1982

An analytical study of a truss bridge - modeling techniques and stress redistribution, M.S. thesis, October 1982.

Bruce A. Ward

Follow this and additional works at: http://preserve.lehigh.edu/engr-civil-environmental-fritz-lab-reports

AN ANALYTICAL STUDY OF A TRUSS BRIDGE –

MODELING TECHNIQUES AND STRESS REDISTRIBUTION

by

Bruce A. Ward

A Thesis

Presented to the Graduate Committee

of Lehigh University

in Candidacy for the degree of

Master of Science

in

Civil Engineering

Lehigh University

Bethlehem, Pennsylvania

October 1982

This thesis is accepted and approved in partial fulfillment of the requirements for the degree of Master of Science in Civil Engineering.

September 9, 1982

_____
Dr. Ben T. Yen

_____
Dr. David A. VanHorn
Chairman
Department of Civil Engineering

ACKNOWLEDGMENTS

TABLE OF CONTENTS

TABLE OF CONTENTS (continued)

LIST OF TABLES

LIST OF FIGURES

LIST OF FIGURES (continued)

ABSTRACT

A discussion of different modeling techniques for a truss bridge is discussed. Three general model types are examined; plane truss, rigid frame truss, and space frame. The results are compared with field measured stresses obtained from measurements of the Atbara Bridge in the Sudan. The study selects the analytical model that best approximates the measured stresses and uses this model to investigate the stress redistribution characteristics of a truss bridge.

In addition, the study examines the effect that stress redistribution has on the fatigue resistance of the structure.

1. INTRODUCTION

1.1 Purpose of the Study

The purpose of this study is to compare the observed behavior of a truss bridge with several analytical models of the bridge and to suggest alternatives to the present design procedure. The study has two objections; to develop an analytical model of the bridge, and to examine the redundancy of the truss bridge using the model.

The study is organized unto five chapters. Chapter 2 describes the data gathering process and the data. Chapter 3 describes the development of several analytical models and their comparison with the actual structure. Chapter 4 uses the analytical model to show the redundant nature of the structure. Chapter 5 examines briefly the effects of member modifications on fatigue strength and Chapter 6 presents the conclusions and recommendations for further investigation.

1.2 Truss Bridges

A truss bridge is composed of a deck supported by longitudinal stringers that frame into floor beams (cross girders) which are connected to the main trusses. Lateral bracing and wind bracing are added to improve the stability of the structure and carry wind loads.

-2-

A truss is characterized by straight structural members, rigidly connected at their joints, with loads only at the joints.[1] The loads induce axial force and bending moments in the truss members. The bending moments, however, are considered to be secondary forces of small magnitude. As a result, the standard design practice has been to analyze the truss as a pin connected structure, developing only axial member forces. The floor beams, stringers, and wind bracing have been designed as simply supported beams. This approach is intended to give an upper bound solution to the member forces.[1,2,9,10,11]

Truss bridges were a popular bridge system for all span lengths until the latter half of the twentieth century. Development of reinforced concrete, precast concrete, plate girders and cable stayed bridge systems provided economically competitive alternatives to truss bridges for spans of 200 to 400 feet. For spans of less than 200 feet the alternative systems were cheaper. In addition, the aesthetics of the alternative bridge systems were considered better for short and medium spans. As a result, the use of truss bridges decreased. At present, truss bridges are most efficiently utilized for spans of 200 to 1500 feet.[1,2]

The advantages of truss bridges over alternative systems are economy of material, because of the open web system, and an easier analysis and design procedure, because the primary member forces are axial. Consequently, the dead weight of the structure is reduced, resulting in a reduction in material costs.[1]

In the last decade, truss bridges have developed problems with fatigue cracking. The cracks have occurred mainly at the floor beam hangers, the floor beams, and the stringers. These are riveted or bolted built-up structural members. As a result, numerous studies of truss bridges have been undertaken and the results indicate that these members are stressed more highly than the design procedure predicts.[3,4] Hence, these members are emphasized in this study.

1.3 Atbara Bridge

The Atbara Bridge of the Sudan Railway System is used in this study as the source of the field data. The bridge is a single track, Pratt Through Truss, with pedestrian and automobile roadways supported from the outside of each truss. Member dimensions and views of the bridge are shown in Figs. 1-1 through Fig. 1-7. The structural members are made of steel plates and angles riveted together. From samples obtained from the bridge, the steel is close in properties and composition to ASTM A7 structural steel, having a yield strength of approximately 255.1 MPa (37 ksi). In addition, the steel has a high level of toughness as indicated by a Charpy V-Notch (CVN) value of 169.5 J (125 ft-lbs.) at an average temperature of 40° F. This compares with an acceptable CVN value of 195.5 J (15 ft-lbs.) at a minimum service temperature of 40° F.[5] A complete list of the properties and composition of the steel is given in Table 1.

A visual inspection of the bridge was made when the field data was obtained. There was no indication of any problems such as cracking of members, excessive deflections, or lack of maintenance. The climate of the Sudan is arid, hence no corrosion of the structure was observed.

The rail traffic using the bridge has consisted of freight and passenger trains. From the opening of the bridge until 1960, the rail system used steam locomotives and trains up to 35 cars in length. Starting in 1960, the steam locomotives were replaced by diesel locomotives and the length of the trains increased to a maximum of 50 cars. The cantilever roadways were added in the early 1960's and have been used extensively by pedestrians, autos, and truck traffic.

2. FIELD MEASUREMENTS

2.1 Purpose of Measuring

In 1980, the Sudan Railway System began a program to assess the condition of their bridges and to project the strength and anticipated life of the structures. Fritz Engineering Laboratory was retained to do a segment of the study. In January and February of 1981, the live load stresses in a number of members in five bridges were measured to provide a data base for the evaluation. The structures examined were located at Atbara, Port Sudan, Khartroum, El Butana, and Kosti.

2.2 Setup and Procedure

In late January of 1981, the south end of one span of the Atbara Bridge was instrumented with electrical resistance strain gages at 17 different locations to monitor strains caused by train traffic. Table 2.1 lists the location of the gages and Fig. 2-1 shows the location of the gages on the structure.

The surfaces of the members were ground smooth and the gages were attached to the surface with epoxy cement and connected to a recording oscillograph. All strain gages were 6 mm long, electrical resistance, temperature compensating, foil gages.

The strain data was recorded in analog form by amplifying and converting the current in the gage to a factored measure of the strain by a Wheatstone Bridge circuit. The impulse was recorded by an analog trace recorder. A typical trace is shown in Fig. 2-2.

The strain response was recorded during the passage of trains for several days. The train traffic during this period consisted of normal traffic and special test trains. The data generated by the normal traffic was used to determine a typical stress range spectrum. The special trains consisted of two coupled diesel engines of known weight and were used to determine the response of the structure to specific loads. A description of the weight and dimension of the test train engines are included in Fig. 2-3.

A summary of the maximum stresses and stress ranges reduced from the field data for the special trains is presented in Table 2.2 and 2.3 for the seventeen gages. The stress values shown are an average for two, 99 ton, coupled diesels, making six trips across the bridge at speeds ranging from 16 kilometers (10 miles) per hour to 32 kilometers (20 miles) per hour. This data is used as the basis for developing an analytical model of the bridge.

2.3 Evaluation of Data

The majority of the field data consists of strain readings from the east and west hangers, U6L6, floor beam L6, and stringers L4L5 and L5L6. Data for the lower chords is limited to one excursion of one scheduled freight train of unknown weight.

Prior to developing an analytical model, an evaluation of the data is presented to determine the data that can be used and the data that is not applicable to the modeling technique.

The lack of data on the lower chord could be due to shear lag and the response of the structure to the first load excursion. In duscussions with the field investigator, gages C2 and C10W were placed near the edges of the top flange along the lower chord. No strain response was recorded in either gage by the passage of one regularly scheduled freight train. Thus the field investigators deleted these gages from future recordings.

Gages C2 and C10W did not show any response for the one load excursion that was recorded due to the effects of shear lag at the splice. Two types of splices are possible that would agree with the measured field data. The first consists of connecting the webs of the lower chord member at the splice and not providing a connection for the flanges. In effect, this type of connection acts as a pin (if designed properly) that tends to allow the beam ends to rotate due to the member moment, releasing the moment stresses. If the web connection is too stiff to allow rotation, the flange stresses are drawn down to the web to be transmitted through the connection with the web stresses. If the gages are near the flange ends, no strain would be recorded. This type of connection is of concern for fatigue and fracture consideration of the structure since stress magnification would occur in the webs of the members and in the connection plate.

The second type of splice consists of web-to-web connections in conjunction with flange-to-flange connections. The flange forces are transferred by the flange-to-flange connection, eliminating the shear lag effect in the web. However, the flange forces are transferred between the chord members by bolts acting as point loads on the flange connection plate. Consequently, the load is not distributed uniformly across the plate, resulting in stresses that are highest at the holes, decreasing toward the edges of the plate (shear lag effect). Hence, if the gages were placed at the edges of the plates, small strains would be recorded. This type of connection is much better for fatigue and fracture resistance by the structure, since more of the member cross section is mobilized to resist the member forces, reducing stress concentration. Unfortunately, the plans of the bridge obtained from the Sudan Railroad do not specifically detail the connections.

The response of gage 12 located on the lower chord, was not recorded as a result of a decision by the field investigators. The trace of regularly scheduled trains showed very small strain ranges for gages 12 and 17. Consequently, the field investigators decided to delete gage 12 from future recordings. The one trace available for gage 12 indicates a maximum stress range response of 0.62 MPa (0.9 ksi) for loads of unknown magnitude. Gage 17 was retained and recorded for the two 99 ton test diesels. However, the location of this gage on the structure is not known.

No field data was recorded for gages C7, C9, C10, C15 and C16 for the test train. The field investigation examined the trace of the first load excursion resulting from the passage of a regularly scheduled freight train and determined that the strain measurements were insignificant. Therefore, they were deleted from further load excursion.

The results from gages C3 and C6 have to be interpreted carefully. They are located on the top of the stringers at the connection of the stringer and the floor beam. From the photographs taken of the bridge, this connection is a shear connection with the top of the stringer coped to allow clearance for the floor beam flanges. Gages C3 and C6 are placed at the edges of the coped flanges of the stringers. The coping of the stringers affects the stresses in the members in two ways. First, removing part of the web and the flange, shifts the neutral axis of the member down toward the bottom flange, significantly modifying the stress distribution in the member. Secondly, the edge of the flange at the cope is subjected to shear lag effects similar to those described above. Both of these effects are localized aberrations in the member and as the cross section becomes complete, the stress distribution becomes linear and symmetric about the neutral axis. In the modeling techniques utilized by this study and described in the following chapters, the structural members are assumed to be complete cross section and fully effective in resisting the applied loads. Therefore, the results obtained from gages C3 and

C6 can not be used to compare the results of the analytical model with the field measured stresses.

The strains recorded in gages C4, C5, and C8 describe the stress distribution in the Hanger U6L6. Since the three gages record different strain values for the same load, the stresses are not uniform across the cross section. This implied that the forces in the hanger are a combination of axial forces (constant stress) and moments (stress varies from tension to compression across the member cross section).

In summary, the analytical bridge model will be developed based on the field data obtained from the hangers, floor beam, and stringers at the south end of the bridge. Qualitative consideration will be given to the lower chord, since the loads causing the recorded strains are unknown and of limited number.

3. DEVELOPMENT OF THE ANALYTICAL BRIDGE MODEL

3.1 Introduction

The development of an analytical model for the truss bridge considers three general structural models; a two-dimensional pin-connected truss, a two-dimensional rigid frame, and a three-dimensional frame. By using a finite element program (SAP IV), the results of analysis from the three structural models are compared with the field data to develop the model that best approximates the observed field measurements. The dimensions and member properties of the bridge are developed from plans and field observations and are presented in Table 3.1 and Fig. 1.1.

The modeling technique consists of two phases. First, the SAP IV program is used to develop member forces resulting from the application of unit loads to the model of the structure. Second, the member forces from the model are used as input to a computer program developed at Fritz Laboratory, Lehigh University, to construct influence lines and stress-time relations for the points of interest on the structure for a given loading condition. The stress-time relations are compared with the field data for the same loading condition to develop a correlation between the stresses on the analytical model and the real structure.

3.2 Pin-connected Truss Model

The pin-connected model analyzes the structure as a series of pin-connected truss members with loads applied only at the connection (joints) along the lower chord. As a consequence, the member forces are axial and no moments are generated. The structure is modeled treating each truss as an independent, planar, two-dimensional structure. The floor beams and stringers are modeled as simply supported members, connected at the hanger/floor beam joint of the truss, transmitting only vertical force. The bracing is not included since no lateral loads are considered.

Two support conditions are examined for the truss. The first support condition prevents any translation horizontally or vertically but allows rotation at all four support points (pins). The second condition allows horizontal translation and rotation (roller) at two support points and pins at the other two points. The results of the analysis for both types of boundary conditions and the field data are shown in Tables 3.2 and 3.3 for hanger U6L6.

A number of observations can be made in comparing the results. First, the largest field measured stress in the hanger is more than twice the maximum model stress, 51.75 MPa (7.50 ksi) versus 22.06 MPa (3.20 ksi). Comparing the influence lines and stress time relationship of the model hanger with the recorded stress variation of the actual hanger, Figs. 3.1, 3.2 and 3.3 gives an indication of the reason for this discrepancy. The model analysis

-13-

results indicate that the hanger U6L6 is not subjected to any stress until the load is applied to panels L5L6 or L6L7, as shown in Figs. 3.1 and 3.2. The field record for the actual structure indicates that hanger U6L6 is stressed by a load applied anywhere on the structure as shown in Fig. 3.3. Consequently, all wheel loads cause stresses in the actual hanger as the train moves onto the bridge and the stress in the hanger predicted by the model would be lower than the stress the actual system experiences. However, a discrepancy of a factor of two between the model stresses and field measured stresses appears to be high.

Second, the number of stress range cycles the hanger experiences in the model is larger than the actual number of stress cycles. This is due to the difference in response between the model and the actual structure. This model assumes that the structure will react instantaneously to the applied loads. In reality, the rate of load application is intermediate between static and dynamic. Damping and the inertia of the members causes the structure to respond more slowly to the applied loads. Hence, the actual structure does not experience the same number of stress range cycles as the model does.

Third, the model predicts only axial forces; thus only uniform stress in the hanger. The field data from Gages C4, C5 and C8 indicates the stresses are a combination of axial and bending stresses.

Fourth, the effects of different boundary conditions on the hangers are insignificant. Each boundary condition results in a maximum tensile stress of 22.06 MPa (3.20 ksi) in the hanger.

As discussed previously, extensive field data for the lower chord is not available. However, for the one train excursion with loads of unknown magnitude, a stress of 6.20 MPa (0.9 ksi) was recorded. The train, noted as a typical train using the Sudan Railway system by the field investigators, consisted of one diesel engine, passenger cars, and freight cars. Consequently, the twin diesel test train is expected to produce a significantly larger stress in bridge members than the normal train traffic. The ratio between the two stress conditions is difficult to predict, however, because of the complex nature of the interaction of the wheel loads, the load spacing, and the number of loads on the bridge. Therefore, the comparison between the model stresses and the measured stresses can only be used to determine if the structure model develops a realistic approximation of the stresses.

For lower chord member L4L5, the maximum measured value is 6.20 MPa (0.9 ksi) under a train with a single engine and freight and passenger cars. The maximum computed stresses for twin 99 ton diesel engines are 24.06 MPa (3.49 ksi) and 10.13 MPa (1.47 ksi) for the pin-roller and pin-pin conditions, respectively. For a single engine, the maximum computed stresses are 16.89 MPa (2.45 ksi) and 6.96 MPa (1.01 ksi) respectively. The measured and computed values are of the same order of magnitude.

The stresses in the floor beams and stringer are computed by a classical approach assuming each is a pin connected member.[1,2]

Due to the length of the stringer (25.4 mm, 252") and the spacing
of the diesel engines, the maximum stress is generated when the
centroid of one of the engines is located at the center of the
stringer. No other combination of load applications will result in
a higher stress. The resulting maximum computed stress is 65.08 MPa
(9.44 ksi).

The maximum stress in the floor beam is determined by
placing the centroid of one of the diesel engines over the floor
beam. The vertical forces acting on the floor beam are taken as
the summation of the wheel loads acting on the stringers. Since no
moments are generated at the floor beam/stringer connection due to
the assumption of pin connection, no torque is developed in the floor
beams by the stringer loads. Hence, the maximum stress is 30.52 MPa
(4.37 ksi).

The maximum measured stresses for the floor beam and
stringer are 12.08 MPa (5.1 ksi) and 43.99 MPa (6.3 ksi), respec-
tively as shown in Table 3.4 with the calculated stresses. The
maximum field measured floor beam stresses are larger than the
maximum computed stresses. The stringer stresses measured during
the field investigation are smaller than the calculated stresses.

In summary, four conclusions can be drawn. First, the truss
model appears to significantly underestimate the stresses and over-
estimates the number of cycles in the hanger. Second, the truss
model generates stresses in the lower chord that qualitatively
agree with the observed stresses. Third, the calculations of

-16-

stresses in a stringer with pin supports results in substantially higher maximum stresses than is obtained from the field measurements. Fourth, the calculations of the floor beam with pin supports results in lower maximum stresses than result from the field measurements.

3.3 Two-Dimensional Plane Frame Model

The second model examined a truss as a two-dimensional plane frame truss, characterized by rigid joints that allow force and moment transfer to adjacent members. The structure is modeled considering each truss member as a beam element. The results of the computed hanger stresses and comparison with the actual hanger stresses are shown in Table 3.5 for hanger L6U6 with pin supports at one end of the bridge and roller supports at the other. Table 3.6 presents the results for the model with pinned supports at both ends. The wind bracing is not considered since it is intended to resist horizontal loads. Only vertical loads are applied to the structure.

Examination of the stress magnitudes reveals the following. First, the maximum tensile stress in the hanger is 23.05 MPa (3.30 ksi), about half of the maximum field measured tensile stress of 52.38 MPa (7.50 ksi). Second, the plane frame truss model generates tensile hanger stresses (23.05 MPa, 3.30 ksi) which is about equal to the pin truss model prediction of 22.35 MPa (3.20 ksi). Therefore, applying the loads at the truss joints does not produce significant moment forces in the truss members.

The model influence lines for a unit load, Fig. 3.4, indicate that as the load enters the bridge and proceeds across the structure to the end of panel L4L5, the hanger stresses are divided into moment stresses and axial stresses. For this region of load application, the axial hanger stresses are insignificant and the moment induced stresses reach a maximum tensile value. As the unit load is applied to panel L5L6, the moment stresses begin to decrease and the axial stresses become dominant. When the unit load is at the hanger, the moment forces are non-existent and the axial forces reach a maximum tensile value. Therefore, the occurrence of the maximum moment stress and the maximum axial stress do not occur at the same load location.

With a series of loads crossing the structure, however, the interaction of loads would be expected to produce a simultaneous moment stress and axial stress in the hanger. Therefore, the higher stresses in the plane frame truss model than the pin-truss model is expected. However, the plane frame truss model stresses are only 3% higher. An examination of the model stress time relationship, Fig. 3.5, indicates that the tensile stress in the hanger are 3.49 MPa (0.5 ksi) when the first wheel is at the end of panel L4L5, a stress of 15% of the maximum stress. This stress is attributed solely to moment effects in the structure since no loads have been placed on panel L5L6. The decrease in the affect of the moment in the structure from 15% of the maximum stress to 3% of the maximum stress is due to the spacing of the applied loads. The spacing of

the wheels of the diesel engines do not produce a maximum moment stress at the same time as a maximum axial stress is produced.

Third, a comparison of the stress time relationships for the model, Fig. 3.5, and actual structure, Fig. 3.3, indicate that model and structure react to loads in a similar manner. The relationships generated from the model indicate that the hanger member is stressed as soon as the load is applied to the bridge; a consequence of the rigid joint connections that transfer the applied loads throughout the structure. As the loads cross the bridge, the stresses increase slowly until the train reaches panel L4L5. At this point the stresses increase dramatically.

The stress time relationship for the real structure indicates that the structure is stressed as the train enters the bridge. As the train crosses the bridge, the stresses increase slowly until the train reaches the panel adjacent to the hanger and then increase dramatically, agreeing with the model. Therefore, even though this analytical model does not develop a good approximation of the maximum stresses, it does generate a stress pattern similar to the field measured stresses.

Fourth, the number of stress ranges predicted by the model is larger than the number of stress ranges recorded by the field measurements. This agrees with the findings of the truss model evaluation and is a consequence of the inertia effects of the actual structural members.

The analytical model with pinned supports at both ends develops results that agree with the above discussion, as shown in Table 3.6. As shown, the largest stress difference between the two models for the hanger is 0.98 MPa (0.14 ksi) and the observations described above are applicable to this model.

The analysis of the floor beams and stringers assumes pin ended members, with the floor beams connected to the hanger/lower chord connection by pins (the same procedure used for the pin truss model). As a consequence, the only loads acting at the frame joints are the vergical end reaction of the floor beam. No moments are induced in the truss from the floor system.[1,2] The results are the same as those obtained for the pin truss model.

The maximum stresses induced at the center of the lower chord L4L5 using the plane frame truss model is -27.80 MPa (-3.98 ksi) (tension) for the pin/roller model and -9.64 MPa (-1.38 ksi) (tension) for the pin/pin model compared with the pin truss model of -24.06 MPa (-3.49 ksi) and -10.26 MPa (-1.47 ksi). The plane frame truss model values are 14% and 6% higher, respectively, than the stress values for the pin truss model. This compares with an observed tensile value of 6.28 MPa (0.9 ksi). The results of the plane frame truss model agree qualitatively with the observed data.

In summary, four conclusions can be stated regarding the stresses generated by this model. First, this plane frame model generates hanger stresses lower than the field measured stresses and overestimates the number of stress ranges experienced by the hangers.

Second, the model does exhibit structural response to loads in a
manner that is similar to the observed field stresses. Third, the
effect of induced moments on the stresses in the structure is small.
The maximum moment stress is 15% of the total stress and does not
occur in conjunction with the maximum total stress. Hence, the
effect of the moment depends on the spacing of the loads. For this
structure, moment stress resulted in a 3% increase in the total
stresses compared with the truss model. Fourth, the stresses in the
lower chord generated by this model agree qualitatively with the
field measured stresses.

3.4 Three-Dimensional Space Frame

The third model used to compute member stresses is a three-
dimensional space frame. This model assembles all the components
(bridge deck, cantilevered walkways, bracing, and main trusses) into
a single structure as shown in Fig. 3.6. (For ease of model develop-
ment, the walkway stringers are treated as one stringer attached to
the end of the cantilever bracket.) The model represents a
structure with greater stiffness and a higher degree of redundancy as
ompared to those models of two-dimensional structures.

Several variations of this model are developed by modifying
the boundary condition of the substructures. Cases 3A and 3B
assume that all member connections are continuous and capable of
carrying bending moment. Case 3A has pin/pin global boundary
conditions, and Case 3B has pin/roller supports. Case 3C and 3D

treat the stringers of the outrigger bracket as pin ended members and the remaining bridge members as continuously connected. Case 3C has pin supports and Case 3D has pin/roller global boundary conditions. Case 3E treats all the floor beams, stringers, and outrigger bracket stringers as pin-ended members and the structural supports are simulated by pins at both ends. Case 3F models the floor beams only as pin-ended members and the rest of the structural members as continuously connected. Case 3F has pin/pin global boundary conditions.

The maximum stresses developed in the model hangers are presented in Table 3.7 with a comparison to the field measured stresses. A comparison between the maximum model floor beam stresses and the maximum measured floor beam stresses is presented in Table 3.8 and a comparison between the maximum model stringer stresses and the maximum measured stresses is presented in Table 3.9. Note that due to the number of models developed, the data presented compares the maximum stresses in the subject member. No listing of stress cycles is included. Similar to the pattern shown by the previous models, the model presenta a larger number of stress cycles than the actual structure experiences.

3.4.1 Hanger Stress Results

A comparison between Case 3E, the pin truss model, and the plane frame truss model is presented below for hanger U6L6A.

    1. Pin Truss σ_{max} = 22.35 MPa (3.20 ksi) (t);

2. Plane Frame Truss $\sigma_{max.}$ = 23.05 MPa (3.30 ksi) (t);

3. Space Frame Truss $\sigma_{max.}$ = 23.82 MPa (3.41 ksi) (t).

Case 3E treats the floor system as a series of pin-ended members with the floor beams connected to the truss by pin connection. The correlation between these models is expected since Case 3E introduces only vertical forces into the truss joints from the end reaction of the floor beams. No moments are induced in the truss from the floor system. This loading condition is the same as the loading condition used for the pin truss and plane frame truss models. Hence, the stress resultants in the hanger should be similar for the three models.

The maximum hanger stress of 31.99 MPa (4.58 ksi) developed by Cases 3B and 3C is one-third higher than the maximum stress of 23.81 MPa (3.41 ksi) in Case 3E. Cases 3B and 3C are characterized by a continuously connected floor system which induces moments in the floor beam/truss connections. Due to the geometry of the joint, this moment is resisted entirely by the hanger. The stresses induced in the hanger by the moment are not large (8.17 MPa, 1.17 ksi). This is expected since the floor beam has a larger moment of inertia 7.58×10^9 mm^4 (18216 in^4) than t he hanger 145.6×10^6 mm^4 (350 in^4). The floor beam rotates the hanger with relative ease resulting in a smaller stress than would be expected if the two moments of inertia were closer in value. Hence, the modeling technique agrees with the expected reaction of the actual structure.

The stress obtained by applying an axial load equal to one half the wheel loads of a diesel engine (24.75 MT for the test train) to the hanger is 27.24 MPa (3.90 ksi). This is a conservative approximation to the stresses obtained from Case 3E and the pin truss and frame truss models, since this approach assumed that the entire load is carried axially by a single member with no load distribution to adjacent members. If this stress value is increased by one-third, the difference between Case 3E and Cases 3B and 3C, a value of 36.32 MPa (5.2 ksi) is obtained, a closer approximation to the model stress of 31.99 MPa (4.58 ksi) than to the field measured stress.

Therefore, based on the three items discussed above, the results obtained from the space frame model for the hanger stresses are consistent with the previous modeling techniques and the expected reaction of the structure to applied load. The results of the floor beams and stringer comparisons are described below.

3.4.2 Stringer Stress Results

The stringer stresses are presented in Table 3.9. There is correlation between the Case 3B and 3D stringer stress of 44.70 MPa (6.4 ksi) and the measured stress of 44.7 MPa (6.4 ksi). Cases 3B and 3D are characterized by a continuous floor system, a frame truss, and pin/roller global boundary conditions. From the table it is apparent that the stringer stresses in Cases 3A, 3C and 3F (pin/pin global boundary conditions) are slightly lower than the stresses in Cases 3B and 3D.

It is interesting to note the difference between the model, the observed stresses and the stresses computed assuming the stringer to be simply supported. The maximum stringer stress is 65.65 MPa (9.4 ksi) using the simply supported beam model. This is approximately 1.5 times greater than Cases 3B and 3D and the measured value of 44.70 MPa (6.4 ksi). Case 3E, which models the stringer as pin-ended members, generates a maximum stringer stress of 66.56 MPa (9.53 ksi), agreeing closely with the simply supported beam model.

Two conclusions can be drawn from this observation. First, the assumption of a simply supported beam for the stringers with the engine wheel loads applied at the beam center results in an upper bound solution to the stresses in the member. Second, the stringers act as continuous beams. According to pictures of the structure taken by the field investigators, the stringers are connected to the floor beam by shear connections and the stringer flanges are not continuous across the floor beam. In reality, however, the stringers interact through the floor beam to prevent substantial rotation of the connection. This condition results in vertical moments, bending the stringers about their strong axis of bending. In the space frame analysis models with continuous stringers, the floor beams do not contribute to the joint stiffness because no torsional rigidity of the floor beams was specified. It should be emphasized that some rotation of the stringer ends occurs depending on the stiffness of the joint. The best modeling technique is to use the relative member sizes to determine the joint stiffness.

3.4.3 Floor Beam Stress Resultants

Table 3.8 presents the results of the model stresses for the floor beams. Cases 3B and 3D give good approximations to the measured stresses. These cases, characterized by pin/roller global boundary conditions, develop a maximum stress of 39,3 MPa (5.7 ksi) compared with a measured stress of 35.6 MPa (5.1 ksi), a difference of approximately one-tenth. The pin/pin global boundary conditions substantially underestimate the floor beam stresses, 27.2 MPa (3.9 ksi) for Case 3C versus a measured value of 35.6 MPa (5.1 ksi).

The floor beam stresses computed by assuming a simply supported beam with the diesel engine axel loads applied to the beam as point loads at the stringer/floor beam connection, are listed in Table 3.4. This analysis (Case 3E) generates a maximum stress of 30.7 MPa (4.4 ksi). This was thought to be conservative since it assumes that the wheel load is carried by the floor beam instead of being shared by adjacent floor beams. However, the computed stress is about 85% of the measured stress and two-thirds of the model stresses generated by Cases 3B and 3D. Therefore, this does not result in an upperbound solution to the member stresses.

An examination of the structure indicates why this approach is not conservative. The stringers acts as continuous beams, as discussed earlier. Therefore, the application of loads at any location on the stringer will generate forces in the floor beams. Assuming that the floor beams are influenced only by the stringers on either adjacent span, as was assumed in 3E, does not take into

account the effect of loads beyond these spans. Hence, it is not a good assumption.

A better model would treat the stringers as continuous members with pinned supports. To find the forces in the floor beams, the reaction at the supports are determined. This model would be expected to give a closer approximation to the observed stress and to Case 3B and Case 3D, but is not conducted as part of the analysis.

3.4.4 Global Boundary Condition

From an examination of Tables 3.7, 3.8 and 3.9 it is apparent that the real structure responds as though the global boundary conditions are pin and roller supports. Table 3.8 indicates that the closest approximations to the measured stresses in the floor beam L7 are generated by pin and roller boundary conditions. Table 3.9 indicates that there is better correlation between the model stresses and the observed stresses when the model global boundary conditions are simulated by pins at one end of the structure and rollers at the other end. Therefore, the conclusions that the structure acts as though the global boundary conditions are pin/roller is realistic.

3.4.5 Space Frame Model Conclusion

In summary, four general conclusions can be drawn regarding this modeling concept:

1. The field measured hanger stresses do not agree with the hanger stresses developed by this model. The model gives results similar to those obtained by previous models and by a single hanger axially loaded;

2. Modeling the stringers as continuous members and as part of the entire structure results in close agreement between the model stresses and the field measured stresses. The simply supported stringer model generates an upper bound solution to the member stresses;

3. Modeling the floor beams as continuous members and as part of the entire structure results in close agreement between the model stresses and the field measured stresses. Assuming the floor beam to be simply supported does not produce a good correlation;

4. The best agreement to the field measured stresses is obtained when the structure model global boundary conditions are simulated by pins at one end and rollers at the other.

3.5 Conclusions

Table 3.10 lists the hanger, floor beam and stringer
stresses for the models developed above and the field measured
stresses. The lowest model hanger stress is obtained from the pin
truss model, a value of 22.3 MPa (3.2 ksi). The largest model
hanger stress, 31.99 MPa (4.58 ksi), is developed by the space frame
model assuming all of the members are continuously connected, Case 3B.
No model develops hanger stresses similar to the field measured
magnitude of 52.4 MPa (7.50 ksi). In addition, if the hanger is
treated as a single beam with an axial load equal to the weight of
one-half the diesel engine wheel loads, a stress of 27.2 MPa
(3.90 ksi) is developed, substantially below the measured hanger
stress. If the hanger stress is increased by one-third, to approxi-
mate the effect of impact and end moments, the hanger stress is
increased to 36.3 MPa (5.2 ksi). This is still substantially below
the field measured stresses.

A comparison of the floor beam and stringer stresses for the
simply supported beam model and the best space frame model (Case 3B)
is shown below.

Member	Simply Supported Beam Model	Case 3B Stress	Field Measured Stress
Floor Beam	30.5 MPa (4.37 ksi)	39.5 MPa (5.65 ksi)	35.5 MPa (5.09 ksi)
Stringer	65.7 MPa (9.41 ksi)	44.6 MPa (6.38 ksi)	44.9 MPa (6.43 ksi)

As can be seen, the best correlation is obtained using the space
frame model with all beams continuously connected.

The study recommends the use of the space frame model with
continuously connected members and pin/roller global boundary
conditions, Case 3B, for the determining of the member stresses,
even though the model hanger stresses and the field measured hanger
stresses do not agree. This conclusion is based on several con-
siderations. First, intuitively, the structure should act as though
the members are continuously connected. The actual member connections
are not true pins that allow rotation of the member ends. They are
shear connections that provide some joint rigidity. Using the model
that allows continuity at the joints, the joint stiffness can be
determined as a function of the stiffness of each member framing
into the joint. An examination of the floor beam and stringer stress
comparisons indicates that there is substantial joint stiffness
in the actual structure which is not predicted by pin supports,
verifying this assumption.

The interaction of the floor beam and hanger can be
described by assuming continuity at the joint. The geometry of the
truss/floor beam connection indicates that the hanger should resist
the floor beam end rotation. In addition, an examination of photo-
graphs of the joint indicate that the joint is substantially rein-
forced to insure that the hanger/floor beam/lower chord connection
is rigid. Since the hanger moment of inertia is very much
smaller than the floor beam moment of inertia (1:50 ratio), the

hanger experiences displacement induced moments as the end of the floor beam rotates. This is more realistic than to assume that there is no hanger rotations caused by the floor beam (i.e. pin joint).

Second, the hanger stress results in the truss for all of the models are similar in magnitude. This is expected since the vertical truss loads are similar for all the models and the moments in the members generated by the space frame model are not large due to the geometry of the joints. Therefore, the model stresses appear to be a good representation of the hanger stresses in the actual structure. This is reinforced by the results obtained from assuming the hanger to be a simple beam loaded axially by one-half the engine axial weight. The resulting stresses are an upper bound approximation of the hanger model stresses not the field measured hanger stresses.

Third, the correlation between the floor system stresses in Case 3B and the measured stresses is good. This correlation would not exist if the joints did not tend to induce a reversal of curvature in the members. This curvature reversal is induced by the stiffness of the members framing into the joint, including the truss members, that can be best approximated by assuming continous connections.

Fourth, with the agreement between the model floor system stresses and the measured floor system stresses, it is conceivable that the field measured strains in the hanger could be questionable

due to possible errors of the data. It is also likely that the hanger sizes depicted in the drawings are incorrect. Based on the correlation of results obtained from the other members and realizing that the field measured data is not infallible, the space frame model with continuously connected beams is recommended. If at all possible, the strain readings in the hanger and the member sizes should be rechecked.

3.6 Discussion of Models

The study has developed three models and compared them with the field measured stresses. The differences between the models are described below for the hanger anf floor system. The discussion assumes that the space frame model is the best representation of the actual structure.

The stresses developed in the hanger by the pin-truss and plane frame truss models are similar. As presented above, the difference in stress is approximately 0.7 MPa (0.1 ksi). The deference between the models is due to the moment effects in the plane frame truss. Hence, the moment effects are negligible between the two models.

The stresses developed in the hanger by the space frame model are significantly larger than developed in either of the other models. The maximum hanger stress by model analysis is approximately one-third larger in the space frame model than the stress developed in the plane frame model. This increase is due to the connection

connection of the floor beam to the hanger by a rigid joint, resulting in out-of-plane bending moments being induced in the hanger. Therefore, the assumption that the floor system and the truss can be designed as separate sub-assemblages results in an underestimation of the stresses in the hanger.

As described earlier, the first and last hangers of truss bridges have been observed to experience fatigue damage. Typically, truss bridges have been designed using the pin-truss model. Hence, the stresses experienced by the actual hanger are higher than the pin truss model predicts. Since the loads applied to the structure are cyclic, fatigue damage would be expected.[8]

The stresses developed in the stringer of the space frame model are lower than the stress developed in the pin truss and plane frame truss models. The space frame assumes that the stringer floor beam connection allows moment transfer in contrast to the other two models that treat the stringer as pin ended members.

The space frame allows reverse curvature to develop at the ends of the member, reducing the midspan moment. The other two models result in analyses that provide an upperbound on the stresses in the member. Hence, using the space frame model will result in member sizes that are smaller than the other two models.

The floor beam stresses developed by the space frame are larger than the corresponding stresses developed by the pin-truss model and plane frame truss. As discussed earlier, this is a

consequence of the type of stringer model used and the assumption of a pin-ended member. This result indicates that the floor beam is overstressed in actual application and the fatigue problems reported in the literature are expected.[3,4,8,9,10,11]

In summary, the use of a two dimensional model neglects the interaction of the floor system with the trusses. Hence, the member stresses developed by these models are not necessarily upper-bound solutions. The study did not investigate the differences in stress between the upper and lower chord members of these three models. It appears, however, that the chords are minimally affected by the floor system stresses, due to the geometry of the connection, and that the stresses predicted by the two dimensional models are upperbound solutions. The lack of fatigue problems in these members is an indication that this is a correct assumption. Therefore, using a space frame model will result in an improved estimate of the stresses in the structure, compared to the field measured stresses, resulting in improved utilization of material.

4. STRESS REDISTRIBUTION IN TRUSS BRIDGES

4.1 Introduction

Using the model developed in Chapter 3, an investigation of the elastic stress redistribution characteristics of a truss bridge will be investigated. Stress redistribution occurs in a bridge as the result of complete or partial member failure due to overstressing of the member, member buckling, or fatigue and resulting fracture of the member. The model developed in Chapter 3 will be used to determine the effect of complete removal and partial removal of hanger L6U6 and lower chord L3L4, see Fig. 4.1.

As it has been shown in Chapter 3, the space frame model with continuity of the structure at the joints represents best the actual structure. Removal of a member from this model does not result in an unstable structure due to the large degree of redundancy. Hence, failure of a member in a truss is not expected to result in catastrophic failure of the total bridge.

The selection of members in the model to be removed is based on an examination of the structure. The members comprising the floor system are not considered because removal of a stringer or floor beam would result in excessive deflection that would impair the use of the structure. This type of failure would be repaired quickly.

The top and bottom bracing do not significantly affect the response of the structure to traffic loads since their primary function is to resist wind loads. Therefore, these members are not considered for removal.

The truss members are the primary load carrying members in the structure for traffic loads. The first and last hangers, U1L1 and U6L6, respectively, appear crucial to the proper functioning of the truss since no other truss members frame into this lower chord/ hanger joint. In addition, the literature notes that the hanger members experience a significant number of fatigue related failures.[3,4,9,10,11] Therefore, this study examines the effect on the structure of the failure of member U6L6A. See Fig. 4.1 for location.

Another important member in this truss is the lower chord member L3L4. This member experiences tensile stresses under any loading condition and would be expected to be susceptible to fatigue. In addition, if the lower chord L3L4 failed, the counter members U3L4 and U4L3 would experience stresses larger than their intended design stress. Therefore, the study examines the effect on the structure of the removal of lower chord L3L4. See Fig. 4.1 for location.

4.2 Modification to Hanger L6U6

Hanger U6L6 will be treated as though it has been completely incapable of taking loads and removed from the structure, Model 4A, and as though half of the cross section is no longer effective in

resisting loads, Model 4B. A comparison between the stresses
developed by these models and the stresses developed in Model 3B is
presented in Tables 4.2 through 4.22.

Table 4.1 and Fig. 4.2 describe the eleven members in the
model that are examined. Nine of the members are near hanger U6L6
and two members, hanger U1L1 and the top bracing member for the first
full panel, U1AU2B, are at opposite ends of the structure from hanger
U6L6. For ease in computation, the stresses in these members are
determined at joints. The ratio of the stresses will be used for
comparison. For ease in identifying the members, the west truss will
be identified as truss A and the east truss will be identified as
truss B. Stringer will be identified as A or B, depending on their
proximity to the west or east trusses. The members to be modified
are hanger U6L6A, at the south end of the truss, and lower chord
L3L4A, in the center of the truss. The panel points are defined as
the connection of the lower chord, hangers, floor beams, and bracing
members and increase numerically from north to south.

4.2.1 Complete Removal of Hanger U6L6A

The maximum member stresses resulting from the complete
removal of hanger U6L6 and the maximum stresses developed using Model
3B are shown in Table 4.2. Several areas of note are discussed below.

The members at the north end of the structure are not
significantly affected by the removal of hanger U6L6A. The stresses
in hanger U1L1B increase by 0.27 MPa (0.04 ksi), from a tensile stress
of 31.85 MPa (4.56 ksi) to a tensile stress of 32.13 MPa (4.60 ksi),

an increase of approximately 1%. An examination of the magnitude of influence line for this member in Table 4.3 indicates that it is very similar to the values of influence line generated by Model 3B. The principle forces are axial forces and the moments are secondary. Therefore, the removal of hanger U6L7A has no effect on hanger U1U1B.

A similar trend is observed for member U1BU2A, one of the top bracing members of the first panel. The maximum compressive stress developed by Model 4A is at 15.0 MPa (2.18 ksi) versus a maximum compressive stress of 15.44 MPa (2.24 ksi) developed by Model 3B, a difference of 3%. A comparison of the unit load stresses developed in the member by both models is presented in Table 4.4. There is no significant difference between these stresses.

The members in the vicinity of hanger U6L6A are significantly affected by the removal of this member. The most dramatic stress changes occurs to lower chord L6L7A, portal beam U6L7A, and hanger L6U6B, as shown in Table 4.2. It is interesting to note that the stresses in floor beam L6AB decrease in magnitude and that the stresses in stringers L6L7A and L6L7B are not significantly affected. A discussion of the effect on each member is presented below.

The lower chord experiences the largest stress increase, going from 18.06 MPa (2.62 ksi) in Model 3B to 97.07 MPa (14.08 ksi) in Model 4A, a ratio of 5.37. A comparison of the stresses for the unit load influence line is presented in Table 4.5. As can be seen, the axial stresses do not change significantly in Model 4A from Model 3B until the load passes panel point 5. At this point,

-38-

the axial stress in the member decreases. The in-plane moment stresses (i.e. generated by moments bending the lower chord in the plane of the truss) generally follow the same pattern in each model for the lower chord until the load reaches hanger U4L4 (panel point 4). When the load moves beyond panel point 4, the moment stresses in lower chord L6L7 begins to increase above the corresponding stresses in Model 3B. The largest increase occurs when the load is placed at panel point 6A. The Model 4A bending stresses are 14.4 times the Model 3B bending stresses. The lower chord in this region becomes a flexural member supporting the applied loads by bending. The axial stresses in the member are minor, accounting for 5% of the total stress.

The out-of-plane moment stresses (stresses generated about the weak axis of bending, i.e. perpendicular to the plane of the truss) follow the same tendency in both models until the load reaches the connection between lower chords L5L6 and L6L7. At this load location, the stresses are 40% larger in Model 4A than in Model 3B. This increase is not of primary concern due to the decrease in axial stress and the large increase in plane moment stresses.

The next largest increase in stress is observed to occur in the portal beam U6L7A. Removal of the hanger changes the maximum stress from a tensile stress of 24.13 MPa (3.50 ksi) to a tensile stress of 43.29 MPa (6.28 ksi), 2.75 times higher, as presented in Table 4.2. Table 4.6 presents the unit load influence line stresses

-39-

for Models 3B and 4A. The axial stresses are similar for the two models until the load reaches hanger L4U4 (panel point 4). As the load moves from panel point 4 to panel point 5, the axial stresses decrease in the member for Model 4A. The in-plane stresses become dominant in Model 4A as the load is placed beyond hanger L5U5 (panel point 5), reaching a maximum value of 1.03 MPa (0.15 ksi) when the load is placed at the connection between lower chords L5L6 and L6L7. This value is more than fifteen times larger than the corresponding stress in Model 3B. The out-of-plane stresses do not increase significantly. Therefore, similar to the lower chord member, the portal beam in Model 4A carries the stresses induced from the applied load by flexure, not axially as is the case in Model 3B.

Due to the removal of hanger L6U6A, the stresses in hanger L6U6B are increased from 31.44 MPa (4.56 ksi) to 73.76 MPa (10.7 ksi), a ratio of 2.35, as presented in Table 4.2. Table 4.7 compares the unit load influence line stresses between the two models. As can be seen from this table, the major difference between the two models is the in-plane moment stresses. Model 3B develops a tensile stress moment of .123 MPa (0.018 ksi) for a unit load compared to 1.02 MPa (.148 ksi) for Model 4A, a ratio of 8.25. The axial and the out-of-plane stresses do not change significantly between the two models. Therefore, the removal of hanger U6L6A results in an increase in the bending moment stresses in hanger U6L6B.

The most interesting result of the hanger removal occurs in

the floor system. From Table 4.2, the floor beam L6AB tensile

stresses in Model 3B are higher, 41.78 MPa (6.06 ksi) than in

Model 4A, 38.40 MPa (5.57 ksi), implying that removal of the hanger

results in lower stresses in the floor beam. Table 4.8 presents

a comparison of the floor beam stresses for both models. The axial

stresses in the floor beam are the same in both models until the

unit load is at floor beam L6AB. The stresses in Model 4A are

half of the Model 3B stresses at this location of load application.

A comparison of the stress components for both models indicates that

the axial stresses and the out-of-plane moment stresses in the member

are similar for both models.

The in-plane moment stresses, however, are substantially

lower in Model 4A than the stresses developed by Model 3B. The

maximum Model 4A stress from the unit loads is 0.40 MPa (0.058 ksi),

compared to the maximum Model 3B stress of 0.50 MPa (0.072 ksi).

This result is a consequence of a change in the end support

condition of the floor beam. Removing the hanger at one end of the

floor beam results in a more flexible support at this end. Thus

reduces the bending moment in the floor beam.

To describe the consequence of this type of support condition

the study has examined two beams with different boundary conditions

as shown in Fig. 4.3a. The first is a member supported at one end

by a spring and at the other end by a fixed support. This is

analogous to the above described boundary condition when the hanger

is not effective. The other beam is treated as though both ends are pinned, analogous to the case of both hangers U6L6A and U6L6B being in place. Both models are loaded with two unit loads at the third point of the members.

The results of this analysis indicate that the maximum moment developed by the first model occurs under the load applied closest to the end of the member if the spring support is assumed to accept three-eights of the total applied load. The maximum moment shifts to the fixed support if the string is assumed to carry a smaller percentage of the total applied load. In addition, the maximum moment developed by this model is less than the maximum moment developed by the pin supported model, as shown in Fig. 4.3b. Therefore, the more flexible structure develops a smaller stress than the stiffer structure. Analogously, the removal of hanger U6L6A in the computer model results in a more flexible floor beam and the stresses in the floor beam are smaller than the Model 3B stresses.

As a consequence of the decrease in the floor beam stresses, the study compared the stresses that occur at the connection of floor beam L5AB and stringer L5L6A and L5L6B. The results are shown below.

Member	Hanger U6L6A in Place	Hanger U6L6B Removed	Floor Beam L5AB/ Stringer L5L6B Connection
Floor Beam L5AB	35.0 MPa (5.07)	35.4 MPa (5.14)	36.4 MPa (5.28)

The increase in stresses in floor beam L5AB is expected due to the removal of hanger U6L6A because a larger portion of the applied load must be transmitted to the truss through L5AB.

In contrast to the floor beam stresses, the stringer stress increase as a result of removal of hanger U6L6B. The maximum stringer tensile stresses are shown in Table 4.2. Stringer L6L7A experiences a 10% increase in stress at the floor beam L6AB stringer connection. Stringer L6L7B, however, experiences little change in stress. In addition, the study determined the maximum stringer stresses that occur at the floor beam L5AB/stringer connection. These results are shown below.

Location	Hanger U6L6A in Place, Max. Stress	Hanger U6L6B Removed, Max. Stress
Stringer L5L6A/ Floor Beam L5AB	48.81 MPa (7.08 ksi)	32.75 MPa (4.75 ksi)
Stringer L5L6B/ Floor Beam L5AB	48.81 MPa (7.08 ksi)	47.36 MPa (6.87 ksi)

Stringer L5 L6A experiences a decrease in stress of 67% and stringer L5L6B experiences a decrease in stress of 3%.

The stress changes in these stringers are a result of a change in the stiffness of the structure. Removal of hanger U6L6A, in effect, increases the span length of the stringer, since the support offered by floor beam L6AB is significantly reduced. Consequently, the relative stiffness of the floor beam L5AB/ stringer L5L6A connection is reduced since the moment resistance of

the joint is a function of the moment of inertia of the member

divided by the length (I/L). Doubling the length of the span

reduces the amount of moment that the joint can resist resulting

in greater joint rotation, as shown in Fig. 4.4 and Fig. 4.5.

The computer analysis indicates that the rotation at this connection,

presented below, is more in Model 3B (higher I/L ratio) than in

Model 4A (lower I/L ratio).

Rotation of Floor Beam L5/Stringer L5L6A Joint

(in Radiant)

Load Location	Model 3B Hanger U6L6A in place	Model 4A Hanger U6L6B Removed
At Floor Beam L5	$- 0.52145 \times 10^{-5}$	$- 0.19621 \times 10^{-5}$
Halfway Across Panel L5L6	0.56972×10^{-4}	0.15136×10^{-4}
At Floor Beam L6	0.50881×10^{-4}	0.35325×10^{-4}

Therefore, the resisting moment at the floor beam L5AB/Stringer L5L6A

connection should be lower for Model 4A than for Model 3B. Hence,

there is less reverse curvature effect at the support for Model 4A.

The increase in the stringer L7L7A stress at the floor beam

L6AB connection is due to the reduction in restraint at the floor

beam L5AB support for stringer L7L7A. The results indicate that the

stress increase is due to an increase in the in-plane moment

stresses since the axial and out0of-plane moment stresses do not

change. Hence, the increase in stress is due to moment, agreeing

with the above discussion.

The similarity in stresses observed in stringers L5L6B and L6L7B is a consequence of their distance from hanger U6L6A. The deflection of the floor beam L6AB/stringer L6L7B joint is not as large as occurs on the A side of the structure. Consequently, the decrease in stiffness of the joints does not occur to such an extent and the members stresses are not changed significantly.

The amount of reverse curvature introduced into the stringer is less in Model 4A than in Model 3B. Therefore, as shown in Fig. 4.5, the moment reduction at the middle of the stringer span (i.e. connection point with floor beam L6AB) in Model 4A will be less than in Model 3B, resulting in a higher moment in Model 4A at the floor beam L6AB stringer connection. This description agrees with the results presented in Table 4.2. In addition, Table 4.9 depicts the unit load stresses which agree with the above discussion.

The remaining two members examined are top bracing U5AU6B and truss diagonal L5U6A. Member U5AU6B is located on top of the bridge in the last panel of the top chord bracing system. Member L5U6A is located in the second last panel of the west truss and is adjacent to hanger L6U6A.

Member U5AU6B experiences a modest increase in maximum stress of 15% as shown in Table 4.2. Table 4.10 indicates that the increase is due to an increase in the axial stresses in the members. The bending stresses remain similar between the two models.

Member L5U6A experiences an increase in stress of 80%, from a tensile stress of 24.3 MPa (3.52 ksi) to a tensile stress of 47.4 MPa (6.88 ksi), as shown in Table 4.2. A comparison of the member unit stresses between Model 4A and Model 3B, Table 4.11, indicates that the increase is due to bending of the member about its principle axis of bending. The axial stresses and the weak axis bending stresses are not affected.

In summary, the effects of removal of hanger U6L6A are varied. Generally, the stress redistribution in the truss members adjacent to hanger U6L7A results in large increases in the bending moments experienced by the members. Hence, the truss members become flexural members as opposed to axial loaded members. This tendency occurs for the lower chords, portal members, and diagonal members. The upper chord is expected to develop substantial flexural stresses as well. This moment effect decreases rapidly for members further away from U6L7A, as evidenced by the small increase in stresses in hanger U1&1B. This is expected since the maximum carry-over factor for moment from one end of a beam to the other end is 0.5 per moment distribution concepts.

The effect of removing hanger U6L6A on the top bracing of the structure is minor. The largest increase in maximum stress is 15% at the end where the member is removed. The bracing at the opposite end experience an increase of 3%. The stress increase in these members is due to an increase in axial stresses. The moment stresses are small for both Model 3B and Model 4A.

The effect on the floor system due to the removal of a hanger varies. The stresses in floor beams near hanger U6L6A decrease, while the stringer stresses remain the same or increase. The effect on adjacent floor beams is to increase the stresses as a consequence of the increased stringer span length between floor beams L5 and L7. The stresses in the adjacent stringers increase at the floor beam L6/ Stringer connection and decrease at the floor beam L5/stringer connection due to variations in the stiffnesses of the respective joint.

4.2.2 Partial Removal of Hanger U6L6A - Model 4B

Model 4B treats hanger U6L6A as though half of its cross section had been removed. A comparison of the Model 4B and Model 3B stresses are presented in Table 4.12. As would be expected, the members that experience the largest stress increases in Model 4A are the members that experience the largest stress increases in this model. The magnitude of the stress increases, however, are significantly lower in Model 4B than in Model 4A.

The members at the opposite end of the structure examined by this study, hanger U1&1B and top bracing U1AU2B do not experience a significant change in stress between Models 4B and 3B. The stresses in hanger U1L1B decline from 15.6 MPa (2.24 ksi) to 15.1 MPa (2.17 ksi) (a 3% difference). In addition, an examination of the influence line unit stresses in this member, presented in Table 4.13, indicate that the axial and moment stresses are similar for Models 3B and 4B.

Member U1U2B, a top chord member in the second panel, also experiences a 3% decline in stress, from 15.6 MPa (2.24 ksi) to 15.1 MPa (2.17 ksi). This is not considered a significant deviation between the models. An examination of the influence line unit stresses in Table 4.14, indicates that the axial stresses and the moment stresses in this member are similar for Models 3B and 4B.

The members that exhibit the largest increase in stresses are the lower chord L6L7A, hanger L6U6A, truss diagonal member L5U6A, and portal beam U6L7A. These members are adjacent to the modified member. The remaining members examined by this study are marginally affected. A discussion of each member is presented below.

The lower chord, L6L7A, experiences the largest stress increase. The stresses change from a tensile stress of 18.06 MPa (2.62 ksi) to a tensile stress of 33.57 MPa (4.87 ksi), an increase of approximately 86 percent. A comparison of the stresses developed in this member by two unit loads crossing the bridge is presented in Table 4.15. The major change in the stresses occurs in the panel in-plane moment stresses. The in-plane moment stresses increase from .173 MPa (0.025 ksi) in Model 3B to .101 MPa (0.015 ksi) in Model 4B, a 67% increase. The axial and out-of-plane moment stresses remain consitent for both models as the unit loads cross the bridge. Hence, the result of removing half of the effective cross section of the hanger results in increased in-plane bending stresses in the lower chord member, similar to the results for complete removal of the hanger.

The next largest increase in stress occurs in hanger U6L6A. The maximum stress developed by Model 3B is a tensile stress of 31.44 MPa (4.56 ksi). When the effective cross section of the member is reduced by one-half the stresses increase to 46.88 MPa (6.80 ksi), an increase of approximately one-half.

Table 4.16 presents a comparison of the unit load stresses for this hanger for Models 3B and 4B. In this case, the axial tensile stresses increase significantly, increasing from 0.0442 MPa (0.064a ksi) for Model 3B to 0.85 MPa (0.1227 ksi) for Model 4B. The in-plane moment stresses decrease from a maximum value of 0.123 MPa (0.0179 ksi) for Model 3B to 0.045 MPa (0.0066 ksi) for Model 4B, and the out-of-plane moment stresses do not change significantly. Therefore, in contrast to the other members where the stress increases were due to moment, the stress increase in this member is due to an increase in axial stresses.

These results agree with the expected outcome. The cross-sectional area has been reduced by half, reducing the amount of material available to resist the axial forces. Therefore, the axial stresses will increase (force divided by area). The moment stresses decrease as a consequence of a decrease in the in-plane moment of inertia of the member from 146×10^6 mm^4 (350 in.^{4}) to 64×10^6 mm^4 (154 in.^{4}). Consequently, the member is more flexible, decreasing the amount of the applied moment it will accept and decreasing the corresponding moment stresses.

Portal beam U6L7A experiences the third largest increase in stress. The maximum Model 3B stress is 17.23 MPa (2.50 ksi) compared with a maximum Model 4B stress of 30.96 MPa (3.04 ksi). An examination of Table 4.17 indicates that the increase is due to an increase in out-of-plane moment stresses and in-plane moment stresses. The axial stresses remain similar between the two models.

The maximum out-of-plane moment stress in Model 3B is .0029 MPa (0.0042 ksi). The corresponding Model 4B maximum stress, .013 MPa (0.0019 ksi), is substantially below this value. However, the influence line magnitude of the out-of-plane moment stresses at other panel points are higher in Model 4B than in Model 3B, by factors of two to three. The maximum in-plane moment stress increases significantly for Model 4B (.050 MPa, 0.0072 ksi) over Model 3B (.012 MPa, 0.0017 ksi) but the influence line magnitudes at other panel points show a marked decrease in Model 4B compared with Model 3B. Therefore, decreasing the cross sectional area of hanger U6L7A increases the maximum in-plane moment stress.

The last member to experience a significant change in stress is truss diagonal member L5U6A. The stress increases from 26.33 MPa (3.82 ksi) in Model 3B to 30.13 MPa (4.37 ksi) in Model 4B. Table 4.18 presents the unit load stresses for the member. As can be seen, the axial stresses and the outof-plane moment stresses remain the same. The in-plane moment stresses increase from .0365 MPa (0.0053 ksi) for Model 3B to .0558 MPa (.0081 ksi) for Model 4B, an increase of 53%. Hence,

stress redistribution due to removal of hanger U6L7A results in an increase in bending moment in the bracing member.

The remaining members, floor beam L6AB, stringer L6L7A, stringer L6L7B, hanger L6U6B, and top bracing member U5AU6B, do not exhibit any substantial increase in stresses as a result of the modification of hanger U6L6A. Tables 4.10, 4.20, 4.21 and 4.22, corresponding to the above listed members, do not show any significant differences between the unit load axial and moment stresses developed from either Model 3B or Model 4B. Hence, removal of half of the cross-sectional area of hanger U6L6A does not result in significant stress redistribution to the floor system or the opposite truss member.

In summary, removal of half of the effective cross section of the hanger affects the truss that contains the modified member. The adjacent truss members become bending members instead of axial force members. The effects of the hanger removal are localized in the truss as shown by the small stress changes that occur in hanger U1L1B and U6L6B and by the small stress changes that occur in the floor system and top bracing members.

4.2.3 Comparison and Discussion of Models 4A, 4B and 3B

A comparison of the stresses in the three models results in the following observations. First, the stress changes to the members adjacent to the hanger are significantly larger in the Model 4A A truss than in Model 4B A truss. Second, the floor system

stresses in Model 4A change to a much greater degree than in Model 4B. Third, the effect on the trusses is different for the two models. In Model 4A, the members in both trusses experience stress redistribution. In Model 4B, however, truss B does not experience any significant change in member stresses.

In the first instance, complete fracture of the hanger results in lower chord L5L7 acting as a continuous beam since the loads from the floor system are not applied to the truss at a truss joint. Therefore, the member acts as a flexural member carrying the loads by bending. The bending stresses are transmitted to the adjoining members, resulting in increased moment stresses. In contrast, removing half of the effective area of the hanger does not affect how the truss is designed to function. The loads from the floor system are applied at the truss joints. Therefore, the bending stresses induced in the truss members would be expected to be less in Model 4B than in Model 4A. As shown in Tables 4.2 and 4.12, the stress increases in the Model 4B truss members are generally much less than the stress increase in the Model 4A truss members.

The change in the floor system stresses are due to the change in deflection of the panel point 6. The deflection of the joint is shown below.

VERTICAL DEFLECTION OF PANEL POINT 6

Model	Vertical Deflection (in.)
3B	$- 0.16099 \times 10^{-2}$
4A	$- 0.13629 \times 10^{-1}$
4B	$- 0.22061 \times 10^{-2}$

Model 4A exhibits the largest deflection, and therefore, has the most flexible floor system. From previous discussions, it has been shown that the more flexible a structure the lower the stresses in the structure. Model 4A exhibits deflections that are eight and one-half times greater than Model 3B. Model 4B deflections are one and one-third times greater than Model 3B. Hence, the lower stresses in Model 4A than in Model 4B is expected. Note that the increase in deflection in Model 4A affects the floor system member stresses by approximately 10%. Hence, a much smaller increase in deflections, such as those developed by Model 4B, would be expected to have little effect on the floor system stresses compared with Model 3B. The floor system stresses in Table 4.12 confirm this expectation.

The stress changes due to the hanger U6L6A modifications are not carried over to the opposite truss in Model 4B because of the continued presence of the hanger in the truss structure. A comparison of the end rotations of floor beam L6AB at the truss B end of the member is presented below.

FLOOR BEAM L6AB END ROTATION

Model	Rotation (rads)
3B	0.71530×10^{-5}
4A	0.65711×10^{-4}
4B	0.10137×10^{-4}

The rotation in Model 4A is larger than the rotation in Model 3B by a factor of nine, resulting in a moment in Model 4A being two and one-third times larger than in Model 3B. The rotation in Model 4B is larger than the Model 3B rotation by a factor of one and one-half, resulting in a 5% increase in moment stresses. Therefore, the stresses are not redistributed to the opposite truss.

In summary, the study indicates that the loss of a hanger has a significant impact on the way the structure functions. The presence of the hanger even if the cross section is not complete, is sufficient to insure that the trusses will carry the loads as axial forces in the members. In addition, the presence of the hanger controls the zone of stress redistribution. When the hanger is not effective, the truss members near the hanger develops large bending stresses and sections of the truss function as continuous beams. In addition, complete fracture of the hanger results in stress redistribution in both trusses.

4.3 Modification to Lower Chord L3L4A

The structure is modeled with lower chord member L3L4A completely removed, Model 4C, and with the lower chord member L3L4A

cross section reduced by one-half, Model 4D. See Fig. 4 for member location. A comparison between the stresses developed by these models and Model 3B is presented in Tables 4.24 through 4.47.

Table 4.23 describes the eleven members that are examined by the study. Nine of the members are near lower chord L3L4A and two members are at the south end of the structure. For ease in computation, the stresses in these members are determined at joints. The ratio of stress will be used for comparison.

4.3.1 Complete Removal of Lower Chord L3L4A

The maximum member stresses resulting from complete removal of chord L3L4A and the maximum stresses developed using Model 3B are shown in Table 4.24. The results are discussed below.

The largest increase in stress occurs in the members immediately adjacent to the lower chord at midspan. Floor beam L4AB, counter L4U3A, counter L3U4A, lower chord L3L4B and lower chord L6L7A are affected to the greatest extent. The remaining members do not experience stress increases larger than 50% above the stresses developed in Model 3B.

The largest stress increase occurs in floor beam L4AB. The stresses increased from 9.86 MPa (1.43 ksi) to 67.35 MPa (9.77 ksi), an increase of approximately seven-fold. Note that the maximum stresses in both models are compressive and are located at the end of the member, i.e. the connection with the truss. From an examination of Table 4.25, the member experiences an increase in axial

stress, in-plane moment stress, and out-of-plane moment stress.
The maximum axial stress in the member increases from .007 MPa
(0.001 ksi) to .021 MPa (0.003 ksi), an increase of threefold.
The in-plane moment stress increase from .012 MPa (0.017 ksi) to
.016 MPa (0.002 ksi), an increase of approximately one-third. The
out-of-plane moment stresses increase from .08 MPa (0.0113 ksi) to
0.70 MPa (0.102 ksi), an increase of approximately ninefold. The
increase in outof-plane moment stresses indicates that the member
is being bent along its minor axis, perpendicular to the floor beam.

An examination of the geometry of the member explains why
the floor beam is experiencing out-of-plane stresses. Removal of
lower chord L3L4A creates a discontinuity in the truss. Hence, the
forces in the lower chord are transferred to the adjacent members.
As discussed later in this study, a large portion of the axial stress
is carried by the adjacent stringer, L3L4A. The lower chord axial
forces are transferred to the stringer by floor beam L4AB as shear
forces perpendicular to the web of the member. As a result, the
floor beam experiences out-of-plane bending stresses. In addition,
the displacement is toward the side of the structure where the lower
chord has been removed (i.e. the negative Y-direction, see Fig. 4.6).

The small increase in the in-plane moment stresses in the
floor beam is due to the support condition of the beam. As discussed
in previous sections of this study, the hangers are critical to the
support of the floor system. Removal of the lower chord does not
significantly affect the hanger stresses. An indication of this is

given by the vertical displacements of the bottom of the hanger as shown below.

MODEL   HANGER U4L4A VERTICAL DISPLACEMENT

3B $- 0.35742 \times 10^{-2}$

4D $- 0.47745 \times 10^{-2}$

The difference in deflection is not substantial (approximately one-third) and, as shown previously, a change in deflection of the same order of magnitude does not significantly affect the stresses. Therefore, the floor beam supports do not change as a result of the lower chord modification and the in-plane moment stresses developed in the member would be expected to be similar to Model 3B.

The increase in the axial stresses in the floor beam is of minor concern. The axial loads in the member increase between Models 3B and 4C as a result of increased differential displacements along the axis of the beam. In Model 3B, the differential displacement is 1.0×10^{-8} mm (4×10^{-10} in.) according to the analytical model. This results in a force of 240.2 N (54 lbs.) in the member. In Model 4C, the differential displacement increases to 0.54×10^{-3} mm (2.110^{-5} in.) resulting in an axial force of 774.0 N (174 lbs.). The increase in axial stress between the two models is 200%, but the effect on the total stresses in the member is small. The total stress in the members from the unit loads in Model 4C is 0.72 MPa (0.105 ksi) while the axial stress is 0.02 MPa (0.003 ksi), approximately 3% of the total.

The second largest increase in stress occurs in counter member L3U4A. The stresses increase from a tensile stress of 8.27 MPa (1.2 ksi) in Model 3B to a tensile stress of 37.23 MPa (5.4 ksi) in Model 4C, an increase of four and one-half times. An examination of Table 4.26 indicates that axial and in-plane moment stresses in Model 4C are larger than the corresponding Model 3B stresses until the load passes panel three. As the load moves from panel 3 to the end of the bridge, the axial and in-plane moment stresses are lower in Model 4C than the corresponding stresses in Model 3B. The out-of-plane moment stresses in Model 4C and in Model 3B also follow the same trend, but to a lesser degree. In addition, the axial stresses in Model 4C are tensile stresses for any load application. Model 3B develops compressive stresses as the load moves across the bridge.

Member L4U3A experience stresses that are opposite member L3U4A, as shown in Table 4.27. The axial stresses in Model 4C are lower than the Model 3B stresses until the load passes the center panel. When the load is applied at panel point 4 or beyond, the axial stresses are higher in Model 4C than in Model 3B. The same tendency occurs for the in-plane moment stresses. The out-of-plane moment stresses for the two members are similar. The total stress in L3U4A is slightly less than member L4U3A and larger than the member stress developed in Model 3B as shown in Table 4.24.

Members U3L4A and L3U4A act in tandem to resist the applied loads. As the load is applied to the north end of the bridge, L4U3A

is in axial compression and U4L3A is in axial tension. When the load is at the opposite end of the bridge, the direction of axial stress in the members is interchanged as shown in Tables 4.26 and 4.27.

Removal of the lower chord removes the compressive stresses in the members. As the load is applied to the north end of the structure, member L4U3A in Model 4C experiences small axial forces, one or two orders of magnitude below the comparable Model 3B stresses. The negative signs (tension) in Model 4C are not of consequence since the stresses are small. Member U4L3A experiences significant tensile axial forces under the same loading condition. As the load is applied to the opposite end of the bridge, the members reverse their stresses with member U4L3A experiencing small stresses and member U4L4A experiencing large axial tensile stresses. In both cases, the axial tensile stresses are approximately two and one-half times larger in Model 4C than in Model 3B.

The in-plane moment stresses in the two members are similar to the axial stresses. The in-plane moment stresses in Model 3B for L3U4A are the reverse of the in-plane moment stresses in Model 3B for L3U4A are the reverse of the in-plane moment stresses in member L4U3A. Removal of the lower chord L3L4A decreases the in-plane moment stresses in L4U3A at the start of the load application and increases these stresses as the load reaches panel 3. The stress increases in L3U4A approximately three and one-half times, including a change in stress from compression to tension. Hence, the counter

experiences curvature in the same direction for all load application
in Model 4C, whereas Model 3B experiences a curvature reversal as
the load crosses the structure. Note that the first in-plane
stresses are small in Model 4C for member L4U3A.

Counter L3U4A in-plane moment stresses experiences a
similar tendency but in reverse order of L4U3A. The positive
stresses, however, are similar in magnitude in Model 4C to the
corresponding stresses in Model 3B. This is different from the
L4U3A results.

The results of the axial and in-plane moment stresses in
the counters indicate that the removal of lower chord member L4L4A
results in a reduction in the compressive stresses that the counter
experience. An examination of the joint forces indicate why this
occurs. When the lower chord L3L4 is in place, panel point 3 is
displaced downward as the load is placed on panels 1, 2, and 3.
As a consequence panel point 4 is displaced toward panel point 3.
Therefore, the counter member L3U4A is in tension along with the
other members framing into panel point 3 and counter member U3L4A is
placed in compression as a result of these displacements.

Removal of lower chord member L3L4 results in no transfer
of the displacements between the two joints. In effect, the joints
are independent of one another. Loading the north end of the bridges
does not result in any significant displacements in the southern
half of the bridge. Hence, there would be no significant stresses
in the counter member U3L4A and counter member U4L3A experiences

tension stresses. As the load moves onto the southern half of the bridge, member U4L4A is stressed and the stresses in U4L3A are not significant.

The out-of-plane moment stress increase between the two models in the counter members is a consequence of the out-of-plane movement of the structure. The counter members are bent about their weak axis of bending. Therefore, the observed stress increases are expected.

The next highest increase occurs in member L3L4B, the lower chord member opposite the removed chord member. The tensile stresses in this member increase from 23.85 MPa (3.46 ksi) to 69.62 MPa (10.09 ksi), a three-fold increase. Table 4.28 presents a comparison of the stresses developed in the member from two unit loads crossing the structure for Models 3B and 4C. As can be seen the in-plane moment stresses are similar for Models 3B and 4C. Hence, there is no significant in-plane bending stress increase.

The axial stresses are similar until the load is applied to panel point 5. At this location, the loads result in an axial stress increase from 0.090 MPa (0.0131 ksi) to 1.002 MPa (0.145 ksi) an increase by an order of magnitude. As the load is moved further the stresses in the two models are similar. Hence, the maximum axial stress affects in Model 4C are delayed until the load is placed at the beginning of the second panel beyond the removed lower chord member.

The in-plane moment stresses are increased in Model 4C above the corresponding Model 3B stresses. The largest increase is from 0.005 MPa (0.0008 ksi) in Model 3B to 0.031 MPa (0.0045 ksi) in Model 4C, an increase of approximately six times. Therefore, it appears that the structure is moving sideways in reaction to the vertical loads. An examination of the displacement of panel point 4 indicates that the structure does move in the Y-direction as shown below.

PANEL POINT 3 – DISPLACEMENT IN Y-DIRECTION

Model	Node Y-Displacement
3B	0.30860×10^{-5}
4C	-0.4086×10^{-2}

Hence, the increase is a result of the out-of-plane displacement of the structure, bending the chord member about its minor axis of bending.

Lower chord L6L7A experiences the lowest significant stress increase of the members studied. The maximum stress increased from 18.06 MPa (2.62 ksi) in Model 3B to 44.95 MPa (6.52 ksi) in Model 4C, an increase of two and one-half times as shown in Table 4.24. Table 4.29 presents a comparison between the unit stresses in Models 3B and 4C. An examination of the table indicates that the axial stresses are of the same order of magnitude for the two models. The in-plane moment stresses are similar for the two models, except when the load is applied at the fifth panel point. This point of load

-62-

application results in maximum tensile stress of 0.179 MPa (0.026 ksi) in lower chord L6L7A from Model 4C compared with a maximum stress of 0.014 MPA (0.002 ksi) from Model 3B, an increase in excess of an order of magnitude.

The out-of-plane moment stresses increase by a factor of approximately two between the two models. Similar to the previous members, the cause of this increase is the out-of-plane displacement due to the removal of lower chord L3L4A, resulting in lower chord L6L7A being bent about its minor axis of bending.

The differences in stress between the remaining members shown in Tables 4.30 through 4.35 are not marked with the exception of stringer L3L4A. The stresses in stringer L3L4A are appoximately 50% greater in Model 4C compared with Model 3B, as shown in Table 4.24. This is expected because of the proximity of this stringer to the removed lower chord member. Table 4.30 compares the unit stresses in the member for the two models. As can be observed, the magnitude of the stress increase is due to an increase in the axial stresses and the out-of-plane moment stresses in the member. The in-plane moment stresses in the member do not change significantly.

The increase in axial stress in stringer L3L4A is expected due to the removal of the lower chord L3L4A. Since this stringer is located next to the lower chord, removal of the lower chord requires that the stringer carry a substantial portion of the axial forces, formerly carried by the lower chord. The lower chord axial forces are transferred through the floor beam as out-of-plane

bending moment and are introduced into the stringer as axial
forces. In effect the stringer functions as a flexural member and
a tension member.

The results presented in Table 4.30 substantiates this
conclusion. The axial stresses increase from a maximum tensile
stress of 0.029 MPa (0.0042 ksi) to a maximum tensile stress of
0.108 MPa (0.0157 ksi), approximately a fourfold increase, as a
consequence of the removal of the lower chord.

The in-plane moment stresses due to unit loads are affected
to a small degree, increasing from a maximum value of 0.163 MPa
(.0236 ksi) to 0.186 MPa (0.0270 ksi), an increase of 15%. Hence,
the in-plane bending stresses in the stringer are not substantially
increased. This is expected since the stringer supports do not
experience any differential displacements, as discussed previously.
The increase in out-of-plane moment stresses between the two models
is due to the out-of-plane displacements of the structure. The
maximum stress increase from 0.014 MPa (0.0021 ksi) to 0.050 MPa
(0.0072 ksi), an increase of approximately two and half times. ·
Hence, the magnitude of stress increase in this stringer is due to
an increase in axial stresses.

The small increase in stress that occurs in the upper chord
member is surprising. Member U3U4A increases from 29.92 MPa
(4.34 ksi) to 33.92 MPa (4.92 ksi), an increase of 13% and member
U3U4B increases from 29.92 MPa (4.34 ksi) to 34.74 MPa (5.04 ksi),

an increase of 16% as presented in Table 4.24. From Tables 4.31 and 4.32, the axial and in-plane moment unit load stress increases approximately 10% for both members. The out-of-plane moment stresses experience a five-fold decrease. Note the out-of-plane moment stresses are much smaller than either the axial stress or in-plane moment stress in either model, hence a large decrease will not significantly affect the stresses. Therefore, the upper chords are not affected by the out-of-plane bending stresses and the axial stresses and the in-plane moment stresses are not increased significantly. Consequently, the stress redistribution due to removing the lower chord L3L4A does not affect the upper chord. The lower chord and floor system carry the stress increases. In addition, the upper chord of the truss does not displace out-of-plane of the truss. Apparently the differential out-of-plane movement of the upper and lower chords is absorbed by the hangers.

Stringer L3L4B and hanger U6L6B experience small increases in stress, 13% and 11%, respectively, as shown in Table 4.24. Tables 33 and 34 present the unit load stresses for Models 3B and 4C. As can be observed, the axial and in-plane moment stresses are not significantly affected by removal of the lower chord member. The out-of-plane moment stresses increase by a factor of two and one-half, but they are secondary stresses with respect to the axial and in-plane moment stresses. The stress redistribution effects have been absorbed by the members closer to the removed lower chord.

Stringer L3L4B and hanger U6L6B are far enough removed from lower chord L3L4A that these stresses are not significantly altered.

The last member discussed by this study is lower chord member L4L5A. As it is listed in Table 4.24 the maximum stress in the member decreases by 11%. Table 4.35 present the stresses resulting from the application of unit loads to the structure. Similar to the previous members, the out-of-plane moment stresses show a significant increase due to the out-of-plane bending affects that result from removal of the lower chord member. The in-plane moment stresses are similar between the two models as would be expected since this member is not a flexural member.

The axial stresses decrease to the greatest extent of the three stresses in the member. This is most noticeable when the load is placed on the northern half of the bridge, panels 1, 2, and 3. When the load is on the southern half of the bridge, the axial s stresses are smaller, but of the same order of magnitude in both models. An examination of the geometry of this member indicates that the forces would not tend to enter the member when the loads are applied at the north end of the bridge. Forces tend to follow smooth flow lines, and the location of the lower chord L4L5A, with respect to the removed member, precludes the member from being significantly stresses.

As the load is applied to the south end of the structure, the member is instrumental in transferring the lower chord forces to the floor system. Hence, the stresses due to this load are

expected to be larger than stresses resulting from loads applied at the northern end of the structure, but smaller than the Model 3B stresses.

In summary, the complete removal of the lower chord member L3L4A results in five general observations. First, the structure experiences a significant out-of-plane displacement. As a result, the lower chord is bent about its outof-plane bending axes, significantly increasing the total member stresses. The axial stresses and the in-plane bending stresses are not affected as significantly as the out-of-plane stresses.

Second, the stringer adjacent to the removed lower chord member carries a large proportion of the axial forces formerly carried by the lower chord. The bending stresses in the stringer are not affected. The floor beam stresses in the out-of-plane direction are also increased as a consequence of the axial stress redistribution from the lower chord to the stringer.

. Third, the upper chord members are not significantly affected by the lower chord removal. There is no out-of-plane displacement from computation for these members, hence out-of-plane stresses are not developed. The in-plane and axial stresses are increased slightly.

Fourth, the counters in the middle panel are not loaded in compression by any load application to the structure. These members are loaded in tension depending on the location of the load on the structure.

Fifth, the stress redistribution effects are limited to a number of members immediately adjacent to the removed lower chord. Streinger L3L4B, hanger U6L6B, and the upper chord members do not experience a significant stress increase. Hence the redistribution is carried by the counters, the floor systems adjacent to the lower chord, and the lower chord members adjacent to the removed member.

4.3.2 Partial Removal of Lower Chord L3L5

Model 4D treats lower chord L3L5A as though half of its cross section has been removed. A comparison of the Model 4D and Model 3B stresses is presented in Table 4.36. Four members, counters L3U4A and L4U3A, lower chord L6L7A, and floor beam L4AB, experience the largest increase in maximum stress. Member U3U4A experiences a 12% decrease in maximum stress. The remaining six members are not significantly affected by the cross section reduction of the lower chord. A discussion of the results is presented below.

The largest stress increase occurs in counter L3U4A as shown in Table 4.36. The stresses change from a tensile stress of 8.62 MPa (1.25 ksi) to a tensile stress of 25.64 MPa (3.72 ksi) approximately a threefold increase. Table 4.37 presents a comparison of unit load stresses between Models 4D and 3B. As can be observed the axial stresses and the in-plane bending stresses are larger in Model 4D for loads applied to the first three panel points. When the load is applied to the next two panel points, the Model 4D axial and out-of-plane bending stresses are lower than the corresponding Model 3B stresses. However, when the load is applied

-68-

to panel point 6, the Model 4D axial stress is eight times higher than the Model 3B axial stress. Note that the out-of=plane bending stresses do not contribute significantly to the increase in member stresses in either model.

Therefore, removal of a portion of the lower chord cross section increases the axial and in-plane bending moment in these members are not affected. Note that this member experiences both compressive and tensile axial stresses in comparison with Model 4C.

The second largest increase in stress occurs in lower chord member L6L7A according to Table 4.36. The tensile stresses approximately double from 18.06 MPa (2.62 ksi) to a tensile stress of 34.61 MPa (5.02 ksi). As presented in Table 4.38, the axial and in-plane bending moment stresses are similar for the two models. However, the out-of-plane bending moment stresses are approximately 12% higher in Model 4D than in Model 3B.

Since the loads are transferred to the truss such that the forces are in the plane of the trusses, the out-of-plane bending stresses are a result of the out-of-plane displacements. An examination of the out-of-plane displacements of panel point 6 is presented below for loads applied at this panel point.

MODEL	DISPLACEMENT
3B	-0.32083×10^{-5}
4D	-0.16269×10^{-2}

The out-of-plane displacement in Model 4D is approximately five

hundred times larger than the corresponding Model 3B displacement.

Hence, reduction of the member cross section in lower chord L3L4A

results in out-of-plane displacements of the lower chord.

The third largest increase in stress occurs in floor beam

L4AB, as shown in Table 4.36. The stresses increase from a compres-

sive stress of 9.86 MPa (1.43 ksi) in Model 3B to a tensile stress

of 14.13 MPa (2.05 ksi) in Model 4D, an increase of approximately

50%. Table 4.39 compares the stresses developed by unit loads

applied to Models 3B and 4D. As can be observed, the axial and

in-plane bending stresses do not experience a significant increase

due to removal of a portion of the lower chord cross section. The

out-of-plane bending stresses increase significantly, with the

maximum calculated stress increasing from a tensile stress of

0.063 MPa (0.0091 ksi) to a compressive stress of 0.108 MPa (0.0157

ksi).

The increase in out-of-plane bending stresses in this

member can be explained by an examination of the geometry of panel

point 4. Due to the reduction in cross-sectional area of lower

chord L3L4, the relative displacement of the member ends increases.

The length increase is resisted by the adjacent lower chords, the

floor beams, and, to a lesser extent, by the hangers. Consequently,

the floor beams are bent about their out-of-plane bending axes by

the additional displacement, i.e. the force in the lower chord is

transferred to the adjacent stringer through the floor beam. Hence,

an increase in the out-of-plane stresses in the floor beam occurs. This is similar to the effect on the floor beam stresses of complete removal of the lower chord discussed previously.

The last significant increase in member stresses observed by this study due to removal of the lower chord occurs in member L4U3A. As shown in Table 4.33, the maximum compressive stresses increase from 10.75 MPa (1.56 ksi) to 12.13 MPa (1.76 ksi), a 13% increase. The stresses due to unit loads presented in Table 4.37 indicate that the axial stresses vary by an average of approximately 15%. The compressive axial stresses in Model 4D are lower than the stresses in Model 3B while the tensile axle stresses in Model 4D are higher. The in-plane bending stresses are similar between the two models except for panel point 4. When the load is placed here, the Model 4D in-plane stresses are more than two times larger than the corresponding Model 3B stresses. The out-of-plane stresses in the member are not significantly affected until the load is placed on the last panel point where the stress in Model 4D is 150 times larger than the Model 3B stress.

The increases in axial and in-plane bending stresses are expected. The axial stress increase is not large and is consistent with the expected reaction of the structure. The in-plane moment stresses are consistent with the expected reaction of the structure and the increase in stress at panel point 4 is consistent with previous results. The larger increase in out-of-plane stresses where the load is applied at panel point 6 is unexpected. Note

-71-

that this member experiences both compressive and tensile stresses as compared with Model 4C.

The remaining members, with the exception of upper chord U3U4A experience minor variations in stress as a consequence of the lower chord modification. The stress changes range from an increase of 3% to a decrease of 8%, as shown in Table 4.36. Tables 4.41 through 4.47 present the stresses developed in these members by application of unit loads to the bridge. As can be seen, the stresses do not change significantly between the two models. Hence, the modification of the lower chord does not affect the stresses in these members.

Upper chord U3U4A experiences a decrease in compressive stress from 29.92 MPa (4.34 ksi) to 26.47 MPa (3.84 ksi), a change of 11%, as shown in Table 4.47. From an examination of Table 4.47 it is evident that the decrease is due to a reduction in axial tension stresses and out-of-plane bending stresses. The in-plane bending stresses are slightly larger in Model 4D than in Model 3B with the exception of panel point 3 where the reverse occurs. Hence, a reduction in the lower chord cross section results in an unloading of upper chord U3U4A.

In summary, four conclusions can be drawn regarding the removal of part of the cross sectional area of the lower chord. First, out-of-plane displacements occur in the floor beams and the lower chord. Second, the stress redistribution occurs in a small number of adjacent members consisting of the lower chord, the

-72-

midspan connectors, and the floor beams. Third, the connector members experience both compressive and tensile stresses. Fourth, the stresses in the upper chord are reduced as a consequence of the cross section reduction.

4.3.3 Comparison and Discussion of Models 3B, 4C, and 4D

Comparison of the stresses in the members of Models 3B, 4C, and 4D results in four observations. First, the modification of the lower chord member induces out-of-plane displacements in the floor beam and lower chord members. As discussed above, this displacement accounts for a large portion of the increased stress in these members.

It is interesting to note the effect on these adjacent members that results from reduction in the lower chord cross section. The out-of-plane displacements for panel point 3 of the three models is presented below.

Model	Panel Point 3 Out-of-Plane Displacement
3B (Full Area)	0.30860×10^{-5}
4C (Zero Area)	-0.4086×10^{-2}
4D (Half Area)	-0.11342×10^{-3}

This displacement generated by Model 3B is negligible. The displacements induced by Models 4C and 4D differ by an order of magnitude. Hence, the relationship between the reduction in cross-sectional area and the resulting stresses is not linearly

proportional as is expected. In addition, when any portion of the lower chord cross section is effective, the integrity of the structure remains. Hence, the effects of out-of-plane displacements are of secondary importance. An examination of Table 4.36 indicates this tendency. Comparing the Model 3B and 4D stresses for lower chord L3L4B, an increase in stress of 1% between the two models is noted.

Complete removal of the lower chord cross section results in the out-of-plane displacements accounting for a significant portion of the total stress in the member. An examination of Table 4.24 indicates this tendency. Comparing the Model 3B and 4C stresses for lower chord L7L7A, an increase in stress of two and one-half times is noted.

The floor beams are affected by the modification to the lower chord member as well. The out-of-plane stresses in floor beam L4AB are larger in Model 4C than in Model 4D as can be observed by comparing Tables 4.24 and 4.36. As discussed above the difference in stress is due to an increase in out-of-plane stresses. Similar to the lower chord stresses, the presence of the lower chord member to any degree results in lower out-of-plane stresses in the floor beam than occurs when the member is completely removed.

In conclusion, by examining the lower chord and the floor beam in Models 3B, 4C and 4D, complete removal of the member results in a significant change in the load carrying characteristics

of the structure. Partial removal of the effective cross section does not cause a significant change in the response of the structure to loads.

The second observation, as a result of the comparison of the three models, concerns the size of the area of stress redistribution. Model 4D was a significantly smaller number of affected members than does Model 4C. This result is expected due to the differences in severity of the modifications described by the two models. However, neither model predicts the effects of the member's modification to extend beyond one or two panels adjacent to the modified member. This agrees with the findings of Models 4A and 4B presented earlier. As is expected, the Model 4D stress redistribution affects a smaller number of members than the Model 4C stress redistribution.

The third observation concerns the midspan connecters. In Model 3B, the member forces alternate between compression and tension depending on the location of the load on the bridge. In Model 4C, the members experience only tensile forces and in Model 4D, they experience compressive forces (smaller than the forces in Model 3B) and tensile forces.

The final observation concerns the upper chord members. Modification of the lower chord does not increase the stresses in the upper chord. For Model 4D the stresses are lower in the upper chord than those in Model 3B. The upper chord stresses in Model 4C are similar to the Model 3B stresses.

5. EFFECTS ON FATIGUE LIFE DUE TO MEMBER MODIFICATION

5.1 Introduction

As shown in Chapter 4, modification of a member in the truss results in stress redistribution to the adjacent members. In the majority of cases, the total stresses are lower than the yield stresses, including the live load stress increases. However, the effect on the fatigue life of the member can be significantly affected. This section of the study is intended to present a qualitative discussion of the effects of the increased member stresses on the fatigue life of the structure.

The study presents the equivalent Miner's stress range for the measured stresses for hanger U6L6A and stringer L5L6A. The increase in stress in these members due to the failure of the hanger is determined and the effect on the fatigue life is qualitatively determined. For purposes of this section of the study, failure of a member occcurs when the effective cross section is one-half of the full cross section.

5.2 Equivalent Stress Range and Fatigue Consideration

From Measured Stress

The equivalent stress range in hanger U6L6A and stringer L5L6A is determined using the measured field stresses and the

stress range-cycle life (S-N) curves in the American Institute of Steel Construction Bridge Fatigue Guide. To use the S-N curves, evaluation of the type of detail used at the point of interest has to be determined. Six categories of details are possible, A through E', and are described in American Institute of Steel Construction Bridge Fatigue Guide. Category A is the best category for fatigue resistance, i.e. largest life before fracture occurs, and Category E' is the worst category. The members examined by this study are riveted, built-up members. approximately seventy years old. In research conducted at Fritz Engineering Laboratory, riveted connections can be included in either Category C or Category D if the members are subjected to zero-to-tension or partial tension-to-tension load cycles. Category D applies if the rivets have "severely reduced levels of clamping force".[14] Since the structure under investigation is seventy years old, the clamping force of the rivets most likely have been reduced, and Category D is applicable.

Using a computer program developed at Fritz Engineering Laboratory, Lehigh University, the field measured stresses from the regularly scheduled train traffic were used to develop histograms of selected members. The histograms are included as Figs. 5.1 and 5.2 for gages C1 (stringer L5L6A) and C4 (hanger U6L6A). The resulting Miner's Stress Range is presented below:

Gage	Miner's Stress Range
C1	24.27 MPa (3.52 ksi)
C4	17.31 MPa (2.51 ksi)

Using the S-N curve presented in Fig. 5.3 and a category D detail classification, the estimated fatigue life of each member is presented below.

Gage	Life (cycles)
C1 (stringer)	Infinite*
C4 (hanger)	$/x\ 10^9$

*Maximum stress is below the threshold value.

The number of cycles predicted by the study using the S-N curves is extremely large. Hence, the stress ranges that the structure is subjected to will not produce fatigue cracking.

5.3 Effect of Reduction in Hanger Cross Section

From the discussion presented above it is obvious that hanger L7L6A, the most stressed member, is unlikely to develop fatigue cracks. However, if the hanger cross section were to be reduced by one-half, the study has qualitatively examined the effort on the adjacent members.

As presented in Chapter 4, the member that is affected to the largest extent is lower chord L5L6A due to a reduction in hanger cross section. The maximum stresses increase from 18.06 MPa

(2.62 ksi) to 33.58 MPa (4.87 ksi), an increase of approximately
1.75. Therefore, the fatigue life is expected to be affected.
In this instance, however, the increased live load stress is below
the threshold stress for fatigue crack growth (see Fig. 5.3) for
Category D details. No fatigue crack would be expected.

In conclusion, it is evident that the fatigue life is not
a critical parameter to the service of the structure. If the
fatigue life of the member with the highest stress is not affected
by reduction of area of hanger U6L6A. Then the fatigue life of the
remaining members is not a governing factor at all.

5.4 Conclusion

The study has examined the effect of reducing the effective
cross section of hanger U6L6A by one-half on stringer L6AB and other
members. Two assumptions are inherent in this discussion. First,
it is assumed that the stress ranges and Miner's stress percentage
increase is the same as the live load stress percentage increase.
Second, the study assumes that the percent increase in model stress
due to modification of a member is the same as the percent increase
in the stresses in the actual structure.

The results indicate that the fatigue life of the examined
members is not a critical parameter to the service of the structure.
Reducing the cross-sectional area of hanger U6L6A increases the
stress in lower chord L5L6A by a factor of 1.75. Hence, this
member has the largest stress increase in the bridge and

and consequently, the largest stress range. The study concludes
that since the fatigue life of this member is not affected by the
hanger modification then the structure does not have a fatigue
problem.

6. CONCLUSION AND RECOMMENDATIONS

6.1 Conclusion

The results of the study can be summarized in three general areas; modeling techniques, stress redistribution, and fatigue response.

The results of the investigation of the modeling techniques indicate that the space frame model provides the best approximation of the field measured stresses. The plane truss and plane frame truss models do not take into account the effect of the moments induced in the truss members by the forces carried in the floor system. Hence, these models underestimate the total stresses in some members. It is interesting to note that the moments in the plane frame truss are minor and the total stresses in the plane frame truss model are similar to the plane truss model. The results indicate that the best model to use to approximate the actual stresses is the space frame model.

The stress redistribution portion of the study is based on modification of two members. In the first instance, hanger U6L6A was modified to reflect a member with half of the cross section no longer effective and a member completely fractured. The results are summarized below:

1. The modification to the hanger results in the lower

    chord acting as a flexural member;

2. Total removal of the member results in a decrease

    in the floor beam stresses and an increase in the

    maximum stress in the stringer;

3. Partial reduction of the effective cross section

    results in minor changes in the floor system

    stresses;

4. The axial stress in the truss members bracing connected

    to the hanger increases due to hanger modification.

5. The upper chord stresses are not significantly

    affected.

In the second instance, the lower chord member L3L4 was
modified to reflect a member with half of its cross section no
longer effective and a member completely fractured. The results
are summarized below:

1. Modification to the lower chord results in out-of-

    plane displacements that bend the lower chord members

    about their minor axes;

2. The adjacent stringers to carry a large portion of

    the axial loads formerly carried by the lower chord;

3. The transfer of loads from the lower chord to the

    stringer result in bending of the floor beam along

    its weak axis of bending;

4. The upper chords are marginally affected by the member modification.

The final conclusions to be drawn concerning the stress redistribution characteristics of the structure are presented below:

1. The extent of stress redistribution is a localized characteristic. In most instances examined, the effect of a member modification was not noticeable in members more than two panels away from the modified member;

2. The modification of a member does not ensure an increase in stress in the adjacent members. The resulting decrease in the stiffness of the structure causes a reduction in stress in some members;

3. There are significant changes in the load carrying characteristics of the structure as a result of complete removal of a member in the structure. As far as a damaged member remains functional, the structure will tend to act as it was designed. However, once the member is totally removed, the loss of symmetry results in displacements that change the stress patterns.

The last area examined by the study discusses the effects that member modification has on the fatigue resistance of the structure. As would be expected, the increase in adjacent member stresses due to modification of a member results in decreased fatigue life of the members.

6.2 Recommendations for Further Studies

6.2.1 Field Data

The study utilized field data obtained from the Atbara Bridge. As presented earlier, the study concluded that the data for hanger U6L6A did not agree well with computed values. In addition the data collected for the truss members of the bridge was limited. Hence, the following is recommended:

1. Additional data is recommended to be obtained for the hanger in question. The data should include member sizes and a new field measurement of the stresses;

2. Additional field measured stresses of the other truss members are recommended to be obtained. The additional data recommended above can be used to confirm the analytical model that best approximates the measured stresses.

6.2.2 Analytical Consideration

There are several areas that can be addressed in future studies. These are presented below:

1. This study did not include the dead weight of the structure in the analytical model. It has been assumed that the dead weight does not affect the modeling of the structure subjected to live load stresses. However, for future work the dead load should be included, especially if compression effects are to be studied.

2. The study has assumed a perfectly elastic response of the structure. There is no yielding of the structure due to increased stresses resulting from member modification. This is not a realistic consideration. With inclusion of the dead load, some of the members adjacent to the modified member could yield. Therefore, the stress redistribution characteristics of the structure would be changed from those presented above. Hence, for future investigations the study recommends that the members be checked for yielding and the member properties be modified subsequently. It is expected that this would result in an increase in the zone of stress redistribution to a small extent;

3. No dynamic effects were included in this study. The field data did not show strong effects of impact due to an increase in speed of the test locomotives. It would be of interest to obtain additional data for high speed test train excursions and to compare their effects between the analytical model and the actual structure.

4. Only minor consideration was given to the stresses in the top chord members. The study suggests that additional field data be obtained to compare the stresses in the top chord with the analytical model. In addition, the maximum possible stress in the top chords is recommended to be investigated.

TABLE 1.1 PROPERTIES AND COMPOSITION OF STEEL

ATBARA BRIDGE

PROPERTIES

Yield Stress	253.74 MPa (36.8 ksi)
Ultimate Stress	435,07 MPa (63.1 ksi)
Strain at Fracture	35.0%
Brinell Hardness No.	73

Charpy V-Notch Temperature

@ 15° ft-lbs

Dynamic	-8.6^{o} C (16.5^{o} F)
Static	-61.8^{o} C (-143.3^{o}F)

CHEMICAL COMPOSITION

	Percentage
Carbon	0.17
Manganese	0.62
Phosphorous	0.045
Silicon	0.01
Sulfur	0.058
Copper	0.021

TABLE 2.1 GAGE LOCATIONS

Gage No.	Location
C1	Bottom center, east stringer Panel L5L6
C2	Top center, east lower chord Panel L5L6
C3	South end east, top stringer Panel L5L6
C4	East Vertical L6 – West Face
C5	East Vertical L6 – East Face
C6	South end west, top stringer Panel L5L6
C7	West Side Top L6 Floor Beam
C8	West Vertical L6 – East Face
C9	West Vertical L6 – West Face
C10R	Top Cantilever L6
C10W	South end of west lower chord Panel L5L6
C11	Floor Beam L6 Center
C12	Top Center of East Lower Chord Panel L4L5
C13	Bottom Center of East Stringer Panel L4L5
C14	Assumed to be center, west stringer Panel L4L5
C15	West Roadway Stringer
C16	Track at Center of Panel L4L5
C17	Location Unknown on Lower Chord

TABLE 2.2 MAXIMUM FIELD MEASURED STRESSES

FROM TEST TRAINS

Gage No.	Maximum Measured Stress MPA (ksi)	General Location
C1	-44.33 (-6.43)	Stringer
C2	N.A.	Lower Chord
C3	33.23 (4.82)	Stringer
C4	-40.61 (-5.89)	Hanger
C5	-20.34 (-2.95)	Hanger
C6	-12.93 (-1.875)	Stringer
C7	N.A.	Floor Beam
C8	-51.71 (-7.50)	Hanger
C9	N.A.	Hanger
C10W	N.A.	Lower Chord
C10R	N.A.	Top Cantilever
C11	-35.10 (-5.09)	Floor Beam
C12	N.A.	Lower Chord
C13	-46.20 (-6.70)	Stringer
C14	-42.47 (-6.16)	Stringer
C15	N.A.	Roadway Stringer
C16	N.A.	Track
C17	N.A.	Lower Chord

TABLE 2.3 MEASURED STRESS CYCLES

Average Measured Stress Cycle Per Passage of Test Train

MPa (ksi)

Gage	North	South
C1	0	0
	5.52 (0.80)	5.52 (0.80)
	-42.50 (-6.16)	-42.50 (-6.16)
	5.52 (0.80)	
	-36.98 (-5.36)	5.52 (0.80)
	- 7.38 (-1.07)	-33.26 (-4.82)
	-36.98 (-5.36)	-5.52 (-0.80)
	5.52 (0.80)	-35.12 (-5.09)
	-44.37 (-6.43)	7.38 (1.07)
	7.38 (1.07)	-36.98 (-5.36)
	0	7.38 (1.07)
		0

TABLE 2.3 MEASURED STRESS CYCLE (continued)

Average Measured Stress Cycle Per Passage of Test Train

MPa (ksi)

Gage	North	South
C3	0	0
	-31.39 (-4.55)	-33.26 (-4.82)
	-16.56 (-2.41)	- 3.73 (-0.54)
	-24.01 (-3.48)	-33.26 (-4.82)
	- 3.73 (-0.54)	- 9.25 (-1.34)
	-29.60 (-4.29)	-29.60 (-4.29)
	- 9.25 (-1.34)	- 3.72 (-0.54)
	-27.54 (-4.02)	-29.60 (-4.29)
	0	0
	-31.39 (-4.55)	
	0	

TABLE 2.3 MEASURED STRESS CYCLE (continued)

Average Measured Stress Cycle Per Passage of Test Train

MPa (ksi)

Gage	North	South
C4	0	--
	-40.64 (-5.89)	--
	-24.01 (-3.48)	--
	-36.98 (-5.63)	--
	-18.49 (-2.68)	--
	-31.39 (-4.55)	--
	9.25 (1.34)	--
	0	
C5	0	0
	-12.97 (-1.88)	--
	-11.11 (-1.61)	--
	-18.49 (-2.68)	--
	-14.77 (-2.14)	--
	-20.35 (-2.95)	--
	0	

TABLE 2.3 MEASURED STRESS CYCLE (continued)

Average Measured Stress Cycle Per Passage of Test Train

MPa (ksi)

Gage	North	South
C6	0	0
	-11.11 (-1.61)	7.38 (1.07)
	7.38 (1.07)	-14.77 (-2.14)
	-12.94 (-1.875)	18.49 (2.68)
	0	-14.77 (-2.14)
	7.38 (-1.07)	9.25 (1.34)
	5.52 (0.80)	- 7.38 (-1.07)
	-12.94 (-1.875)	18.49 (2.68)
	7.38 (1.07)	-11.11 (-1.61)
	-12.94 (-1.875)	0
	7.38 (1.07)	
	0	
C8	0	--
	-42.50 (-6.16)	--
	-29.60 (-4.29)	--
	-51.75 (-7.50)	--
	-31.39 (-4.55)	--
	-48.02 (-6.96)	--
	0	

TABLE 2.3 MEASURED STRESS CYCLE (continued)

Average Measured Stress Cycle Per Passage of Test Train

MPa (ksi)

Gage	North	South
C11	0	0
	-31.46 (-4.56)	-33.26 (-4.82)
	-16.56 (-2.41)	-20.35 (-2.95)
	-29.60 (-4.29)	-35.12 (-5.09)
	-27.54 (-4.02)	-18.49 (-2.68)
	-35.12 (-5.09)	-31.46 (-4.56)
	-18.49 (-2.68)	0
	-33.26 (-4.82)	
	0	
C13	0	0
	7.38 (1.07)	7.38 (1.07)
	-38.82 (-5.63)	-46.23 (-6.70)
	7.38 (1.07)	5.52 (0.80)
	-38.82 (-5.63)	-35.12 (-5.09)
	-11.10 (-1.61)	-11.11 (-1.61)
	-36.82 (-5.36)	-36.98 (-5.63)
	5.52 (0.80)	7.38 (1.07)
	-46.20 (-6.70)	-40.64 (-5.89)
	5.52 (0.80)	7.38 (1.07)
	0	0

TABLE 2.3 MEASURED STRESS CYCLE (continued)

Average Measured Stress Cycle Per Passage of Test Train

MPa (ksi)

Gage	North	South
C14	0	0
	-36.98 (-5.63)	-40.64 (-5.89)
	-33.26 (-4.82)	-33.26 (-4.82)
	-42.50 (-6.16)	-40.64 (-5.89)
	0	0

TABLE 3.1 MEMBER PROPERTIES

Member	Area cm^2 ($in.^2$)	In-Plane Moment of Inertia cm^4 ($in.^4$)	Out-of-Plane Moment of Inertia cm^4 ($in.^4$)	Length m (ft-in)
$L_0 L_1$	167 (25.92)	30,888 (742)	66,231 (1591)	6.40 (21'-0")
$L_1 L_2$	167 (25.92)	30,888 (742)	66,231 (1591)	6.40 (21'-0")
$L_2 L_3$	272 (42.17)	40,421 (971)	108,317 (2602)	6.40 (21'-0")
$L_3 L_4$	335 (51.92)	43,293 (1040)	136,874 (3288)	6.40 (21'-0")
$L_4 L_5$	272 (42.17)	40,421 (971)	108,317 (2602)	6.40 (21'-0")
$L_5 L_6$	161 (24.92)	30,888 (742)	66,231 (1591)	6.40 (21'-0")
$L_6 L_7$	161 (24.92)	30,888 (742)	66,231 (1591)	6.40 (21'-0")
$U_1 U_2$	247 (38.25)	74,473 (1789)	102,530 (2463)	6.41 (21'-5/16")
$U_2 U_3$	284 (44.09)	78,053 (1875)	137,373 (3300)	6.41 (21'-5/16")
$U_3 U_4$	284 (44.09)	78,053 (1875)	137,373 (3300)	6.41 (21'-5/16")
$U_4 U_5$	284 (44.09)	78,053 (1875)	137,373 (3300)	6.41 (21'-5/16")
$U_5 U_6$	247 (38.25)	74,443 (1789)	102,530 (2463)	6.41 (21'-5/16")

LOWER CHORD

UPPER CHORD

TABLE 3.1 MEMBER PROPERTIES (continued)

Member	Area cm^2 (in.^{2})	In-Plane Moment of Inertia cm^4 (in.^{4})	Out-of-Plane Moment of Inertia cm^4 (in.^{4})	Length m (ft-in)
$-U_1 L_1$	91 (14.08)	14,570 (350)	703 (16.9)	7.92 (26'-0")
$-U_1 L_2$	148 (22.88)	20,273 (487)	987 (23.70)	10.19 (33'-5-5/32")
$-U_2 L_2$	130 (20.20)	16,443 (395)	828 (19.90)	7.92 (26'-0")
$U_2 L_3$	91 (14.08)	14,570 (350)	703 (16.9)	10.19 (33'-5-5/32")
$-U_3 L_3$	105 (16.32)	15,069 (362)	720 (17.3)	7.92 (26'-0")
$U_3 L_4$	86 (13.32)	14,237 (342)	700 (16.81)	10.19 (33'-5-5/32")
$U_4 L_3$	86 (13.32)	14,237 (342)	700 (16.81)	10.19 (33'-5-5/32")
$-U_4 L_4$	105 (16.32)	15,069 (362)	720 (17.3)	7.92 (26'-0")
$U_5 L_4$	91 (14.08)	14,570 (350)	703 (16.9)	10.19 (33'-5-5/32")
$-U_5 L_5$	130 (20.20)	16,443 (395)	828 (19.90)	7.92 (26'-0")
$U_6 L_5$	148 (22.88)	20,273 (487)	1428 (34.3)	10.19 (33'-5-5/32")
$-U_6 L_6$	91 (14.08)	14,570 (350)	703 (16.9)	7.93 (26'-0")

BRACING AND HANGERS

TABLE 3.1 MEMBER PROPERTIES (continued)

	Member	Area cm^2 (in.^{2})	In-Plane Moment of Inertia cm^4 (in.^{4})	Out-of-Plane Moment of Inertia cm^4 (in.^{4})	Length m (ft-in)
PORTALS	$U_1 L_0$	358 (55.5)	65,481 (1573)	50,287 (1208)	10.19 (33'-5-5/32")
	$U_6 L_7$	358 (55.5)	65,481 (1573)	50,287 (1208)	10.19 (33'-5-5/32")
FLOOR SYSTEM	Floor Beams	348 (54)	758,218 (18,216)	9,699 (233)	6.40 (252")
	Stringers	171 (26.48)	150,736 (3641)	1,623 (39)	6.40 (252")

TABLE 3.2 COMPARISON OF PIN TRUSS MODEL STRESSES

WITH MEASURED STRESSES - HANGER $L_6 U_6$

Pin and Roller Boundary Conditions

Gage	Measured Stresses MPa (ksi)	Model Stresses MPa (ksi)
C4	0	0
	-40.64 (-5.98)	-22.01 (-3.19)
	-24.01 (-3.48)	-12.07 (-1.75)
	-36.98 (-5.63)	-22.08 (-3.20)
	-18.49 (-2.68)	-16.70 (-2.42)
	-31.39 (-4.55)	-22.08 (-3.20)
	9.25 (1.34)	-12.07 (-1.75)
	0	-22.15 (-3.21)*
	0	0
C5	0	0
	-12.97 (-1.88)	-22.01 (-3.19)
	-11.11 (-1.61)	-12.07 (-1.75)
	-18.49 (-2.68)	-22.08 (-3.00)
	-14.77 (-2.14)	-16.70 (-2.42)
	-20.35 (-2.95)	-22.08 (-3.20)
	0	-12.07 (-1.75)
		-22.15 (-3.21)*
		0

TABLE 3.2 COMPARISON OF PIN TRUSS MODEL STRESSES

WITH MEASURED STRESSES - HANGER L_6 U_6

Pin and Roller Boundary Conditions

Gage	Measured Stresses MPa (ksi)	Model Stresses MPa (ksi)
C8	0	0
	-42.47 (-6.16)	-22.01 (-3.19)*
	-29.58 (-4.29)	-12.07 (-1.75)
	-51.71 (-7.50)**	-22.08 (-3.20)
	-31.37 (-4.55)	-16.70 (-2.42)**
	-47.90 (-6.96)	-22.08 (-3.20)
	0	-12.07 (-1.75)
		-22.15 (-3.21)*
		0

*Maximum Model Stress
**Measured Stress

TABLE 3.3 COMPARISON OF PIN TRUSS MODEL STRESSES

WITH MEASURED STRESSES – HANGER $L_6 U_6$

Pin and Pin Boundary Conditions

Gage	Measured Stresses MPa (ksi)	Model Stresses MPa (ksi)
C4	0	0
	-40.7 (-5.89)	-22.0 (-3.19)
	-24.0 (-3.48)	-12.07 (-1.75)
	-38.6 (-5.63)	-22.06 (-3.20)
	-18.6 (-2.68)	-16.69 (-2.42)
	-31.7 (-4.55)	-22.06 (-3.20)
	+9.0 (1.34)	-12.07 (-1.75)
	0	-22.13 (-3.21)*
		0
C5	0	0
	-13.0 (-1.88)	-22.00 (-3.19)
	-11.1 (-1.61)	-12.07 (-1.75)
	-18.5 (-2.68)	-22.06 (-3.20)
	-14.5 (-2.14)	-16.69 (-2.42)
	-20.3 (-2.95)	-22.06 (-3.20)
	0	-12.07 (-1.75)
		-22.13 (-3.21)
		0

*Maximum Model Stress
**Maximum Field Measured Stress

TABLE 3.3 COMPARISON OF PIN TRUSS MODEL STRESSES (continued)

WITH MEASURED STRESSES - HANGER $L_6 U_6$

Pin and Pin Boundary Conditions

Gage	Measured Stresses MPa (ksi)	Model Stresses MPa (ksi)
C8	0	0
	-42.5 (-6.16)	-22.00 (-3.19)
	-29.6 (-4.29)	-12.07 (-1.75)
	-51.7 (-7.50)**	-22.06 (-3.20)
	-31.4 (-4.55)	-16.68 (-2.42)
	-47.9 (-6.95)	-22.06 (-3.20)*
	0	-12.07 (-1.75)**
		-22.13 (-3.21)
		0

TABLE 3.4   FLOOR BEAM AND STRINGER PIN TRUSS

MODEL AND FIELD STRESSES

Member	Maximum Model Stress MPa (ksi)	Maximum Field Stress MPa (ksi)
Stringer	65.09 (9.44)	44.3 (6.43)
Floor Beam	30.13 (4.37)	35.1 (5.09)

TABLE 3.5 COMPARISON OF PLANE FRAME TRUSS MODEL STRESSES

WITH MEASURED STRESSES - HANGER L_6 U_6

Pin and Roller Boundary Conditions

Gage	Measured Stresses MPa (ksi)	Model Stresses MPa (ksi)
C4	0	0
	-40.7 (-5.89)	-24.41 (-3.56)
	-24.0 (-3.48)	-15.10 (-2.19)
	-38.8 (-5.63)	-24.62 (-3.57)*
	-18.5 (-2.68)	-18.96 (-2.75)
	-31.4 (-4.55)	-23.51 (-3.41)
	9.2 (1.34)	-13.38 (-1.96)
	0	-21.99 (-3.19)
		0
C5	0	0
	-12.9 (-1.88)	3.24 (0.47)
	-11.1 (-1.61)	-18.82 (-2.73)
	-18.5 (-2.68)	- 8.55 (-1.24)
	-14.8 (-2.14)	-19.10 (-2.77)
	-20.3 (-2.95)	-13.99 (-2.03)
	0	-20.13 (-2.92)
		-10.41 (-1.51)
		-21.65 (-3.14)
		0

*Maximum Model Stress

**Maximum Field Measured Stress

-104-

TABLE 3.5 COMPARISON OF PLANE FRAME TRUSS MODEL STRESSES (continued)

WITH MEASURED STRESSES − HANGER $L_6 U_6$

Pin and Roller Boundary Conditions

Gage	Measured Stresses MPa (ksi)	Model Stresses MPa (ksi)
C8	0	0
	−42.5 (−6.16)	−24.41 (−3.56)
	−29.0 (−4.29)	−15.10 (−2.19)
	−51.7 (−7.50)**	−24.62 (−3.57)*
	−31.4 (−4.55)	−18.76 (−2.75)
	−47.9 (−6.96)	−23.51 (−3.41)
	0	−13.38 (−1.96)
		−22.00 (−3.19)
		0

---

* Maximum Model Stress

** Maximum Field Measured Stress

TABLE 3.6 COMPARISON OF PLANE FRAME TRUSS MODEL STRESSES

WITH MEASURED STRESSES - HANGER $L_6 U_6$

Pin and Pin Boundary Conditions

Gage	Measured Stress MPa (ksi)	Model Stress MPa (ksi)
C4	0	0
	-40.6 (-5.89)	-25.03 (-3.63)*
	-24.0 (-3.48)	-15.38 (-2.23)
	-38.8 (-5.63)	-24.82 (-3.60)
	-18.5 (-2.68)	-19.10 (-2.77)
	-31.4 (-4.55)	-23.58 (-3.42)
	9.2 (1.34)	-13.58 (-1.97)
	0	-22.06 (-3.20)
		0
C5	0	0
	-13.0 (-1.88)	3.31 (0.48)
	-11.1 (-1.61)	-18.75 (-2.72)
	-18.5 (-2.68)	- 8.48 (-1.23)
	-14.8 (-2.14)	-19.03 (-2.76)
	-20.3 (-2.95)	-13.93 (-2.02)
	0	-20.06 (-2.91)
		-10.34 (-1.50)
		-21.58 (-3.13)
		0

*Maximum Model Stress

**Maximum Measured Stress

TABLE 3.6 COMPARISON OF PLANE FRAME TRUSS MODEL STRESSES (continued)

WITH MEASURED STRESSES – HANGER $L_6 U_6$

Pin and Pin Boundary Conditions

Gage	Measured Stress MPa (ksi)	Model Stress MPa (ksi)
C8	0	0
	-42.5 (-6.16)	-23.65 (-3.63)*
	-29.6 (-4.29)	-15.38 (-2.23)
	-51.7 (-7.50)**	-24.82 (-3.60)
	-31.4 (-4.55)	-19.10 (-2.77)
	-47.9 (-6.96)	-23.58 (-3.42)
	0	-13.58 (-1.97)
		-22.06 (-3.20)

---

*Maximum Model Stress

**Maximum Measured Stress

TABLE 3.7 COMPARISON OF MAXIMUM SPACE FRAME MODEL STRESSES

WITH MEASURED STRESSES - HANGER $L_6 U_6$

Case	Description	Maximum Model Hanger Stress MPa (ksi)	Maximum Measured Hanger Stress MPa (ksi)
3A	All members continuous. Boundary condition pin/pin	29.17 (4.23) tension	51.7 (7.5) tension
3B	All members continuous. Boundary condition pin/pin	31.58 (4.58) tension	51.7 (7.5) tension
3C	Outrigger bracket stringer pinned. All other members continuous. Boundary condition pin/pin	31.58 (4.58) tension	51.7 (7.5) tension
3D	Outrigger bracket stringer pinned. All other members continuous. Boundary condition pin/roller	31.23 (4.53) tension	51.7 (7.5) tension
3E	Floor beams, stringer, outrigger bracket stringer pinned. All other members continuous. Boundary condition pin/pin	23.51 (3.41) tension	51.7 (7.5) tension
3F	Floor beams pinned. All other members continuous. Boundary condition pin/pin	25.30 (3.67) tension	51.7 (7.5) tension

TABLE 3.8 COMPARISON OF MAXIMUM SPACE FRAME MODEL

STRESSES WITH MEASURED STRESSES - FLOOR BEAM L_6

Case	Description	Maximum Model Floor Beam Stress MPa (ksi)	Maximum Measured Floor Beam Stress MPa (ksi)
3A	All members continuous. Boundary Condition Pin/Pin	24.55 (3.56) tension	35.2 (5.09) tension
3B	All members continuous. Boundary Condition Pin/Roller	38.96 (5.65) tension	35.2 (5.09) tension
3C	Outrigger Bracket stringer pinned. All other members continuous. Boundary Condition Pin/Pin	26.82 (3.89) tension	35.2 (5.09) tension
3D	Outrigger Bracket stringer pinned. All other members continuous. Boundary Condition Pin/Pin	39.09 (5.67) tension	35.2 (5.09) tension
3E	Floor beams, stringer, outrigger bracket stringer pinned. All other members continuous. Boundary Condition Pin/Pin	26.48 (3.86) tension	35.2 (5.09) tension
3F	Floor beams pinned. All other members continuous. Boundary Condition Pin/Pin	25.44 (3.69) tension	35.2 (5.09) tension

TABLE 3.9   COMPARISON OF MAXIMUM SPACE FRAME MODEL

STRESSES WITH MEASURED STRESSES - STRINGER L5 L6

Case	Description	Maximum Model Stringer Stress MPa (ksi)	Maximum Measured Floor Beam Stress MPa (ksi)
3A	All members continuous. Boundary condition. pin/pin	41.99 (6.09) tension	44.33 (6.43) tension
3B	All members continuous. Boundary condition pin/pin.	4 .99 (6.38) tension	44.33 (6.43) tension
3C	Outrigger bracket stringer pinned All other members continuous. Boundary Condition pin/pin	41.85 (6.07) tension	44.33 (6.43) tension
3D	Outrigger bracket stringer pinned. All other members continuous.	43.99 (6.38) tension	44.33 (6.43) tension
3E	Floor beam, stringer outrigger bracket stringer pinned. All other members continuous. Boundary condition pin/pin	65.71 (9.53) tension	44.33 (6.43) tension
3F	Floor beams pinned. All other members continuous. Boundary condition pin/pin	42.06 (6.10) tension	44.33 (6.13) tension

TABLE 3.10 COMPARISON OF MAXIMUM MODEL AND FIELD MEASURED STRESSES

Member	Pin Truss Max. Stress MPA (ksi)	Plane Frame Truss Max. Stress MPa (ksi)	Space Frame and Maximum Stress						Field Measured Max. Stress MPa (ksi)
			Case 3A MPa (ksi)	Case 3B	Case 3C	Case 3D	Case 3E	Case 3F	
Hanger*	22.13/22.13 (3.21/3.21)	24.62/25.03 (3.57/3.63)	29.17 (4.23)	31.58 (4.58)	31.58 (4.58)	31.23 (4.53)	23.51 (3.41)	25.3 (3.67)	51.71 (7.50)
Floor Beam	30.13 (4.37)	30.13 (4.37)	24.55 (3.56)	38.96 (5.65)	26.82 (3.89)	39.09 (5.67)	26.61 (3.86)	25.44 (3.69)	35.10 (5.09)
Stringer	65.09 (9.44)	65.09 (9.44)	41.99 (6.09)	43.99 (6.38)	41.85 (6.07)	43.99 (6.38)	65.71 (9.53)	42.06 (6.10)	44.33 (6.43)

---

*Pin/Roller/Pin/Pin

TABLE 4.1 MEMBERS OF INTEREST

MODELS 4A AND 4B

MEMBER

Hanger U1L1B

Floor Beam L6AB

Hanger L6U6A

Lower Chord L6L7A

Stringer L6L7A

Top Bracing U1BU2A

Top Bracing U5AU6B

Stringer L6L7B

Portal Beam U6L7A

Truss Diagonal L5L6A

TABLE 4.2   COMPARISON OF MODEL 3B AND MODEL 4A

MAXIMUM MEMBER STRESSES

Member	Model 3B MPa (ksi)	Model 4A MPa (ksi)	Ratio
Hanger U1L1B	-31.30 (-4.56)	-31.72 (-4.60)	1.01
Floor Beam L6AB	-41.78 (-6.06)	-38.41 (-5.57)	0.92
Hanger L6U6A	-31.44 (-4.56)		
Hanger L6U6B	-31.44 (-4.56)	-73.85 (-10.71)	2.35
Lower Chord L6L7A	-16.69 (-2.62)	-94.08 (-14.08)	5.37
Stringer L7L7A	-41.92 (-6.08)	-45.99 (-6.67)	1.10
Top Bracing U1BU2A	15.44 (2.24)	+15.03 (+2.18)	+0.97
Top Bracing U5AU6B	15.44 (2.24)	+17.72 (+2.57)	+1.15
Stringer L6L7B	-41.92 (-6.08)	-42.06 (-6.10)	1.00
Portal Beam U6L7A	17.24 (2.50)	-47.44 (-6.88)	+2.75
Truss Diagonal L5U6A	-26.35 (-3.82)	-47.44 (-6.88)	1.80

Notes:
1. Negative sign implies tension and positive sign implies compression.

2. Stresses are due to two 99 ton diesel locomotives crossing structure.

TABLE 4.3   COMPARISON OF UNIT LOAD INFLUENCE LINE STRESSES

BETWEEN MODEL 3B AND MODEL 4A - HANGER U1L1B

Panel Point	Axial Stress		In-Plane Bending Stresses		Out-of-Plane Bending Stresses	
X Coordinate	Model 3B	Model 4A	Model 3B	Model 4A	Model 3B	Model 4A
0 (0)	0	0	0	0	0	0
252 (1)	− 0.0642	− 0.0660	− 0.0179	− 0.0182	− 0.0005	− 0.0044
504 (2)	− 0.0037	− 0.0025	− 0.0020	− 0.0019	− 0.0049	− 0.0050
756 (3)	0.0012	0.0009	− 0.0005	− 0.0007	− 0.0030	− 0.0030
1008 (4)	0.0002	0.0002	− 0.0006	− 0.0007	− 0.0023	− 0.0023
1260 (5)	0.0003	0.0002	− 0.0004	− 0.0005	− 0.0015	− 0.0015
1512 (6)	0.0001	0.0001	− 0.0002	0.0006	− 0.0007	− 0.0007
1764 (7)	0	0	0	0	0	0

TABLE 4.4   COMPARISON OF UNIT LOAD INFLUENCE LINE STRESSES

BETWEEN MODEL 3B AND MODEL 4A - TOP BRACING U1BU2A

Panel Point	Axial Stress		In-Plane Bending Stresses		Out-of-Plane Bending Stresses	
X Coordinate	Model 3B	Model 4A	Model 3B	Model 4A	Model 3B	Model 4A
0 (0)	0	0	0	0	0	0
232 (1)	0.0083	0.0080	0	0.0001	0.0002	0.0002
504 (2)	0.0156	0.0152	0.0002	0.0002	0.0024	0.0025
756 (3)	0.0127	0.0123	0.0002	0.0002	0.0014	0.0014
1008 (4)	0.0094	0.0091	0.0001	0.0001	0.0026	0.0007
1260 (5)	0.0063	0.0041	0.0001	0.0001	0.0002	0.0002
1512 (6)	0.0032	0.0040	0	0.0001	0.0001	0.0001
1764 (7)	0	0	0	0	0	0

TABLE 4.5 COMPARISON OF UNIT LOAD INFLUENCE LINE STRESSES

BETWEEN MODEL 3B AND MODEL 4A - LOWER CHORD L6L7A

Panel Point	Axial Stress		In-Plane Bending Stresses		Out-of-Plane Bending Stresses	
X Coordinate	Model 3B	Model 4A	Model 3B	Model 4A	Model 3B	Model 4A
0 (0)	0	0	0	0	0	0
252 (1)	− 0.0036	− 0.0036	− 0.0001	0.0001	− 0.0026	− 0.0027
504 (2)	− 0.0074	− 0.0074	− 0.0001	0.0003	− 0.0044	− 0.0046
756 (3)	− 0.0114	− 0.0114	− 0.0002	− 0.0001	− 0.0055	− 0.0057
1008 (4)	− 0.0155	− 0.0156	− 0.0004	0.0014	− 0.0063	− 0.0065
1260 (5)	− 0.0200	− 0.0196	0.0020	− 0.0037	−. 0.0066	− 0.0069
1512 (6)	− 0.0230	− 0.0130	− 0.0150	− 0.2159	− 0.0055	− 0.0077
1764 (7)	0	0	0	0	0	0

TABLE 4.6   COMPARISON OF UNIT LOAD INFLUENCE LINE STRESSES

BETWEEN MODEL 3B AND MODEL 4A - PORTAL BEAM U6L7A

Panel Point X Coordinate	Axial Stress		In-Plane Bending Stresses		Out-of-Plane Bending Stresses	
	Model 3B	Model 4A	Model 3B	Model 4A	Model 3B	Model 4A
0 (0)	0	0	0	0	0	0
252 (1)	0.0033	0.0033	- 0.0009	- 0.0004	- 0.0002	- 0.0004
504 (2)	0.0066	0.0067	- 0.0014	- 0.0007	- 0.0004	- 0.0006
756 (3)	0.0099	0.0100	- 0.0017	- 0.0014	- 0.0007	- 0.0008
1008 (4)	0.0132	0.0133	- 0.0016	- 0.0008	- 0.0009	- 0.0008
1260 (5)	0.0168	0.0164	- 0.0018	- 0.0061	- 0.0008	- 0.0005
1512 (6)	0.0189	0.0100	- 0.0001	0.1521	- 0.0042	- 0.0064
1764 (7)	0	0	0	0	0	0

TABLE 4.7 COMPARISON OF UNIT LOAD STRESSES BETWEEN MODEL 3B

AND MODEL 4A - HANGER U6L6B

Panel Point X Coordinate	Axial Stress		In-Plane Bending Stresses		Out-of-Plane Bending Stresses	
	Model 3B	Model 4A	Model 3B	Model 4A	Model 3B	Model 4A
0 (0)	0	0	0	0	0	0
252 (1)	0.0001	0.0001	−0.0007	−0.0007	−0.0002	−0.0001
506 (2)	0.0003	0.0002	−0.0015	−0.0015	−0.0004	−0.0001
756 (3)	0.0002	0.0001	−0.0023	−0.0023	−0.0006	−0.0006
1008 (4)	0.0012	0.0009	−0.0030	−0.0030	−0.0005	−0.0006
1260 (5)	−0.0037	−0.0028	−0.0049	−0.0050	−0.0020	−0.0056
1512 (6)	−0.0642	−0.0606	−0.0005	−0.0007	−0.0179	−0.1477
1764 (7)	0	0	0	0	0	0

TABLE 4.8 COMPARISON OF UNIT LOAD STRESSES BETWEEN MODEL 3B

AND MODEL 4A - FLOOR BEAM L6AB

Panel Point	Axial Stress		In-Plane Bending Stresses		Out-of-Plane Bending Stresses	
X Coordinate	Model 3B	Model 4A	Model 3B	Model 4A	Model 3B	Model 4A
0 (0)	0	0	0	0	0	0
254 (1)	-0.0001	-0.0001	-0.0066	-0.0069	0.0001	0
504 (2)	-0.0003	-0.0003	-0.0108	-0.0113	0.0002	0
756 (3)	-0.0005	-0.0005	-0.0131	-0.0137	0	-0.0001
1008 (4)	-0.0007	-0.0007	-0.0142	-0.0148	0.0014	0.0006
1260 (5)	-0.0009	-0.0009	-0.0141	-0.0146	-0.0040	-0.0018
1512 (6)	-0.0010	-0.0005	-0.0100	-0.0099	-0.0718	-0.0588
1764 (7)	0	0	0	0	0	0

TABLE 4.9 COMPARISON OF UNIT LOAD STRESSES BETWEEN MODEL 3B

AND MODEL 4A - STRINGER L6L7A AND L6L7B

Panel Point X Coordinate	Axial Stresses			In-Plane Bending Stresses			Out-of-Plane Bending Stresses		
	Model 3B	Model 4A1	Model 4A2	Model 3B	Model 4A1	Model 4A2	Model 3B	Model 4A1	Model 4A2
0 (0)	0	0	0	0	0	0	0	0	0
252 (1)	-0.0007	-0.0007	-0.0007	0.0050	0.0051	+0.0052	0.0002	0.0005	0.0002
504 (2)	-0.0011	-0.0012	-0.0012	0.0083	0.0086	+0.0086	0.0002	0.0010	0.0003
756 (3)	-0.0015	-0.0015	-0.0015	0.0103	0.0106	+0.0106	0.0007	0.0013	0.0006
1008 (4)	-0.0017	-0.0017	-0.0017	0.0115	0.0118	+0.0118	-0.0013	0.0027	-0.0008
1260 (5)	-0.0018	-0.0018	-0.0019	0.0119	0.0122	+0.0121	0.0014	-0.0001	0.0093
1512 (6)	-0.0016	-0.0008	-0.0019	0.0093	0.0090	0.0077	-0.0344	-0.2037	-0.1339
1764 (7)	0	0	0	0	0	0	0	0	0

TABLE 4.10 COMPARISON OF UNIT LOAD STRESSES BETWEEN MODEL 3B

AND MODEL 4A – TOP BRACING U5AU6B

Panel Point	Axial Stress		In-Plane Bending Stresses		Out-of-Plane Bending Stresses	
X Coordinate	Model 3B	Model 4A	Model 3B	Model 4A	Model 3B	Model 4A
0 (0)	0	0	0	0	0	0
252 (1)	0.0032	+0.0031	0.0001	+0.0011	0	0
504 (2)	0.0063	+0.0063	0.0002	+0.0002	0.0001	+0.0001
756 (3)	0.0094	+0.0094	0.0006	+0.0006	0.0001	+0.0001
1008 (4)	0.0127	+0.0126	0.0014	+0.0013	0.0002	+0.0002
1260 (5)	0.0156	+0.0157	0.0024	+0.0025	0.0002	+0.0002
1512 (6)	0.0083	+0.0166	0.0002	+0.0037	0	+0.0001
1764 (7)	0	0	0	0	0	0

TABLE 4.11 COMPARISON OF UNIT LOAD STRESSES BETWEEN MODEL -3B

AND MODEL 4A - TRUSS DIAGONAL L5U6A

Panel Point	Axial Stress		In-Plane Bending Stresses		Out-of-Plane Bending Stresses	
X Coordinate	Model 3B	Model 4A	Model 3B	Model 4A	Model 3B	Model 4A
0 (0)	0	0	0	0	0	0
252 (1)	-0.0081	-0.0080	0.0002	0.0242	0.0013	0.0014
504 (2)	-0.0162	-0.0161	0.0004	0.0004	0.0029	0.0029
756 (3)	-0.0241	-0.0240	0.0003	0.0005	0.0039	0.0039
1008 (4)	-0.0327	-0.0321	0.0008	0.0009	0.0060	0.0067
1260 (5)	-0.0372	-0.0391	0.0057	0.0061	-0.0019	-0.0038
1512 (6)	-0.0049	-0.0202	0.0003	0.0023	-0.0053	-0.0631
1764 (7)	0	0	0	0	0	0

TABLE 4.12 COMPARISON OF MODEL 3B AND MODEL 4B

MAXIMUM MEMBER STRESSES

Member	MODEL 3B MPa (ksi)	Model 4B MPa (ksi)	Ratio
Hanger U1L1B	-31.44 (-4.56)	-30.48 (-4.42)	0.97
Floor Beam L6AB	-41.78 (-6.06)	-43.30 (-6.28)	1.04
Hanger L6U6A	-31.44 (-4.56)	-46.89 (-6.80)	1.49
Hanger L6U6B	-31.44 (-4.56)	-33.03 (-4.79)	1.05
Lower Chord L6L7A	-16.59 (-2.62)	-33.58 (-4.58)	1.86
Stringer L6L7A	-41.92 (-6.08)	-41.78 (-6.06)	1.00
Top Bracing U1BU2A	15.44 (2.24)	-14.96 (+2.17)	0.97
Top Bracing U5AU6B	15.44 (2.24)	-15.65 (-2.27)	1.01
Stringer L6L7B	41.92 (-6.08)	-39.99 (-5.80)	0.95
Portal Beam U6L7A	17.24 (2.50)	-20.96 (-3.04)	1.22
Truss Diagonal L5U6A	-26.34 (-3.82)	-30.13 (-4.37)	1.14

Notes:

1. Negative sign implies tension and positive sign implies compression.

2. Stresses are due to two 99 ton diesel locomotives crossing structure.

TABLE 4.13 COMPARISON OF UNIT LOAD INFLUENCE LINE STRESSES FOR MODEL

3B AND MODEL 4B - HANGER U1L1B

Panel Point	Axial Stress		In-Plane Bending Stresses		Out-of-Plane Bending Stresses	
X Coordinate	Model 3B	Model 4A	Model 3B	Model 4A	Model 3B	Model 4A
0 (0)	0	0	0	0	0	0
252 (1)	-0.0642	-0.0660	-0.0005	-0.0004	-0.0179	-0.0182
504 (2)	-0.0037	-0.0025	-0.0049	-0.0050	-0.0020	-0.0019
756 (3)	0.0012	0.0009	-0.0003	-0.0030	-0.0005	-0.0007
1008 (4)	0.0002	0.0002	-0.0023	-0.0023	-0.0006	-0.0007
1260 (5)	0.0003	0.0002	-0.0015	-0.0015	-0.0004	-0.0005
1512 (6)	0.0001	0.0001	-0.0007	-0.0007	-0.0002	-0.0001
1764 (7)	0	0	0	0	0	0

TABLE 4.14 COMPARISON OF UNIT LOAD INFLUENCE LINE STRESSES FOR

MODEL 3B AND MODEL 4B - TOP BRACING U1U2B

Panel Point	Axial Stress		In-Plane Bending Stresses		Out-of-Plane Bending Stresses	
X Coordinate	Model 3B	Model	Model 3B	Model	Model 3B	Model
0 (0)	0	0	0	0	0	0
252 (1)	0.0083	0.0080	0.0002	0.0002	0	0.0001
504 (2)	0.0156	0.0152	0.0024	0.0025	0.0002	0.0002
756 (3)	0.0127	0.0123	0.0014	0.0014	0.0002	0.0014
1008 (4)	0.0094	0.0091	0.0006	0.0007	0.0001	0.0001
1260 (5)	0.0063	0.0061	0.0002	0.0002	0.0001	0.0001
1512 (6)	0.0032	0.0032	0.0001	0.0001	0	0
1764 (7)	0	0	0	0	0	0

TABLE 4.15 COMPARISON OF UNIT LOAD INFLUENCE LINE STRESSES FOR

MODEL 3B AND MODEL 4B – LOWER CHORD L6L7A

Panel Point	Axial Stress		In-Plane Bending Stresses		Out-of-Plane Bending Stresses	
X Coordinate	Model 3B	Model	Model 3B	Model	Model 3B	Model
0 (0)	0	0	0	0	0	0
252 (1)	-0.0036	-0.0035	-0.0026	-0.0027	-0.0001	-0.0001
504 (2)	-0.0074	-0.0071	-0.0044	-0.0046	-0.0001	-0.0001
756 (3)	-0.0114	-0.0110	-0.0055	-0.0057	-0.0002	-0.0002
1008 (4)	-0.0155	-0.0149	-0.0063	-0.0065	-0.0004	-0.0005
1260 (5)	-0.0200	-0.0191	-0.0066	-0.0068	0.0020	0.0022
1512 (6)	-0.0230	-0.0216	-0.0055	-0.0060	-0.0150	-0.0251
1764 (7)	0	0	0	0	0	0

TABLE 4.16 COMPARISON OF UNIT LOAD INFLUENCE LINE STRESSES. FOR

MODEL 3B AND MODEL 4B – HANGER U6L6A

Panel Point	Axial Stress		In-Plane Bending Stresses		Out-of-Plane Bending Stresses	
X Coordinate	Model 3B	Model 4B	Model 3B	Model 4B	Model 3B	Model 4B
0 (0)	0	0	0	0	0	0
252 (1)	0.0001	0.0001	-0.0007	-0.0008	-0.0002	-0.0002
504 (2)	0.0003	0.0003	-0.0015	-0.0016	-0.0004	-0.0003
756 (3)	0.0002	0.0001	-0.0023	-0.0024	-0.0006	-0.0005
1008 (4)	0.0012	0.0011	-0.0030	-0.0032	-0.0005	-0.0005
1260 (5)	-0.0037	-0.0039	-0.0049	-0.0054	-0.0020	-0.0010
1512 (6)	-0.0642	-0.1227	-0.0005	-0.0004	-0.0179	-0.0066
1764 (7)	0	0	0	0	0	0

TABLE 4.17 COMPARISON OF UNIT LOAD INFLUENCE LINE STRESSES FOR

MODEL 3B AND MODEL 4B – PORTAL BEAM U6L7A

Panel Point	Axial Stress		In-Plane Bending Stresses		Out-of-Plane Bending Stresses	
X Coordinate	Model 3B	Model	Model 3B	Model	Model 3B	Model
0 (0)	0	0	0	0	0	0
252 (1)	0.0033	0.0033	−0.0009	0.0002	−0.0002	−0.0009
504 (2)	0.0066	0.0066	−0.0014	0.0004	−0.0004	−0.0014
756 (3)	0.0099	0.0100	−0.0017	0.0007	−0.0007	−0.0017
1008 (4)	0.0132	0.0133	−0.0016	0.0009	−0.0009	−0.0017
1260 (5)	0.0168	0.0167	−0.0018	0.0008	−0.0008	−0.0015
1512 (6)	0.0189	0.0184	−0.0001	0.0072	−0.0042	0.0019
1764 (7)	0	0	0	0	0	0

TABLE 4.18 COMPARISON OF UNIT LOAD INFLUENCE LINE STRESSES FOR

MODEL 3B AND MODEL 4B - TRUSS DIAGONAL L5U6A

Panel Point	Axial Stress		In-Plane Bending Stresses		Out-of-Plane Bending Stresses	
X Coordinate	Model 3B	Model 4B	Model 3B	Model 4B	Model 3B	Model 4B
0 (0)	0	0	0	0	0	0
252 (1)	+0.0081	+0.0080	0.0002	0.0002	0.0013	0.0014
504 (2)	+0.0162	+0.0161	0.0004	0.0003	0.0027	0.0027
756 (3)	+0.0241	0.0240	0.0003	0.0003	0.0039	0.0039
1008 (4)	+0.0327	0.0323	0.0008	0.0006	0.0060	0.0061
1260 (5)	+0.0372	0.0363	0.0057	0.0042	−0.0019	0.0020
1512 (6)	+0.0049	0.0042	0.0003	0.0007	−0.0053	0.0081
1764 (7)	0	0	0	0	0	0

TABLE 4.19 COMPARISON OF UNIT LOAD INFLUENCE LINE STRESSES FOR

MODEL 3B AND MODEL 4B - FLOOR BEAM L6AB

Panel Point	Axial Stress		In-Plane Bending Stresses		Out-of-Plane Bending Stresses	
X Coordinate	Model 3B	Model 4B	Model 3B	Model 4B	Model 3B	Model 4B
0 (0)	0	0	0	0	0	0
252 (1)	-0.0001	-0.0001	-0.0066	-0.0009	0.0001	0
504 (2)	-0.0003	-0.0003	-0.0108	-0.0113	0.0002	0
756 (3)	-0.0005	-0.0005	-0.0131	-0.0136	0	-0.0001
1008 (4)	-0.0007	-0.0007	-0.0142	-0.0148	0.0014	0.0007
1260 (5)	-0.0009	-0.0009	-0.0041	-0.0146	-0.0040	-0.0022
1512 (6)	-0.0010	-0.0010	-0.0100	-0.0104	-0.0718	-0.0727
1764 (7)	0	0	0	0	0	0

TABLE 4.20 COMPARISON OF UNIT LOAD INFLUENCE LINE STRESSES FOR

MODEL 3B AND MODEL 4B – STRINGER L6L7A AND L6L7B

Panel Point X Coordinate	Axial Stresses			In-Plane Bending Stresses			Out-of-Plane Stresses		
	Model 3B	Model 4B1	Model 4B2	Model 3B	Model 4B1	Model 4B2	Model 3B	Model 4B1	Model 4B2
0 (0)	0	0	0	0	0	0	0	0	0
252 (1)	-0.0007	-0.0007	-0.0007	-0.0002	0.0004	0.0001	-0.0050	0.0051	0.0052
504 (2)	-.0011	-0.0012	-0.0012	0.0002	0.0007	0.0001	0.0083	0.0086	0.0086
756 (3)	-0.0015	-0.0015	-0.0015	0.0007	0.0012	0.0006	0.0103	0.0106	0.0106
1008 (4)	-0.0017	-0.0017	-0.0017	0.0013	0.0011	0.0017	0.0115	0.0118	0.0118
1260 (5)	-0.0018	-0.0019	-0.0018	0.0014	0.0051	0.0123	0.0119	0.0122	0.0122
1512 (6)	-0.0016	-0.0015	-0.0016	-0.0344	0.0397	0.0399	0.0093	0.0095	0.0094
1764 (7)	0	0	0	0	0	0	0	0	0

TABLE 4.21 COMPARISON OF UNIT LOAD INFLUENCE LINE STRESSES FOR

MODEL 3B AND MODEL 4B - HANGER U6L6B

Panel Point	Axial Stress		In-Plane Bending Stresses		Out-of-Plane Bending Stresses	
X Coordinate	Model 3B	Model 4B	Model 3B	Model 4B	Model 3B	Model 4B
0 (0)	0	0	0	0	0	0
252 (1)	0.0001	0.0001	-0.0007	-0.0007	-0.0002	-0.0002
504 (2)	0.0003	0.0002	-0.0015	-0.0015	-0.0004	-0.0003
756 (3)	0.0002	0.0001	-0.0023	-0.0020	-0.0006	-0.0006
1008 (4)	0.0012	0.0009	-0.0030	-0.0030	-0.0005	-0.0005
1260 (5)	-0.0037	-0.0029	-0.0049	-0.0049	-0.0020	-0.0017
1512 (6)	-0.0642	-0.0645	-0.0005	-0.0005	-0.0179	-0.0239
1764 (7)	0	0	0	0	0	0

TABLE 4.22   COMPARISON OF UNIT LOAD INFLUENCE LINE STRESSES FOR

MODEL 3B AND MODEL 4B – TOP DIAGONAL U5AU6B

Panel Point X Coordinate	Axial Stress		In-Plane Bending Stresses		Out-of-Plane Bending Stresses	
	Model 3B	Model 4B	Model 3B	Model 4B	Model 3B	Model 4B
0 (0)	0	0.	0	0.	0	0
252 (1)	0.0032	0.0031	0.0001	0.0001	0	0
504 (2)	0.0063	0.0063	0.0002	0.0002	0.0001	0.0001
756 (3)	0.0094	0.0094	0.0006	0.0006	0.0001	0.0001
1008 (4)	0.0127	0.0126	0.0014	0.0014	0.0002	0.0002
1260 (5)	0.0156	0.0157	0.0024	0.0024	0.0002	0.0002
1512 (6)	0.0083	0.0088	0.0002	0.0003	0	0.0001
1764 (7)	0	0	0	0	0	0

TABLE 4.23   MEMBERS OF INTEREST

MODELS 4C AND 4D

MEMBER

TOP CHORD U3U4A

TOP CHORD U3U4B

TRUSS DIAGONAL L3U4A

TRUSS DIAGONAL L4U3A

STRINGER L3L4A

STRINGER L3L4B

LOWER CHORD L3L4B

HANGER U6L6B

LOWER CHORD L6L7A

FLOOR BEAM L4AB

LOWER CHORD L4L5A

TABLE 4.24 COMPARISON OF MODEL 3B AND MODEL 4C

MAXIMUM MEMBER STRESSES

Member	Model 3B MPa (ksi)	Model 4C MPa (ksi)	Ratio
Top Chord U3U4A	29.92 (4.34)	33.92 (4.92)	1.13
Top Chord U3U4B	29.92 (4.34)	34.75 (5.04)	1.16
Counter L3U4A	- 8.14 (-1.18)	-30.34 (-4.40)	3.73
Counter L4U3A	- 8.14 (-1.18)	-37.30 (-5.41)	4.58
Stringer L3L4A	-39.16 (-5.68)	-57.92 (-8.40)	1.48
Stringer L3L4B	-39.16 (-5.68)	-44.13 (-6.40)	1.13
Lower Chord L3L4B	-23.86 (-3.46)	-69.57 (-10.09)	2.92
Hanger U6L6B	-31.44 (-4.56)	-28.34 (-4.11)	1.11
Lower Chord L6L7A	-16.69 (-2.62)	-44.96 (-6.52)	2.49
Floor Beam L4AB	+ 9.86 (1.43)	67.36 (9.77)	6.83
Lower Chord L4L5A	-26.89 (-3.90)	-23.99 (-3.48)	0.89

Notes:

1. Negative sign implies tension and positive sign implies compression.

2. Stresses are due to two 99 ton diesel locomotives crossing structure.

TABLE 4.25 COMPARISON OF UNIT LOAD INFLUENCE LINE STRESSES FOR MODEL 3B AND

MODEL 4C - FLOOR BEAM L4AB

Panel Point	Axial Stress		Out-of-Plane Bending Stresses		In-Plane Bending Stresses	
X Coordinate	Model 3B	Model 4C	Model 3B	Model 4C	Model 3B	Model 4C
0 (0)	0	0	0	0	0	0
252 (1)	0.0003	0.0009	0.0086	0.0236	−0.0001	−0.0007
504 (2)	0.0006	0.0020	0.0113	0.0435	−0.0001	0.0013
756 (3)	0.0009	0.0031	0.0091	0.0588	−0.0005	0.0023
1008 (4)	0.0009	0.0031	0.0041	0.1020	0.0017	0.0002
1260 (5)	0.0010	0.0025	−0.0031	0.0307	−0.0002	0.0001
1512 (6)	0.0005	0.0012	−0.0053	+0.0113	0	0.0005
1764 (7)	0	0	0	0	0	0

TABLE 4.26 COMPARISON OF UNIT LOAD INFLUENCE LINE STRESSES

FOR MODEL 3B AND MODEL 4C - COUNTER L3U4A

Panel Point	Axial Stress		In-Plane Bending Stresses		Out-of-Plane Bending Stresses	
X Coordinate	Model 3B	Model 4C	Model 3B	Model 4C	Model 3B	Model 4C
0 (0)	0	0	0	0	0	0
252 (1)	−0.0067	−.0142	0	−0.0021	0.0007	0.0010
504 (2)	−0.0143	−0.0299	0.0005	−.0040	0.0028	0.0046
756 (3)	−0.0180	−0.0424	0.0053	−0.0015	−0.0027	−0.0051
1008 (4)	0.0195	−0.0042	0	−0.0070	−0.0043	−0.0022
1260 (5)	0.0158	−0.0001	−0.0004	−0.0050	−0.0036	−0.0031
1512 (6)	0.0075	0	−0.0002	−0.0024	−0.0019	−0.0015
1764 (7)	0	0	0	0	0	0

TABLE 4.27   COMPARISON OF UNIT LOAD INFLUENCE LINE STRESSES FOR

MODEL 3B AND MODEL 4C - COUNTER L4U3A

Panel Point X Coordinate	Axial Stress		In-Plane Bending Stresses		Out-of-Plane Bending Stresses	
	Model 3B	Model 4C	Model 3B	Model 4C	Model 3B	Model 4C
0	0	0	0	0	0	0
252 (1)	+0.0075	-0.0002	0.0002	-0.0022	0.0019	-0.0003
504 (2)	+0.0158	-0.0005	0.0004	-0.0045	0.0036	-0.0004
756 (3)	+0.0195	-0.0051	0	-0.0065	0.0043	-0.0068
1008 (4)	-0.0180	-.0434	-0.0053	-0.0033	0.0027	-0.0057
1260 (5)	-0.0143	-0.0303	-0.0005	-0.0036	-0.0028	-0.0068
1512 (6)	-0.0067	-0.0144	0.0156	-0.0018	-0.0007	-0.0027
1764 (7)	0	0	0	0	0	0

TABLE 4.28 COMPARISON OF UNIT LOAD INFLUENCE LINE STRESSES FOR

MODEL 3B AND MODEL 4C - LOWER CHORD L3L4B

Panel Point X Coordinate	Axial Stress		In-Plane Bending Stresses		Out-of-Plane Bending Stresses	
	Model 3B	Model 4C	Model 3B	Model 4C	Model 3B	Model 4C
0 (0)	0	0	0	0	0	0
252 (1)	-0.0062	-0.0069	0.0007	-0.0020	-0.0006	-0.0009
504 (2)	-0.0131	-0.0145	0.0008	-0.0036	0.0009	0.0009
756 (3)	-0.0199	-0.0222	0.0001	-0.0045	-0.0101	-0.0106
1008 (4)	-0.0199	-0.0222	-0.0005	-0.0040	-0.0002	-0.0006
1260 (5)	-0.0131	-0.1453	-0.0009	-0.0021	-0.0017	-0.0020
1512 (6)	-0.0062	-0.0069	-0.0008	-0.0007	-0.0008	-0.0007
1764 (7)	0	0	0	0	0	0

TABLE 4.29 COMPARISON OF UNIT LOAD INFLUENCE LINE STRESSES FOR

MODEL 3B AND MODEL 4C - LOWER CHORD L6L7A

Panel Point X Coordinate	Axial Stress		Out-of-Plane Bending Stresses		In-Plane Bending Stresses	
	Model 3B	Model 4C	Model 3B	Model 4C	Model 3B	Model 4C
0 (0)	0	0	0	0	0	0
252 (1)	-0.0036	-0.0023	0.0026	-0.0051	-0.0001	0.0001
504 (2)	-0.0074	-0.0047	0.0044	-0.0096	-0.0001	0.0001
756 (3)	-0.0114	-0.0072	0.0055	-0.0133	-0.0002	0.0001
1008 (4)	-0.0155	-0.0113	0.0063	-0.0140	-0.0004	0.0002
1260 (5)	-0.0200	-0.0171	0.0066	-0.0117	0.0020	0.0264
1512 (6)	-0.0230	-0.0218	0.0055	-0.0080	-0.0150	-0.0151
1764 (7)	0	0	0	0	0	0

TABLE 4.30   COMPARISON OF UNIT LOAD INFLUENCE LINE STRESSES FOR

MODELS 3B AND MODEL 4C - STRINGER L3L4A

Panel Point	Axial Stress		Out-of-Plane Bending Stresses		In-Plane Bending Stresses	
X Coordinate	Model 3B	Model 4C	Model 3B	Model 4C	Model 3B	Model 4C
0 (0)	0	0	0	0	0	0
252 (1)	-0.0024	-0.0060	0.0012	-0.0005	-0.0023	-0.0035
504 (2)	-0.0037	-0.0113	0.0010	-0.0027	0.0068	0.0054
756 (3)	-0.0042	-0.0157	-0.0004	-0.0061	-0.0236	-0.0270
1008 (4)	-0.0042	-0.0157	-0.0014	-0.0072	-0.0055	-0.0081
1260 (5)	-0.0037	-0.0113	-0.0021	-0.0057	-0.0028	-0.0052
1512 (6)	-0.0024	-0.0060	-0.0017	-0.0034	-0.0022	-0.0031
1764 (7)	0	0	0	0	0	0

TABLE 4.31 COMPARISON OF UNIT LOAD INFLUENCE LINE STRESSES FOR

MODEL 3B AND MODEL 4C - TOP CHORD U3U4A

Panel Point	Axial Stress		Out-of-Plane Bending Stresses		In-Plane Bending Stresses	
X Coordinate	Model 3B	Model 4C	Model 3B	Model 4C	Model 3B	Model 4C
0 (0)	0	0	0	0	0	0
252(1)	0.0088	0.0092	-0.0001	0.0002	-0.0012	-0.0003
504 (2)	0.0178	0.0185	-0.0028	0.0005	-0.0028	-0.0011
756 (3)	0.0264	0.0233	0.0052	0.0011	0.0052	0.0079
1008 (4)	0.0264	0.0274	0.0033	0.0010	0.0033	0.0061
1260 (5)	0.0178	0.0185	0.0034	0.0007	0.0034	0.0052
1512 (6)	0.0088	0.0092	0.0017	0.0003	0.0017	0.0025
1764 (7)	0	0	0	0	0	0

TABLE 4.32 COMPARISON OF UNIT LOAD INFLUENCE LINE STRESSES FOR

MODEL 3B AND MODEL 4C - TOP CHORD U3U4B

Panel Point	Axial Stress		In-Plane Bending Stresses		Out-of-Plane Bending Stresses	
X Coordinate	Model 3B	Model 4C	Model 3B	Model 4D	Model 3B	Model 4C
0 (0)	0	0	0	0	0	0
252 (1)	0.0088	0.0099	-0.0001	0.0004	-0.0012	-0.0010
504 (2)	0.0178	0.0199	-0.0028	0.0008	-0.0028	-0.0027
756 (3)	0.0264	0.0297	0.0052	0.0010	0.0052	0.0056
1008 (4)	0.0264	0.0297	0.0033	0.0011	0.0033	0.0036
1260 (5)	0.0178	0.0199	0.0034	0.0006	0.0034	0.0037
1512 (6)	0.0088	0.0099	0.0017	0.0003	0.0017	0.0018
1764 (7)	0	0	0	0	0	0

TABLE 4.33 COMPARISON OF UNIT LOAD INFLUENCE LINE STRESSES FOR

MODEL 3B AND MODEL 4C - STRINGER L3L4B

Panel Point	Axial Stress		In-Plane Bending Stresses		Out-of-Plane Bending Stresses	
X Coordinate	Model 3B	Model 4C	Model 3B	Model 4C	Model 3B	Model 4C
0 (0)	0	0	0	0	0	0
252 (1)	-0.0024	-0.0027	0.0012	0.0007	-0.0023	-0.0018
504 (2)	-0.0037	-.0043	0.0010	-0.0003	0.0068	0.0027
756 (3)	-0.0042	-0.0050	-0.0004	-0.0024	-0.0236	-0.0241
1008 (4)	-0.0042	-0.0050	-0.0014	-0.0034	-0.0055	-0.0072
1260 (5)	-0.0037	-0.0043	-0.0021	-0.0033	-0.0028	-0.0038
1512 (6)	-0.0024	-0.0027	-0.0017	-0.0022	-0.0022	-0.0027
1764 (7)	0	0	0	0	0	0

TABLE 4.34   COMPARISON OF UNIT LOAD INFLUENCE LINE STRESSES FOR

MODEL 3B AND MODEL 4C - HANGER U6L6B

Panel Point X Coordinate	Axial Stress		In-Plane Bending Stresses		Out-of-Plane Bending Stresses	
	Model 3B	Model 4C	Model 3B	Model 4C	Model 3B	Model 4C
0 (0)	0	0	0	0	0	0
252 (1)	0.0001	0.0001	-0.0007	0.0008	-0.0002	0.0010
504 (2)	0.0003	0.0003	-0.0015	0.0016	-0.0004	0.0021
756 (3)	0.0002	0.0003	-0.0223	0.0025	-0.0006	0.0032
1008 (4)	0.0012	0.0011	-0.0030	0.0033	-0.0005	0.0032
1260 5)	-0.0037	-0.0028	-0.0049	0.0051	-0.0020	0.0009
1512 (6)	-0.0642	-0.0646	-0.0005	0.0006	-0.0179	-0.0169
1764 (7)	0	0	0	0	0	0

TABLE 4.35   COMPARISON OF UNIT LOAD INFLUENCE LINE STRESSES FOR

MODEL 3B AND MODEL 4C - LOWER CHORD L4L5A

Panel Point X Coordinate	Axial Stress		In-Plane Bending Stresses		Out-of-Plane Bending Stresses	
	Model 3B	Model 4C	Model 3B	Model 4C	Model 3B	Model 4C
0 (0)	0	0	0	0	0	0
252 (1)	-0.0040	-0.0007	-0.0010	-0.0052	-0.0021	-0.0014
504 (2)	-0.0085	-0.0016	-0.0015	-0.0094	-0.0044	-0.0027
756 (3)	-0.0133	-0.0028	-0.0015	-0.0127	-0.0043	-0.0033
1008 (4)	-0.0185	-0.0079	-0.0011	-0.0117	-0.0127	-0.0050
1260 (5)	-0.0228	-0.0162	-0.0003	-0.0066	0.0031	0.0033
1512 (6)	-0.0115	-0.0081	0.0004	-0.0024	0.0001	0.0007
1764 (7)	0	0	0	0	0	0

TABLE 4.36 COMPARISON OF MODEL 3B AND MODEL 4D

MAXIMUM MEMBER STRESSES

Member	Model 3B MPa (ksi)	Model 4D MPa (ksi)	Ratio
Top Chord U3U4A	29.92 (4.34)	26.48 (3.84)	0.88
Top Chord U3U4B	29.92 (4.34)	30.41 (4.41)	1.02
Counter L3U4A	8.62 (1.25)	25.65 (+3.72)	2.98[1]
Counter L4U3A	10.76 (1.56)	12.14 (+1.76)	1.13[3]
Stringer L3L4A	-39.16 (-5.68)	-40.34 (-5.85)	1.03
Stringer L3L4B	-39.16 (-5.68)	-38.82 (-5.63)	0.99
Lower Chord L3L4B	-23.86 (-3.46)	-24.13 (-3.50)	1.01
Hanger U6L6B	-31.44 (-4.56)	-31.10 (-4.51)	0.99
Portal Beam L6L7A	-18.06 (-2.62)	-34.61 (-5.02)	1.92[2]
Floor Beam L4AB	+ 9.86 (+1.43)	-14.13 (-2.05)	1.43[4]
Lower Chord L4L5A	-26.09 (-3.90)	-24.62 (-3.57)	0.92

Notes:

1. Negative sign implies tension and positive sign implies compression.

2. Stresses are due to two 99 ton diesel locomotives crossing structure.

TABLE 4.37 COMPARISON OF UNIT LOAD INFLUENCE LINE STRESSES FOR

MODEL 3B AND MODEL 4D – TRUSS COUNTER L3U4A

Panel Point	Axial Stress		In-Plane Bending Stresses		Out-of-Plane Bending Stresses	
X Coordinate	Model 3B	Model 4D	Model 3B	Model 4D	Model 3B	Model 4D
0 (0)	0	0	0	0	0	0
252 (1)	-0.0067	-0.0074	0	-0.0001	0.0007	0.0005
504 (2)	-0.0143	-0.0156	0.0005	0.0001	0.0028	0.0033
756 (3)	-0.0180	-0.0205	0.0053	0.0048	-0.0027	-.0061
1008 (4)	0.0195	0.0177	0	-0.0007	-0.0043	-0.0042
1260 (5)	0.0158	0.0142	-0.0004	-0.0008	-0.0036	-0.0041
1512 (6)	0.0075	0.0680	-0.0002	-0.0004	-0.0019	-0.0020
1764 (7)	0	0	0	0	0	0

TABLE 4.38   COMPARISON OF UNIT LOAD INFLUENCE LINE STRESSES FOR

MODEL 3B AND MODEL 4D - LOWER CHORD L6L7A

Panel Point	Axial Stress		In-Plane Bending Stresses		Out-of-Plane Bending Stresses	
X Coordinate	Model 3B	Model 4D	Model 3B	Model 4D	Model 3B	Model 4D
0 (0)	0	0	0	0	0	0
252 (1)	-0.0036	-0.0035	0.0026	+0.0029	-0.0001	0
504 (2)	-0.0074	-0.0071	0.0044	+0.0050	-0.0001	-0.0001
756 (3)	-0.0114	-0.0110	0.0055	+0.0064	-0.0002	-0.0002
1008 (4)	-0.0155	-0.0151	0.0063	+0.0071	-0.0004	-0.0002
1260 (5)	-0.0200	-0.0196	0.0066	+0.0074	0.0020	0.0025
1512 (6)	-0.0230	-0.0230	0.0055	+0.0059	-0.0150	-0.0152
1764 (7)	0	0	0	0	0	0

TABLE 4.39 COMPARISON OF UNIT LOAD INFLUENCE LINE STRESSES FOR

MODEL 3B AND MODEL 4D – FLOOR BEAM L4AB

Panel Point X Coordinate	Axial Stress		In-Plane Bending Stresses		Out-of-Plane Bending Stresses	
	Model 3B	Model 4	Model 3B	Model	Model 3B	Model
0 (0)	0	0	0	0	0	0
252 (1)	0.0003	0.0003	0.0086	−0.0107	−0.0001	0.0002
504 (2)	0.0006	0.0007	0.0113	−0.0157	−0.0001	0.0002
756 (3)	0.0009	0.0011	0.0091	−0.0155	−0.0005	0.0006
1008 (4)	0.0009	0.0012	0.0041	−0.0107	0.0017	−0.0015
1260 (5)	0.0010	0.0012	−0.0031	−0.0157	−0.0002	0.0003
1512 (6)	0.0005	0.0006	−0.0053	0.0028	0	0
1764 (7)	0	0	0	0	0	0

TABLE 4.40 COMPARISON OF UNIT LOAD INFLUENCE LINE STRESSES FOR

MODEL 3B AND MODEL 4D - TRUSS COUNTER L4U3A

Panel Point X Coordinate	Axial Stress		In-Plane Bending Stresses		Out-of-Plane Bending Stresses	
	Model 3B	Model 4D	Model 3B	Model 4D	Model 3B	Model 4D
0 (0)	0	0	0	0	0	0
252 (1)	0.0075	+0.0067	0.0002	0.0004	0.0019	0.0021
504 (2)	0.0158	+0.0142	0.0004	0.0008	0.0036	0.0041
756 (3)	0.0195	+0.0174	0	0.0007	0.0043	0.0042
1008 (4)	-0.0180	-0.0208	-0.0053	-0.0047	0.0027	0.0062
1260 (5)	-0.0143	-0.0156	-0.0005	0	-0.0028	-0.0035
1512 (6)	-0.0067	-0.0074	0.0156	0.0001	-0.0007	-0.0004
1764 (7)	0	0	0	0	0	0

TABLE 4.41 COMPARISON OF UNIT LOAD INFLUENCE LINE STRESSES FOR

MODEL 3B AND MODEL 4D - LOWER CHORD L3L4B

Panel Point X Coordinate	Axial Stress		In-Plane Bending Stresses		Out-of-Plane Bending Stresses	
	Model 3B	Model 4D	Model 3B	Model 4D	Model 3B	Model 4D
0 (0)	0	0	0	0	0	0
252 (1)	-0.0062	-0.0062	0.0007	-0.0009	-0.0006	-0.0008
504 (2)	-0.0131	-0.0131	0.0008	-0.0012	0.0009	0.0011
756 (3)	-0.0199	-0.0201	0.0001	-0.0007	-0.0101	-0.0103
1008 (4)	-0.0199	-0.0201	-0.0005	-0.0001	-0.0002	-0.0002
1260 (5)	-0.0131	-0.0131	-0.0009	0.0005	-0.0017	-0.0018
1512 (6)	-0.0062	-0.0062	-0.0008	0.0005	-0.0006	-0.0006
1764 (7)	0	0	0	0	0	0

Panel Point	Axial Stress		In-Plane Bending Stresses		Out-of-Plane Bending Stresses	
X Coordinate	Model 3B	Model 4	Model 3B	Model 4	Model 3B	Model 4
0 (0)	0	0	0	0	0	0
252 (1)	-0.0024	-0.0029	0.0012	0.0012	-0.0023	-0.0026
504 (2)	-0.0037	-0.0047	0.0010	0.0008	0.0068	0.0072
756 (3)	-0.0042	-0.0056	-0.0004	-0.0008	-0.0236	-0.0242
1008 (4)	-0.0042	-0.0056	-0.0014	-0.0018	-0.0055	-0.0053
1260 (5)	-0.0037	-0.0047	-0.0021	-0.0023	-0.0028	-0.0034
1512 (6)	-0.0024	-0.0029	-0.0017	-0.0017	-0.0022	-0.0022
1764 (7)	0	0	0	0	0	0

TABLE 4.43 COMPARISON OF UNIT LOAD INFLUENCE LINE STRESSES FOR

MODEL 3B AND MODEL 4D - TOP CHORD U3U4B

Panel Point	Axial Stress		In-Plane Bending Stresses		Out-of-Plane Bending Stresses	
X Coordinate	Model 3B	Model 4D	Model 3B	Model 4D	Model 3B	Model 4D
0 (0)	0	0	0	0	0	0
252 (1)	0.0088	0.0089	-0.0001	-0.0001	-0.0012	-0.0011
504 (2)	0.0178	0.0179	-0.0028	-0.0001	-0.0028	-.0026
756 (3)	0.0264	0.0265	0.0052	0.0002	0.0052	0.0053
1008 (4)	0.0264	0.0265	0.0033	0	0.0033	0.0036
1260 (5)	0.0178	0.0179	0.0034	0.0001	0.0034	0.0036
1512 (6)	0.0088	0.0089	0.0017	0	0.0017	0.0018
1764 (7)	0	0	0	0	0	0

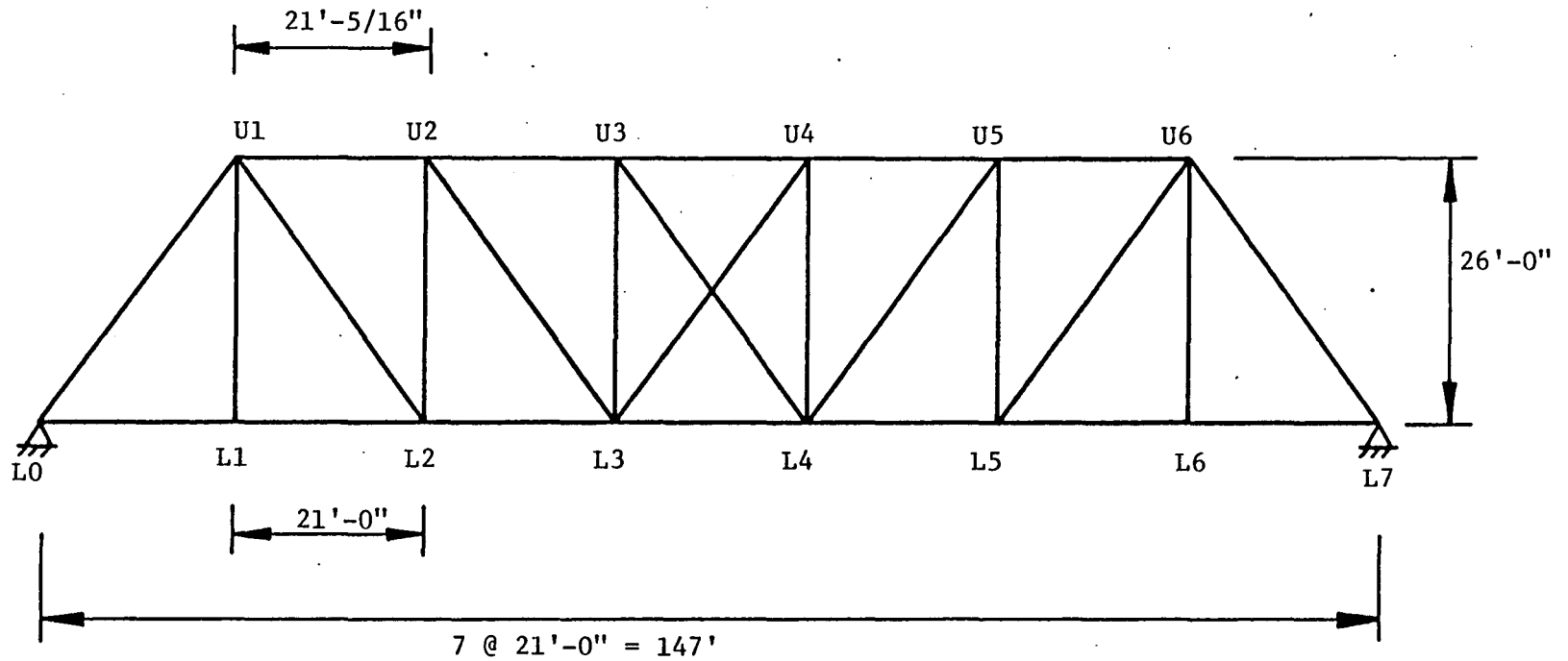TABLE 4.44   COMPARISON OF UNIT LOAD INFLUENCE LINE STRESSES FOR

MODEL 3B AND MODEL 4D – STRINGER L3L4B

Panel Point	Axial Stress		In-Plane Bending Stresses		Out-of-Plane Bending Stresses	
X Coordinate	Model 3B	Model 4D	Model 3B	Model 4D	Model 3B	Model 4D
0 (0)	0	0	0	0	0	0
252 (1)	−0.0024	−0.0025	0.0012	−0.0013	−0.0023	−0.0012
504 (2)	−0.0037	−0.0039	0.0010	−0.0011	0.0068	0.0038
756 (3)	−0.0042	−0.0044	−0.0004	0.0004	−0.0236	−0.0223
1008 (4)	−0.0042	−0.0044	−0.0014	+0.0014	−0.0055	−0.0054
1260 (5)	−0.0037	−.0039	−0.0021	0.0020	−0.0028	−0.0026
1512 (6)	−0.0024	−0.0025	−0.0017	0.0016	−0.0022	−0.0021
1764 (7)	0	0	0	0	0	0

TABLE 4.45 COMPARISON OF UNIT LOAD INFLUENCE LINE STRESSES FOR

MODEL 3B AND MODEL 4D - HANGER U6L6B

Panel Point	Axial Stress		In-Plane Bending Stresses		Out-of-Plane Bending Stresses	
X Coordinate	Model 3B	Model 4D	Model 3B	Model 4D	Model 3B	Model 4D
0 (0)	0	0	0	0	0	0
252 (1)	0.0001	0.0001	-0.0007	-0.0008	-0.0002	-0.0001
504 (2)	0.0003	0.0002	-0.0015	-0.0015	-0.0004	-0.0002
756 (3)	0.0002	0.0001	-0.0023	-0.0023	-0.0006	-0.0003
1008 (4)	0.0012	0.0010	-0.0030	-0.0030	-0.0005	-0.0003
1260 (5)	-0.0037	-0.0029	-0.0049	-0.0050	-0.0020	-0.0014
1512 (6)	-0.0642	-0.0646	-0.0005	-0.0005	-0.0179	-0.0180
1764 (7)	0	0	0	0	0	0

TABLE 4.46   COMPARISON OF UNIT LOAD INFLUENCE LINE STRESSES FOR

MODEL 3B AND MODEL 4D - LOWER CHORD L4L5A

Panel Point	Axial Stress		In-Plane Bending Stresses		Out-of-Plane Bending Stresses	
X Coordinate	Model 3B	Model 4D.	Model 3B	Model 4D.	Model 3B	Model 4D
0 (0)	0	0	0	0	0	0
252 (1)	−0.0040	−0.0036	−0.0010	−0.0015	−0.0021	−0.0017
504 (2)	−0.0085	−0.0077	−0.0015	−0.0023	−0.0044	−0.0035
756 (3)	−0.0133	−0.0121	−0.0015	−0.0024	−0.0043	−0.0039
1008 (4)	−0.0185	−0.0173	−0.0011	−0.0018	−0.0127	−0.0071
1260 (5)	−0.0228	−0.0223	−0.0003	−0.0006	0.0031	0.0030
1512 (6)	−0.0115	−0.0110	0.0004	0.0002	0.0001	0.0004
1764 (7)	0	0	0	0	0	0

TABLE 4.47   COMPARISON OF UNIT LOAD INFLUENCE LINE STRESSES FOR

MODEL 3B AND MODEL 4D – TOP CHORD U3U4A

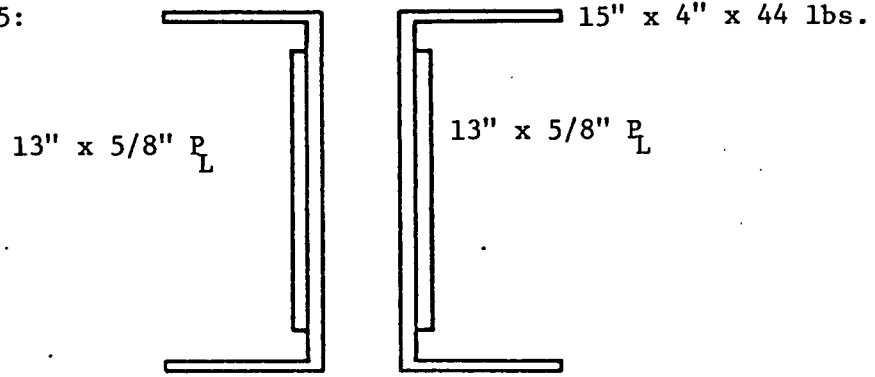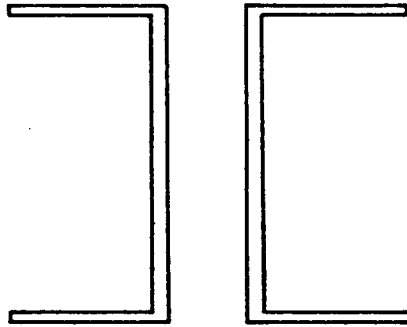| Panel Point	Axial Stress		In-Plane Bending Stresses		Out-of-Plane Bending Stresses	
X Coordinate	Model 3B	Model 4D	Model 3B	Model 4D	Model 3B	Model 4D
0 (0)	0	0	0	0	0	0
252 (1)	0.0088	0	-0.0001	0	-0.0012	0.0021
504 (2)	0.0178	0	-0.0026	0.0001	-0.0028	0.0044
756 (3)	0.0264	0.0227	0.0052	0	0.0052	0.0044
1008 (4)	0.0264	0.0298	0.0033	0.0002	0.0033	0.0060
1260 (5)	0.0178	0.0021	0.0034	-0.0001	0.0034	-0.0035
1512 (6)	0.0088	0.0102	0.0017	-0.0001	0.0017	-0.0013
1764 (7)	0	0	0	0	0	0

Fig. 1.1a Elevation View of Span of Atbara Bridge

21'-5/16"

U1   U2   U3   U4   U5   U6

26'-0"

L0   L1   L2   L3   L4   L5   L6   L7

21'-0"

7 @ 21'-0" = 147'

1' = 0.305 m

1" = 25.4 mm

-159-

L2L3, L4L5:

15" x 4" x 44 lbs.

13" x 5/8" P_L

13" x 5/8" P_L

L0L1, L1L2, L5L6,
   L6L7:

2 Channels - 15" x 4" x 44 lbs. ea.

LoU1 and L7U6:

1" = 25.4 mm

1 lb.= 4.448 N

24" x 1/2" P_L

9" x 4" x 1/2" L
   (Typical)

13" x 1/2" P_L

24" x 1/2" P_L
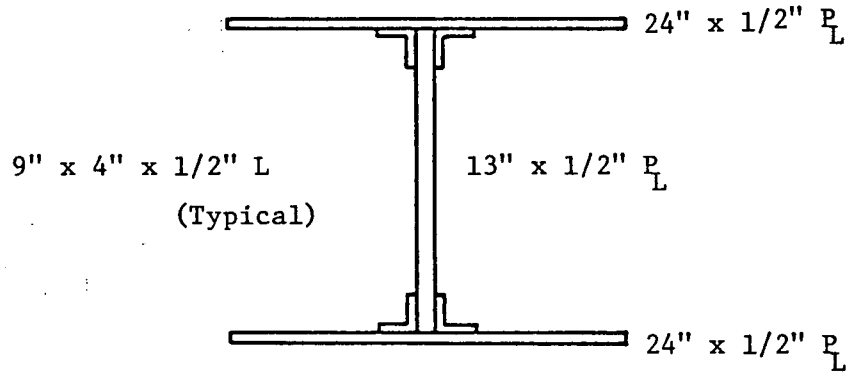
Fig. 1.1b Lower Chord and Portal Members

-160-

L3L4:

13" x 5/8" P$_L$ 13" x 5/8" P$_L$

13" x 3/8" P$_L$ 13" x 3/8" P$_L$

15" x 4" x 4416 [

U1U2, U5U6:

22" x 3/8" P$_L$

18" x 1/2" P$_L$ 18" x 1/2" P$_L$

3-1/2" x 3" x 1/2" L

U2U3, U3U4, U4U5:

22" x 3/8" P$_L$

18" x 1/2" P$_L$ 18" x 1/2" P$_L$

10-7/8" x 3/8" P$_L$ 10-7/8" x 3/8" P$_L$

1" = 25.4 mm
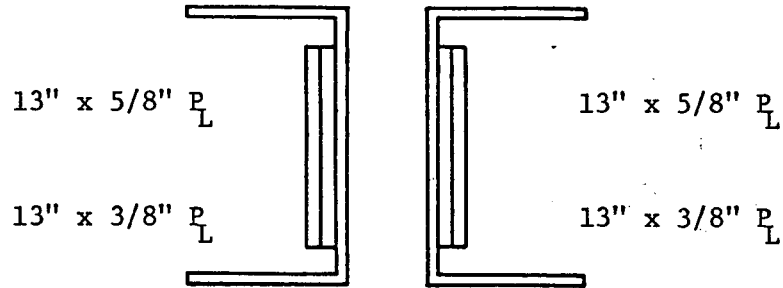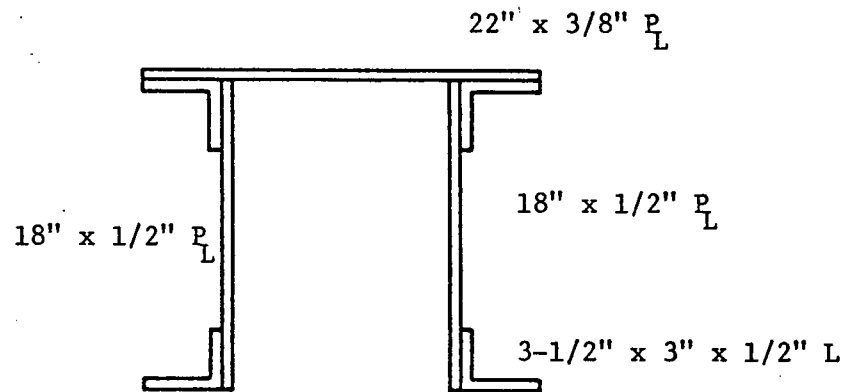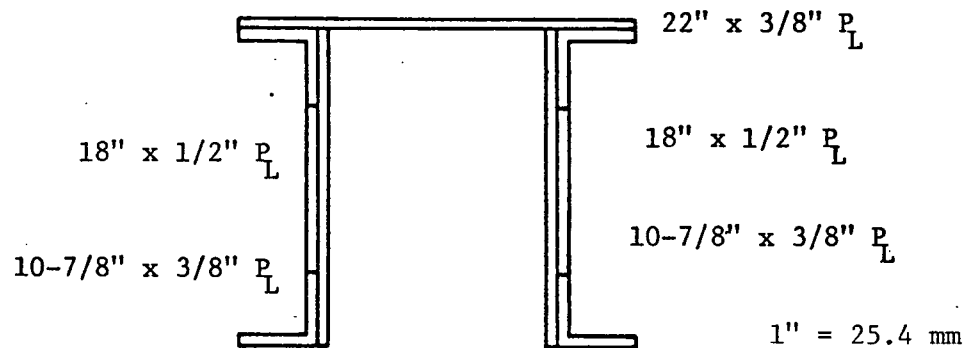
Fig. 1.1c   Lower Chord and Upper Chord Members
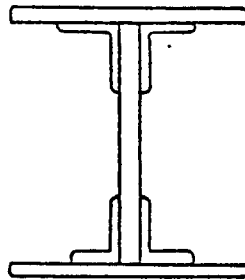
13" x 3/8" P_L
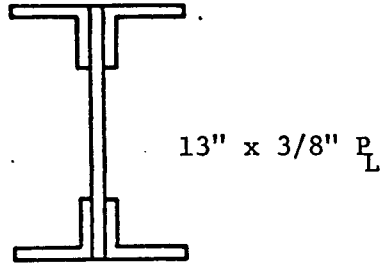
For angle sizes see schedule below

SCHEDULE OF ANGLES

Member	Angle
U1L1	3-1/2" x 3" x 3/8"
U1L2	6" x 3" x 1/2"
U2L2	6-1/2" x 3" x 13 #
U2L3	3-1/2" x 3" x 3/8"
U3L3	5" x 3" x 3/8"
U3L4	3" x 3" x 3/8"
U4L3	3" x 3" x 3/8"
U4L4	5" x 3" x 3/8"
U5L4	3-1/2" x 3" x 3/8"
U5L5	6-1/2" x 3" x 13#
U6L5	6" x 3" x 1/2"
U6L6	3-1/2" x 3" x 3/8"

1" = 25.4 mm

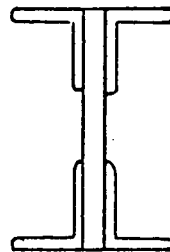Fig. 1.1d   Bracing and Hanger Members

-162-

2 P$_L$'s   13" x 3/8"
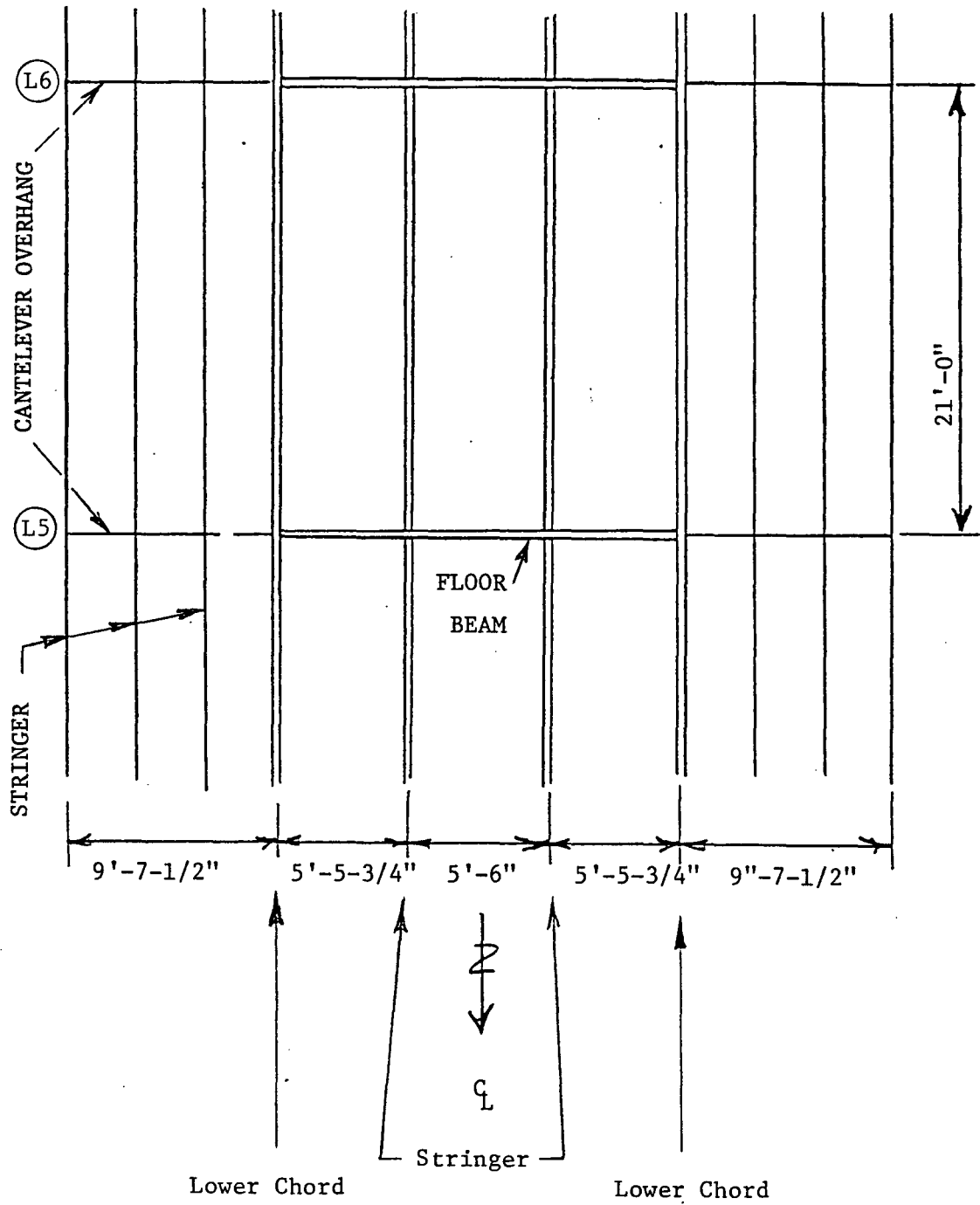
4 L's   6" x 4" x 3/8"

1 P$_L$ 43" x 3/8"

Floor Beam
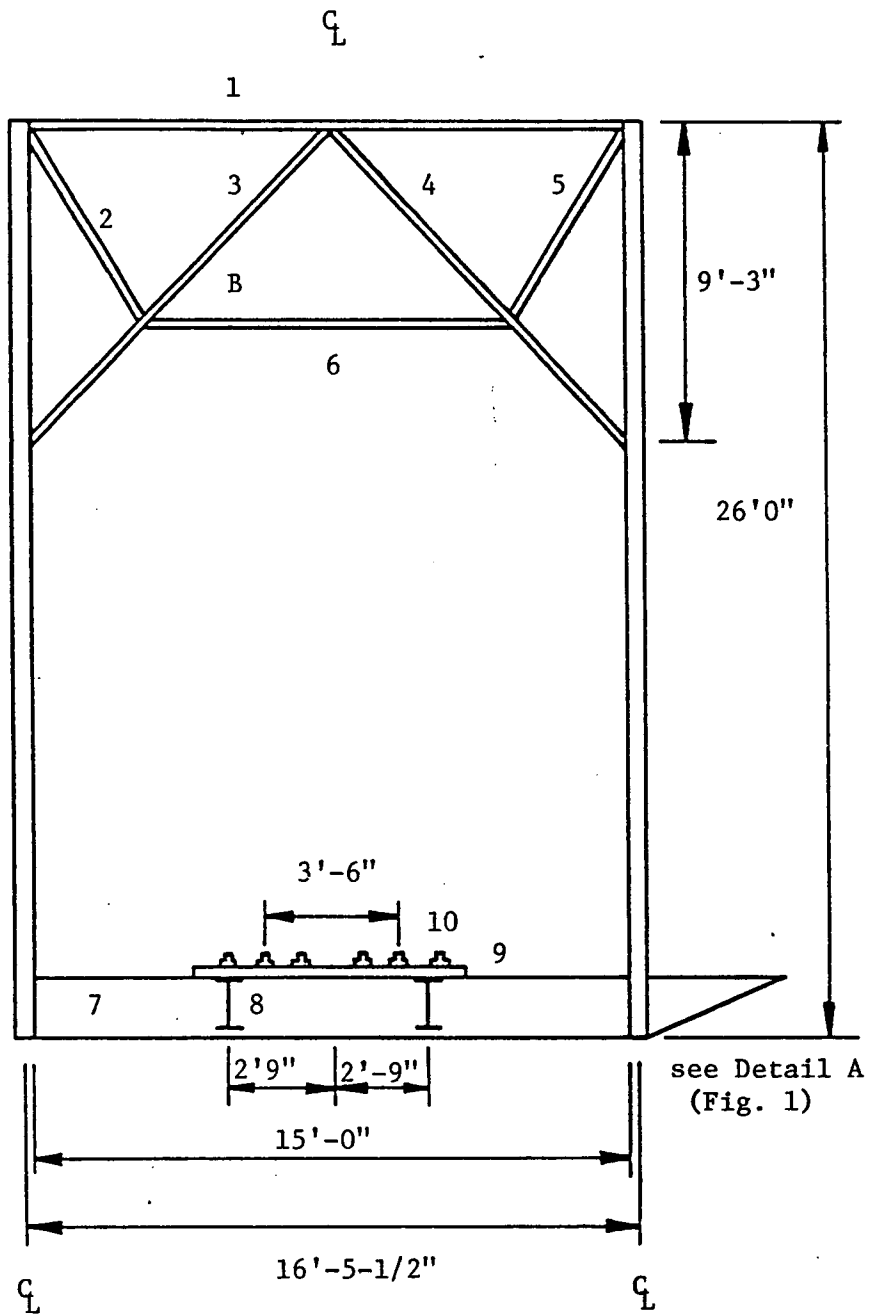

4 L's   5" x 4" x 3/8"

1 P$_L$ 31" x 7/16"

Stringer

1" = 25.4 mm

Fig. 1.1e   Floor Beam and Stringer Members

Fig. 1.2 Plan View of Panel (Typical)

Within the figure:

(L6)

CANTELEVER OVERHANG

(L5)

STRINGER

21'-0"

FLOOR
BEAM

9'-7-1/2" 5'-5-3/4" 5'-6" 5'-5-3/4" 9"-7-1/2"

C
L

Stringer

Lower Chord   Lower Chord

1' = 30.84 N   1" = 25.4 mm

Fig. 1.3a Cross Section A2 Hanger (typical)

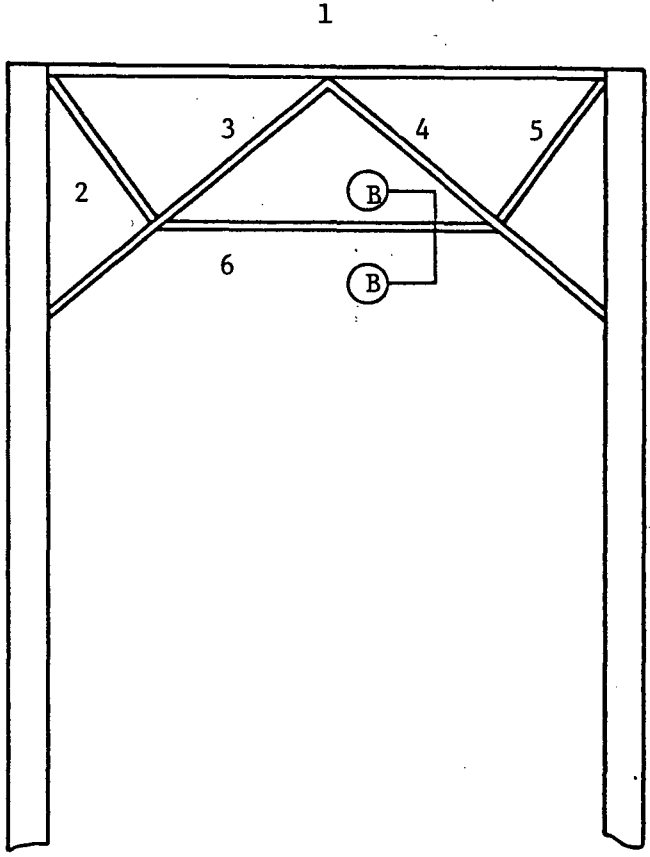|	
<u>MEMBER NUMBER</u>	<u>MATERIAL</u>
1	2 L's 3-1/2" x 3" x 3/8"
2	2 L's 3" x 2-1/2" x 3/8"
3	2 L's 3-1/2" x 3" x 3/8"
4	2 L's 3-1/2" x 3" x 3/8"
5	2 L's 3" x 2-1/2" x 3/8"
6	2 L's 3" x 2-1/2" x 3/8"
7	4 L's 6" x 4" x 3/8" 2 P_L's 13" x 3/8" 1 P_L 43" x 3/8"
8	4 L's 5" x 4" x 3/8" 1 P_L 31" x 7/16"
9	12" x 12" Wood Ties
10	90#/YD Rails

Notes:

1. First bent has no top bracing.   1" = 25.4 mm

2. For Hanger Sizes see Schedule of Member Sizes,

    Fig. 1.1b.
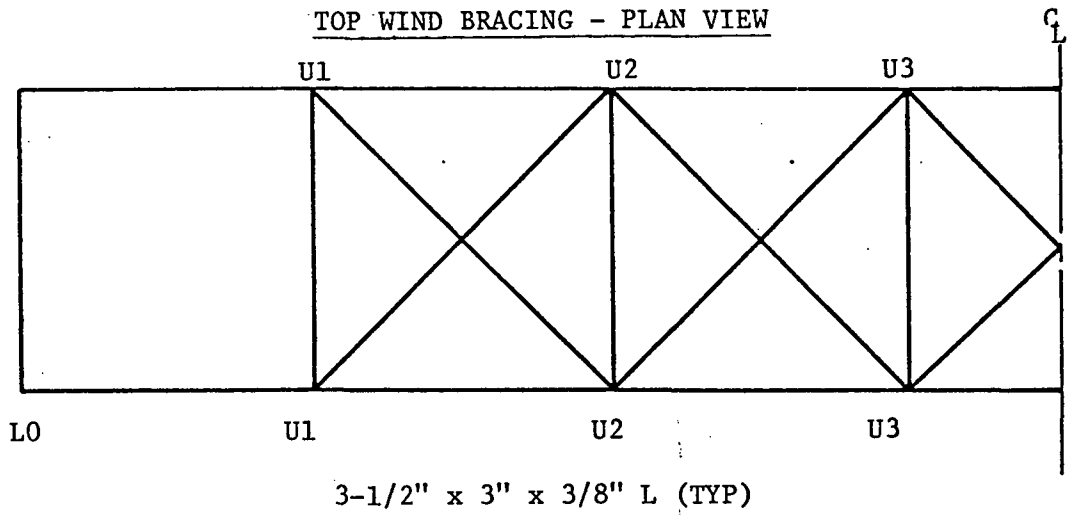
Fig. 1.3b Schedule of Cross Section Members

-166-

SCHEDULE OF PORTAL BRACING   1" = 25.4 mm

Member	Material
1	2 L's 5" x 3-1/2" x 7/16"
2	2 L's 3" x 2-1/2" x 3/8"
3	2 L's 5" x 3-1/2" x 7/16"
4	2 L's 5" x 3-1/2" x 7/16"
5	2 L's 3-1/2" x 3" x 3/16"
6	2 L's 3" x 2-1/2" x 3/8"

Note:

For Portal Member

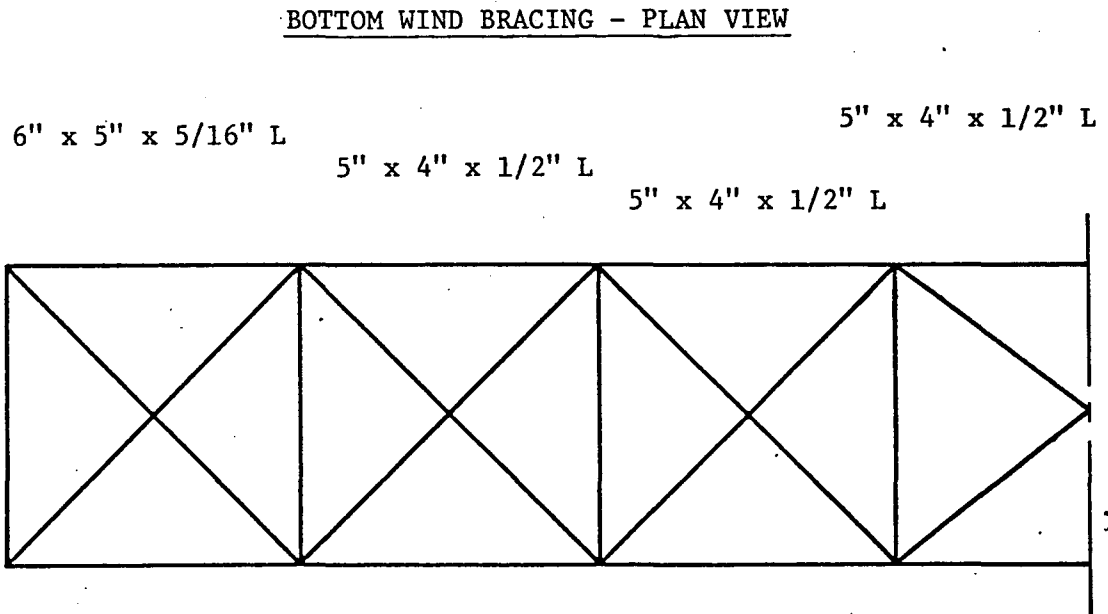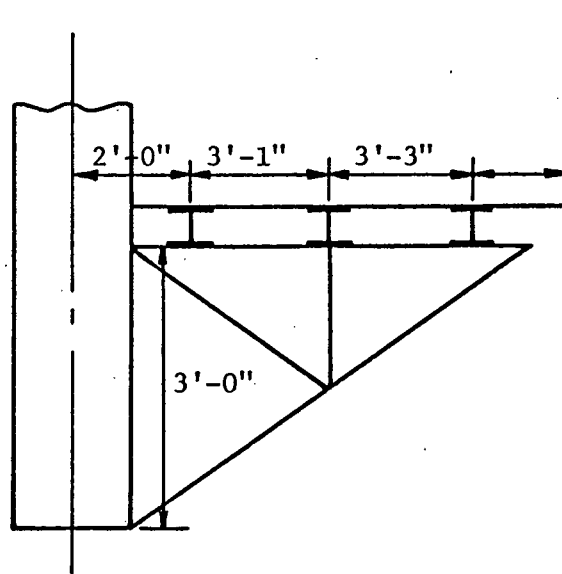Sizes, see Fig.

1.1b

Fig. 1.4 Portal Entrance (Typical)
-167-

TOP WIND BRACING – PLAN VIEW
$_{L}^{C}$

U1   U2   U3

LO   U1   U2   U3

3-1/2" x 3" x 3/8" L (TYP)

1" = 25.4 mm

BOTTOM WIND BRACING – PLAN VIEW

6" x 5" x 5/16" L   5" x 4" x 1/2" L

5" x 4" x 1/2" L

5" x 4" x 1/2" L

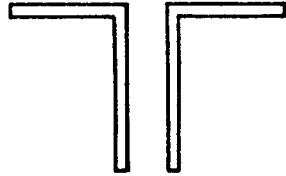Fig. 1.5 Top and Bottom Wind Bracing Plan Views

Hanger

2'-0"   3'-1"   3'-3"   1'-3-1/2"

3'-0"

2-1/2" x 2-1/2" x 5/16" L and Wearing Surface

R.S.J. 12" x 5" x 30# (TYP)

2 L's - 3-1/2" x 3 1/2" x 3/8"

1/2" P_L

3-1/2" x 3-1/2" x 3/8" L.E.S.

Flat 3-1/2" x 3/8" B.S.

1' = 0.305 m
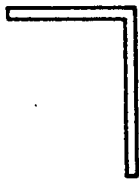
1" = 25.4 mm

Fig. 1.6   Detail A

Angle Sizes as Indicated on
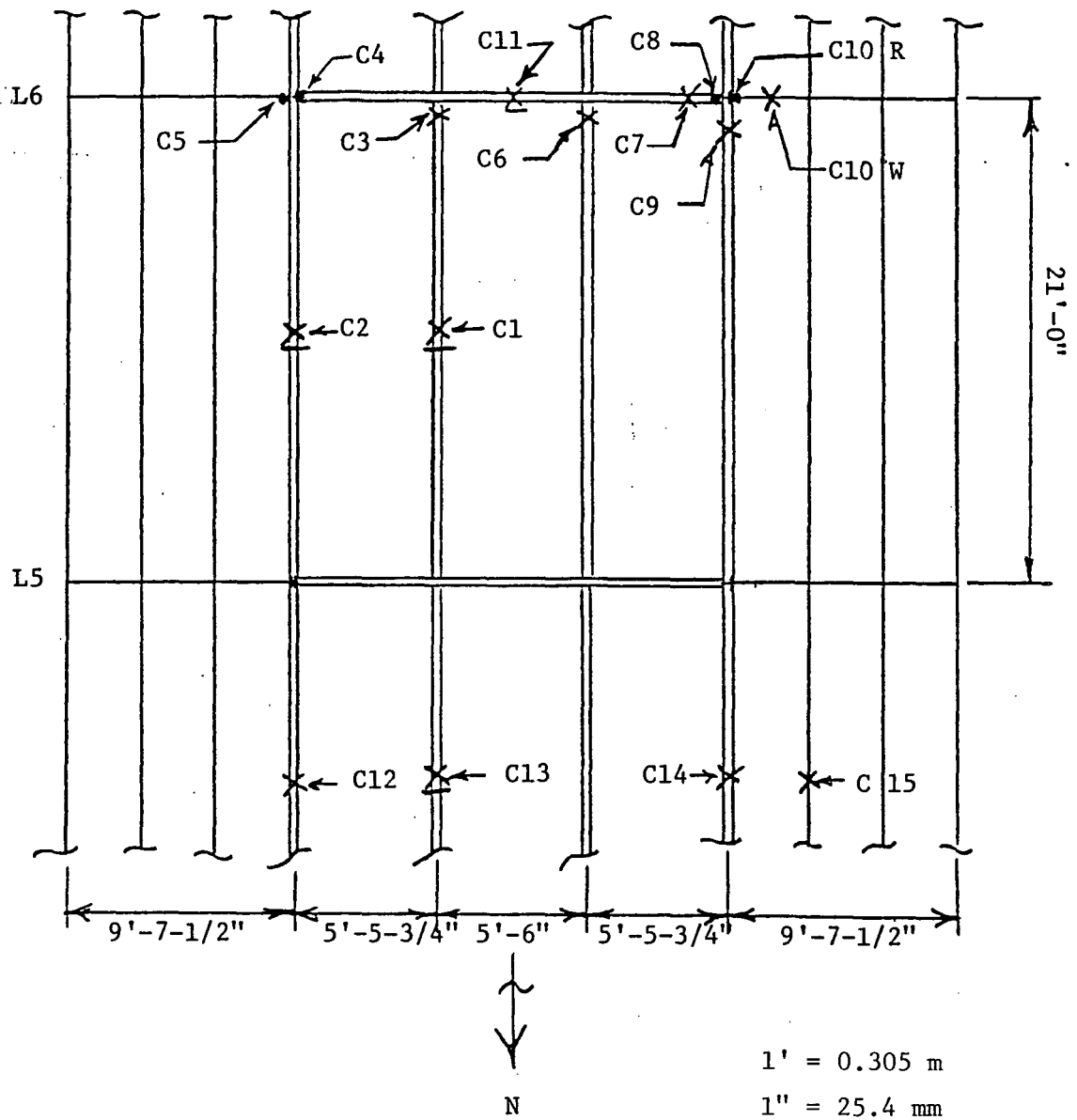
Figs. 1.3a and 1.4

Section   B – Top Bracing

Angle Sizes as Indicated on

Fig. 1.5

Section   C – Top and Bottom Wind Bracing

Fig. 1.7 Orientation of Upper Truss Bracing Members

Fig. 2.1 Gage Locations

TIME

34.5 MPa

GAGE C4

69   MPa

-172-

GAGE C5

17.25 MPa

34.5 MPa

GAGE C8
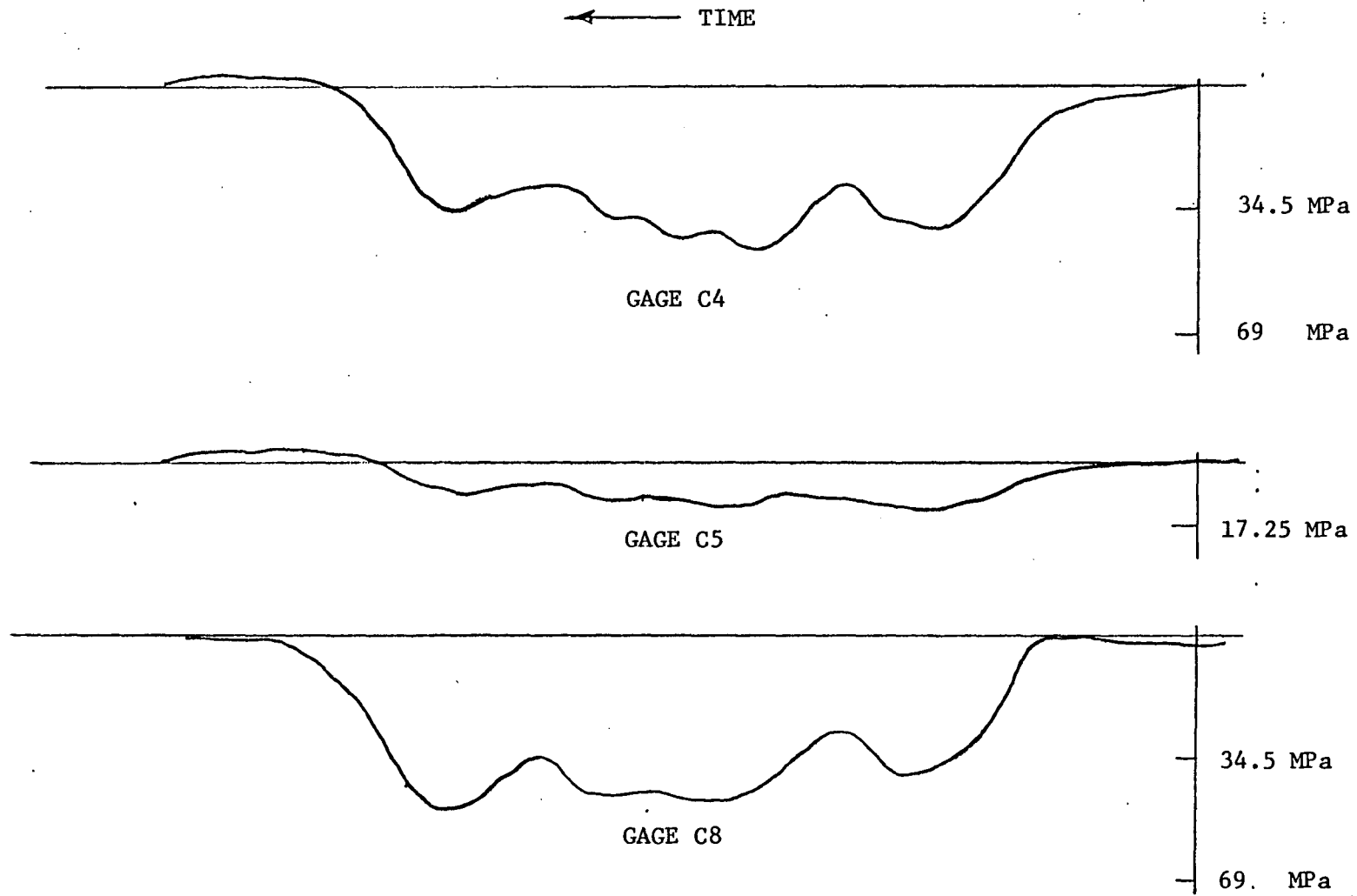
69. MPa

Fig. 2.2 Typical Analog Trace

DIESEL ENGINE – CLASS 1800–1819

87-1/2"   261 M   87-1/2"

62-3/4"   75-1/4"   75-1/4"   62-3/4"
73.9^k 73.9^k 73.9^k 73.9^k 73.9^k 73.9^k
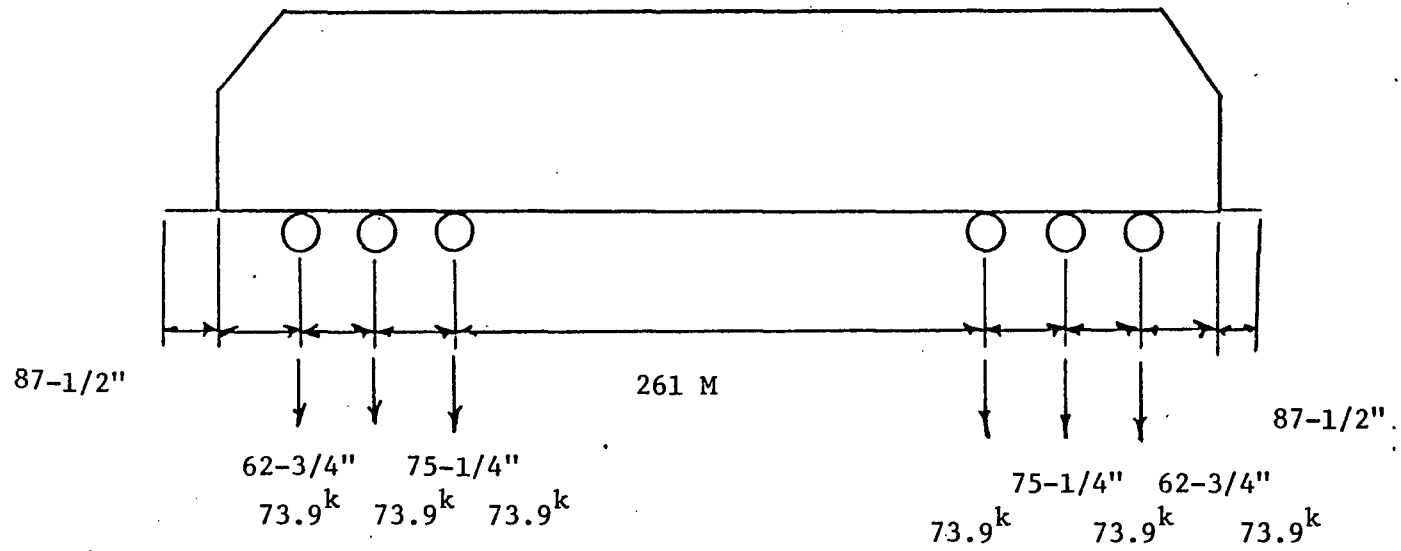
1" = 25.4 mm
1^k = 6.9 MPa

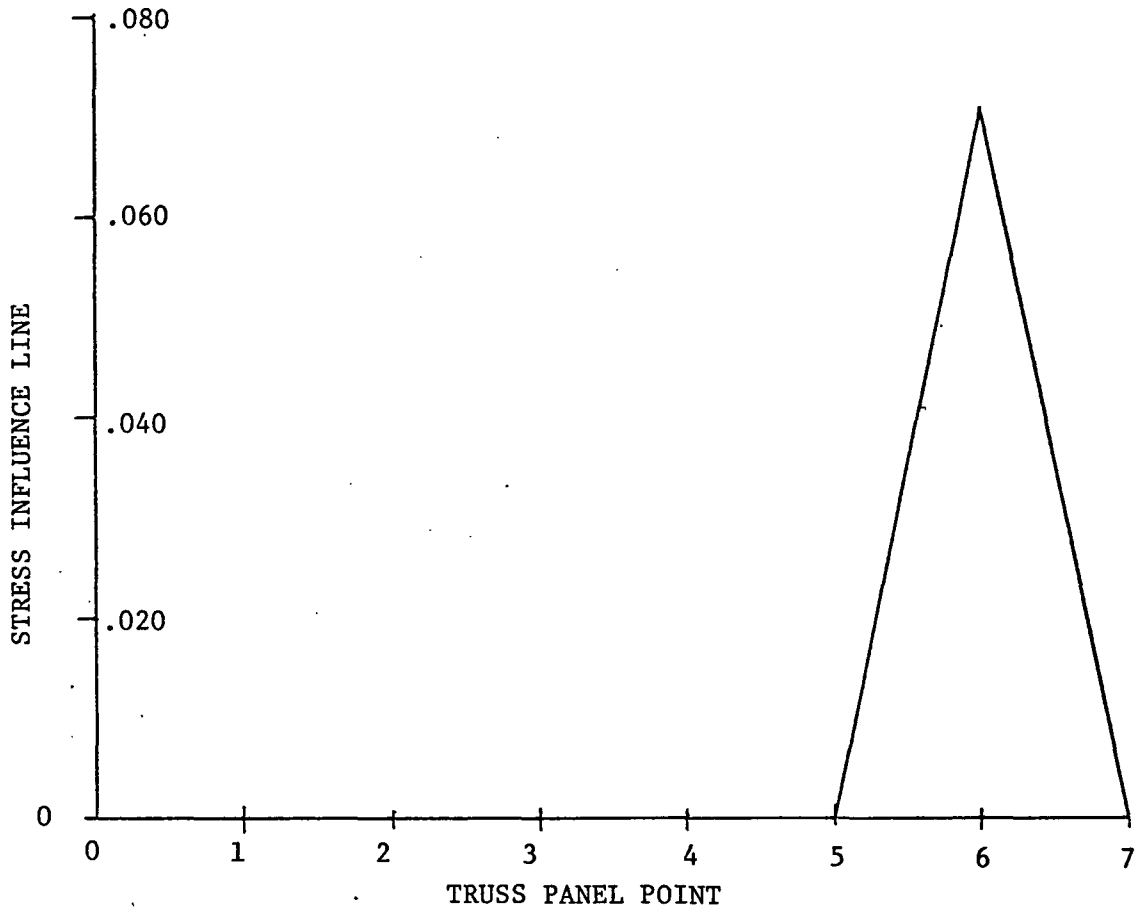Fig. 2.3 Gedmetric Pro perties of 99 ton Diesel Locomotive

Fig. 3.1 STRESS INFLUENCE LINE OF PIN TRUSS
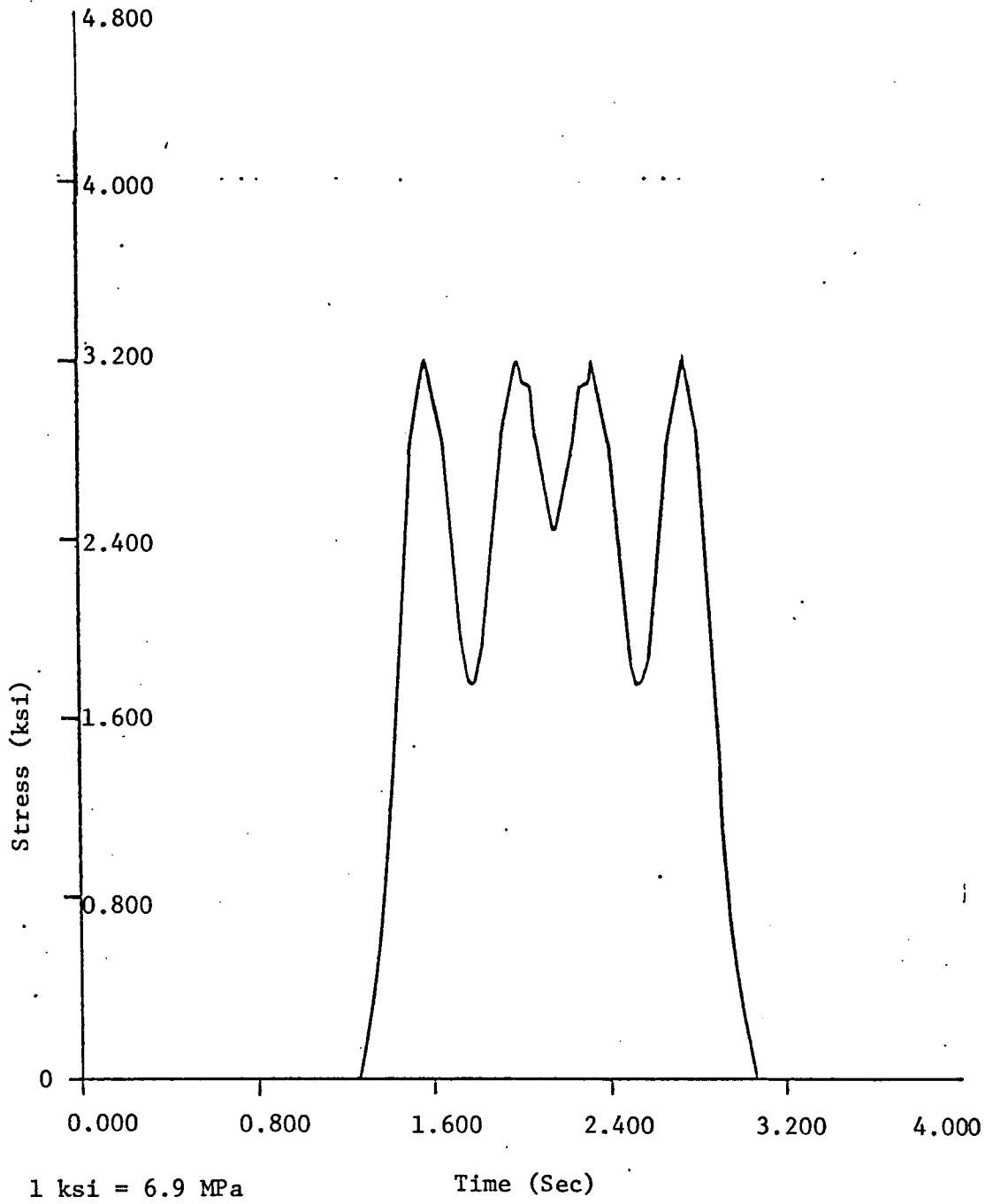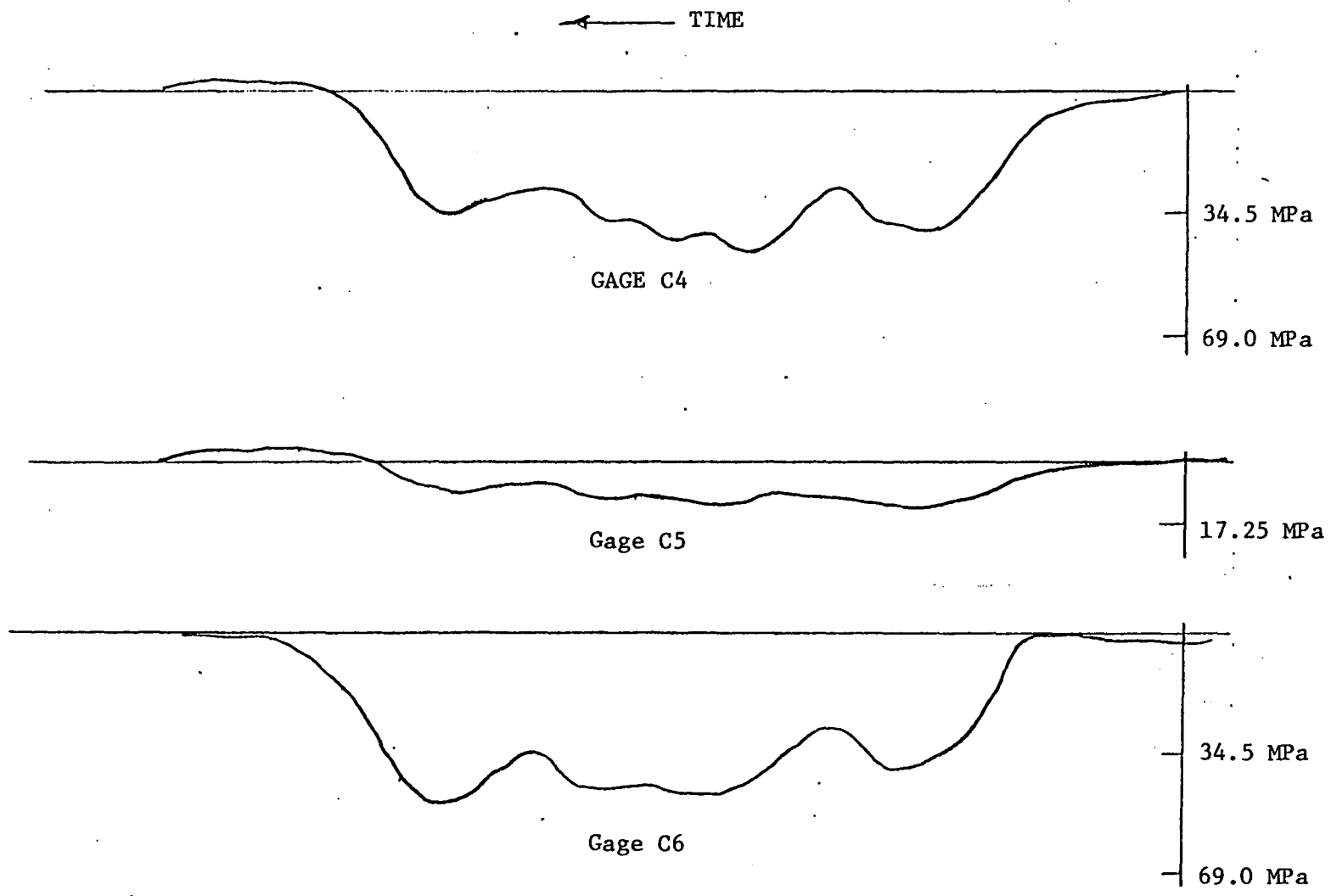
1 ksi = 6.9 MPa

Fig. 3.2   Stress–Time Relationship of Pin Truss
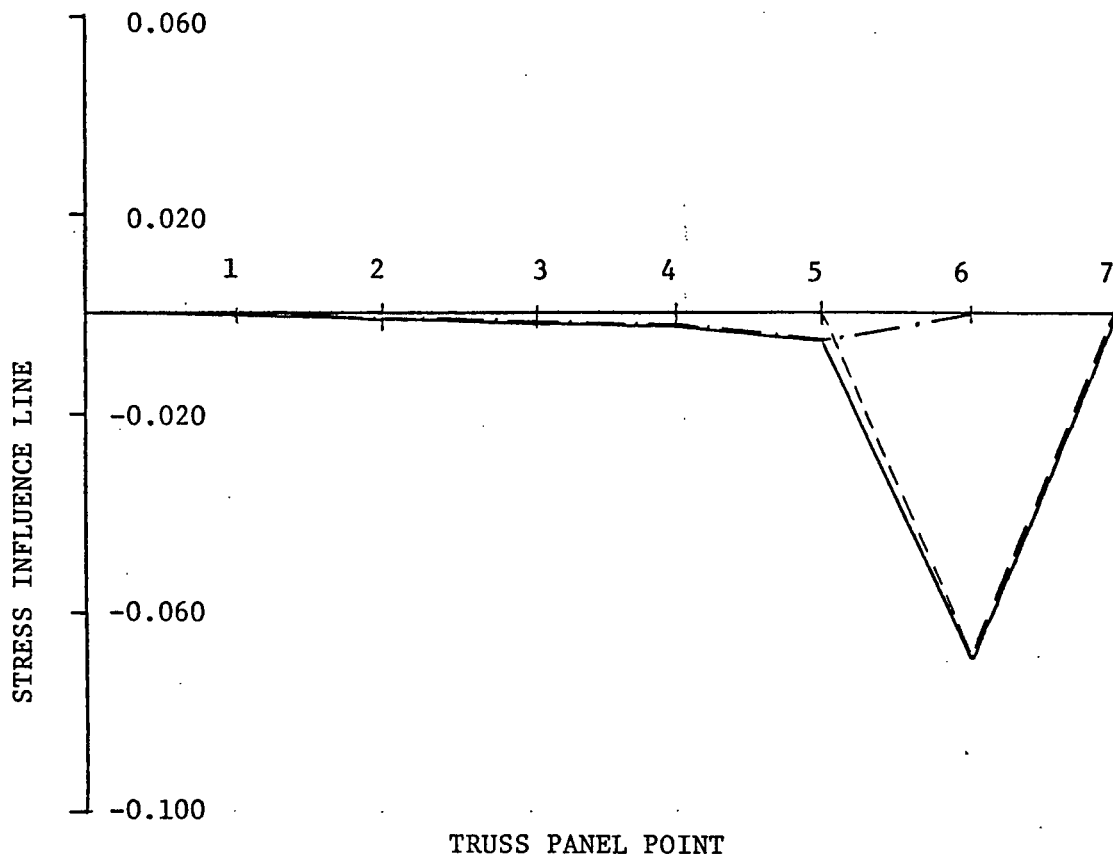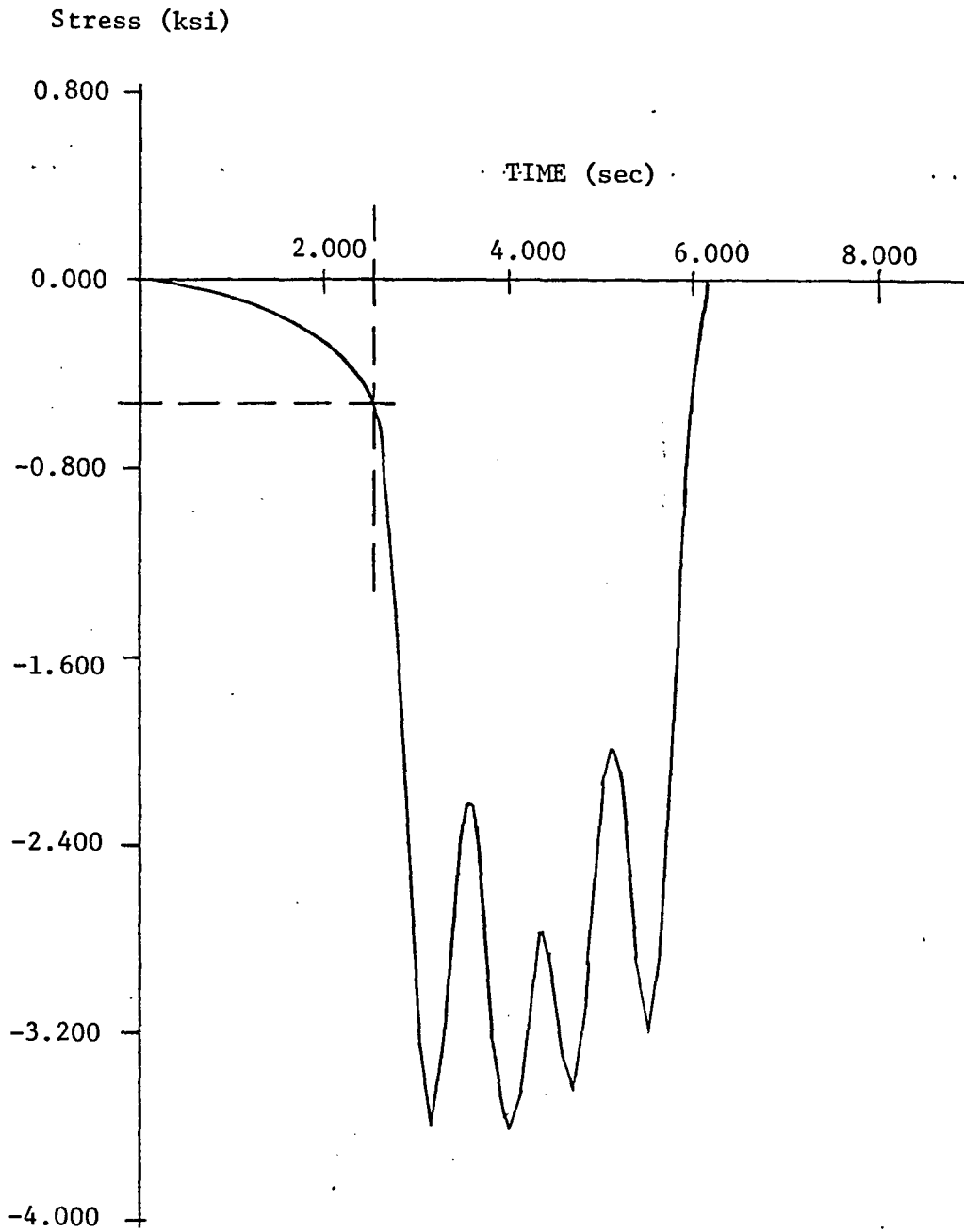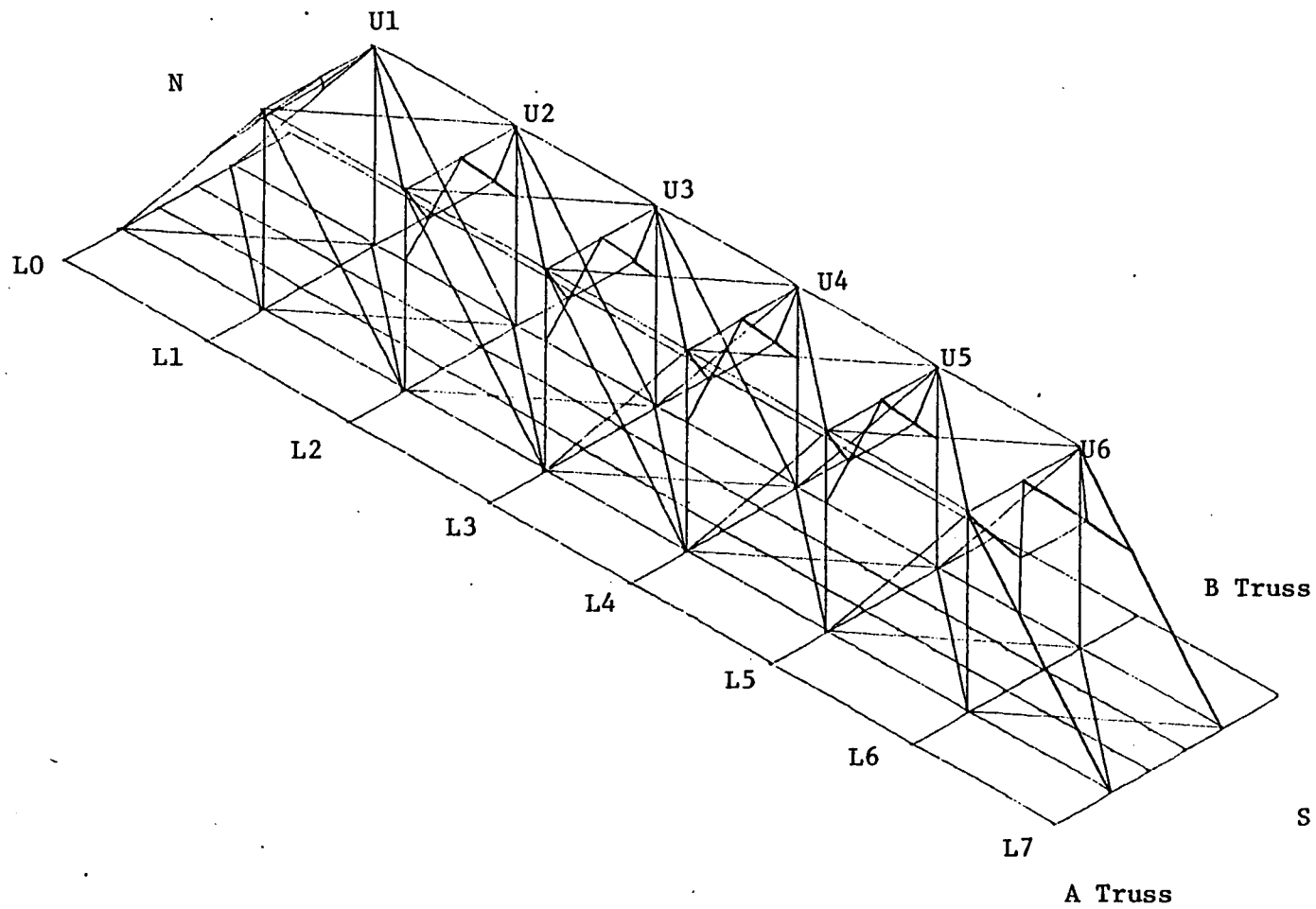
Fig. 3.3 Stress-Time Relationship for Actual Structure

Fig. 3.4 Stress Influence Line of Frame Truss

Fig. 3.5 Stress-Time Relationship of Frame Truss

1 ksi = 6.9 MPa

Fig. 3.6 Space Frame Model

N
U1
U2
U3
U4
U5
U6

L0
Panel
Point 0

L.

Panel
Point 1

L2

Panel Point 2

Panel Point 3

L3

Panel Point 4

L4

Panel Point 5

L5

Lower Chord L3L4A

Panel Point 6

L6

B Truss

Modified for Models 4C and 4D

S

Panel Point 7
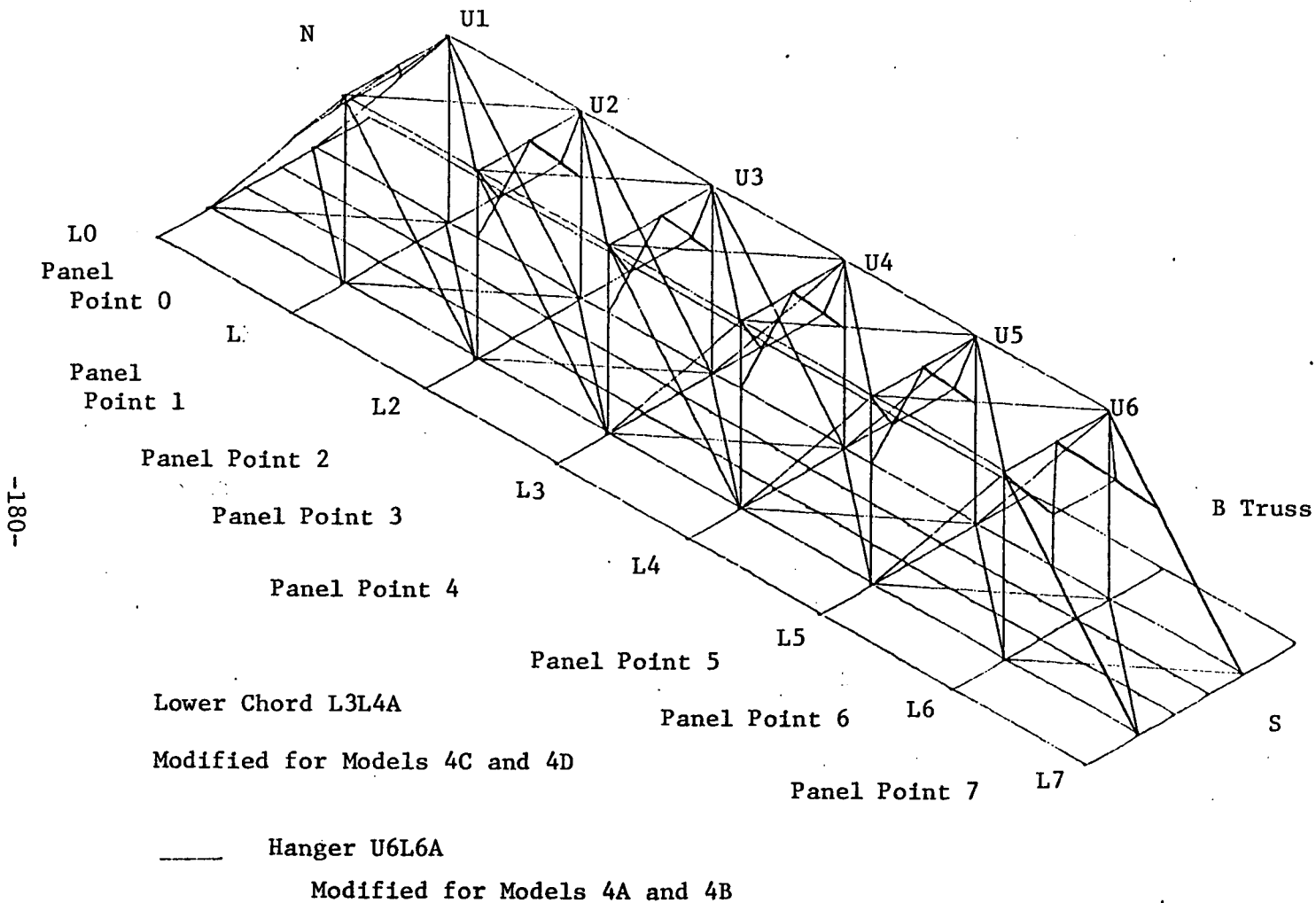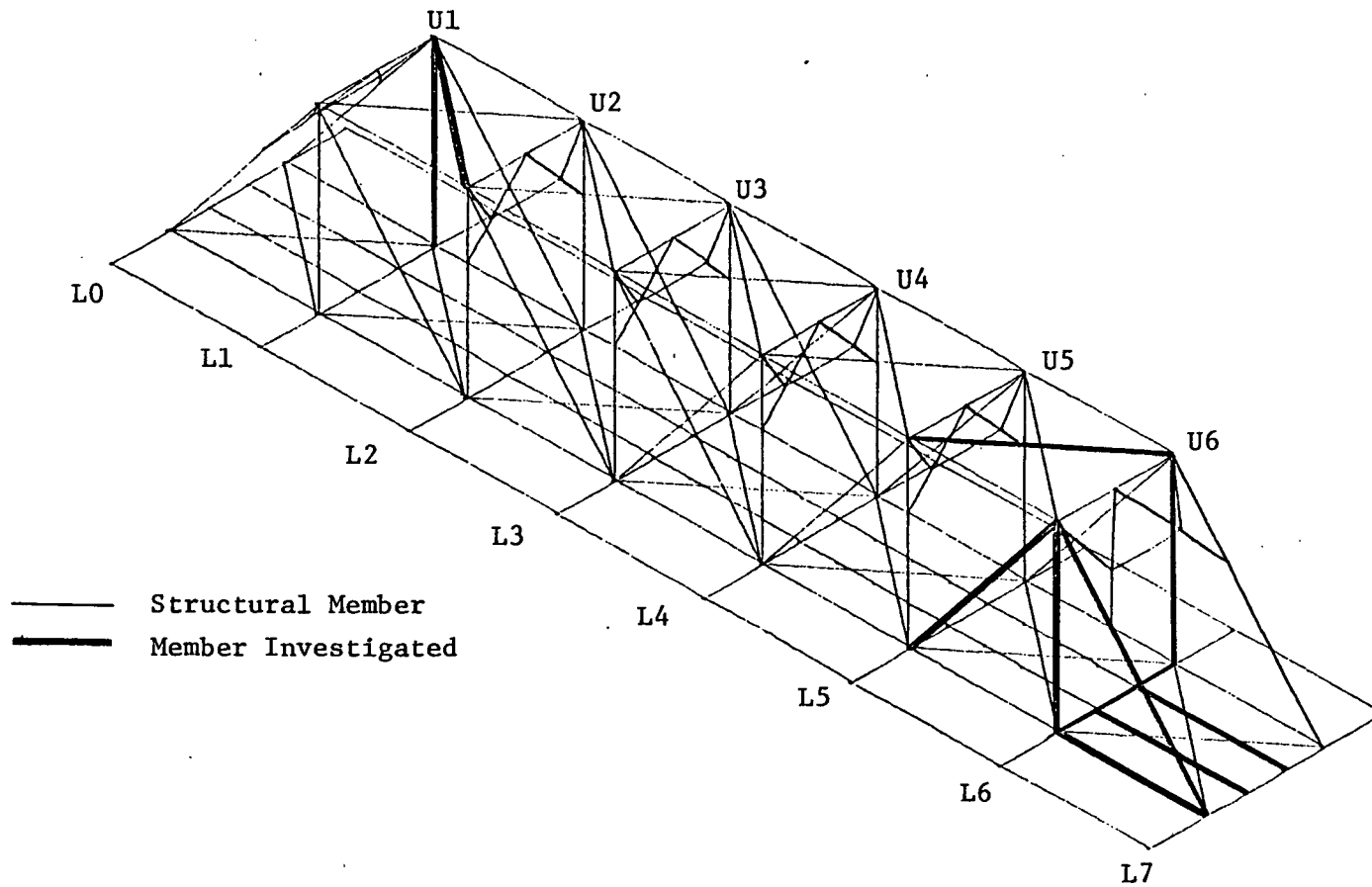
L7

_____ Hanger U6L6A

Modified for Models 4A and 4B

Fig. 4.1 Member Modification for Models 4A, 4B, 4C and 4D

Fig. 4.2 Members of Interest in Models 4A and 4B
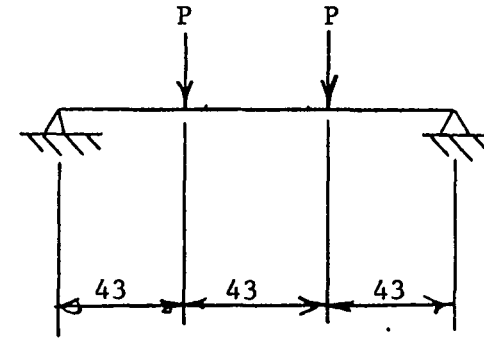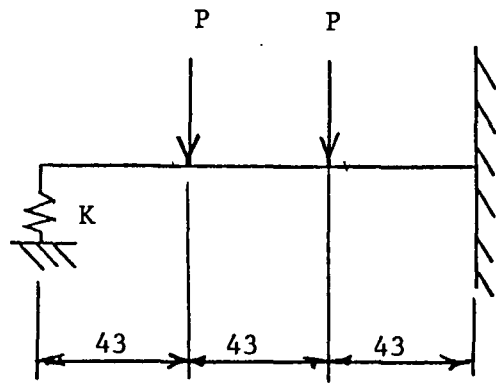
Fig. 4.3a   Equivalent Models
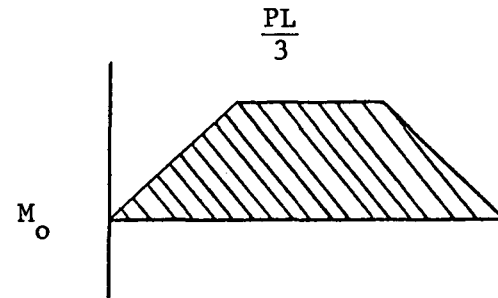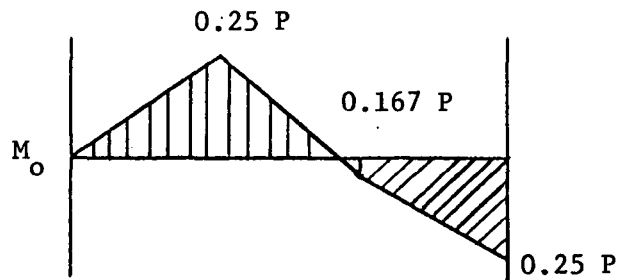
Fig. 4.3b   Moment Diagrams
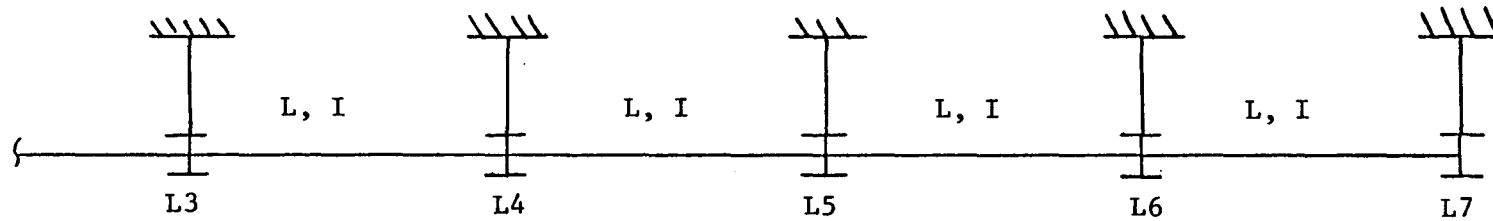
Note: Moment Reversal Developed in this
Model is greater than the moment
reversal in Fig. 4.5.
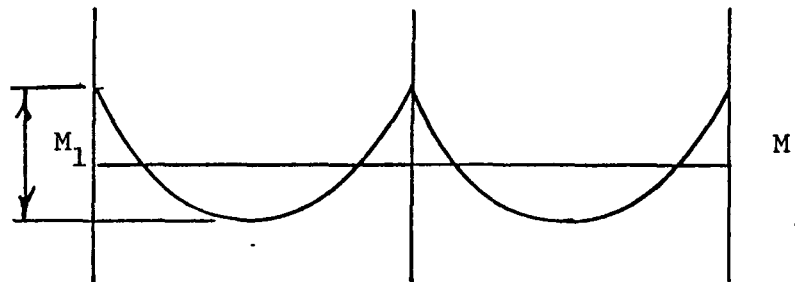
Fig. 4.4 Continuous Beam Moments

L, I   1, I   2L, I

L3   L4   L5   L6   L7
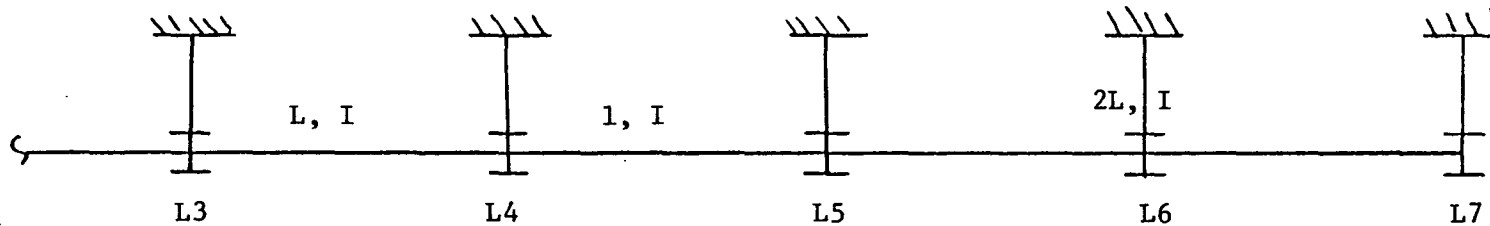
Note: Moment reversal developed in this
Model is less than the moment
reversal developed in Fig. 4.4.

M_2

+

0   M

−
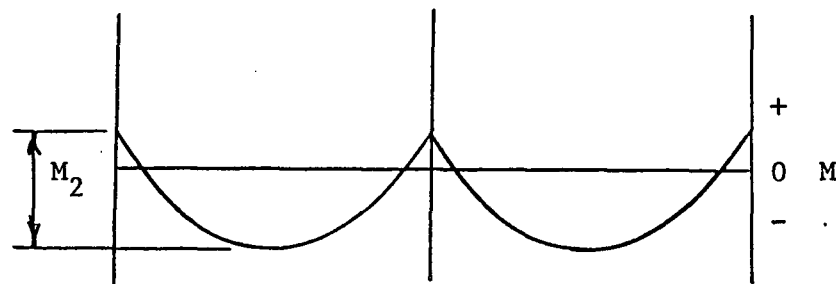
Fig. 4.5   Continuous Beam Moments L6 Removed
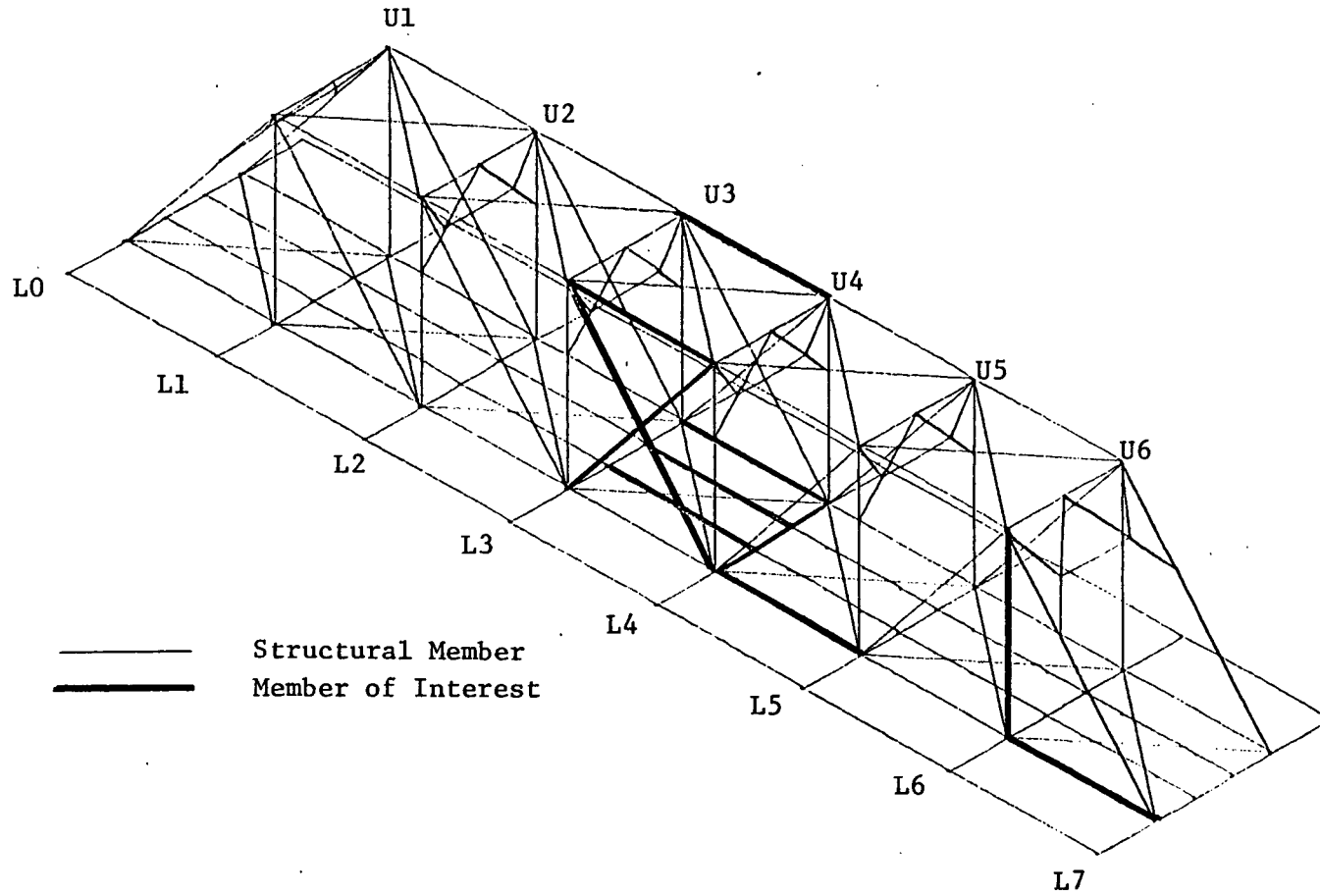
Fig. 4.6 Members of Interest in Models 4C and 4D

LOAD CASE
ONE

GAGE NO. 1

S_{RMINER}= 23.5 MPa

S_{RRMS}= 28.1 MPa

Fig. 5.1 Histogram

-186-
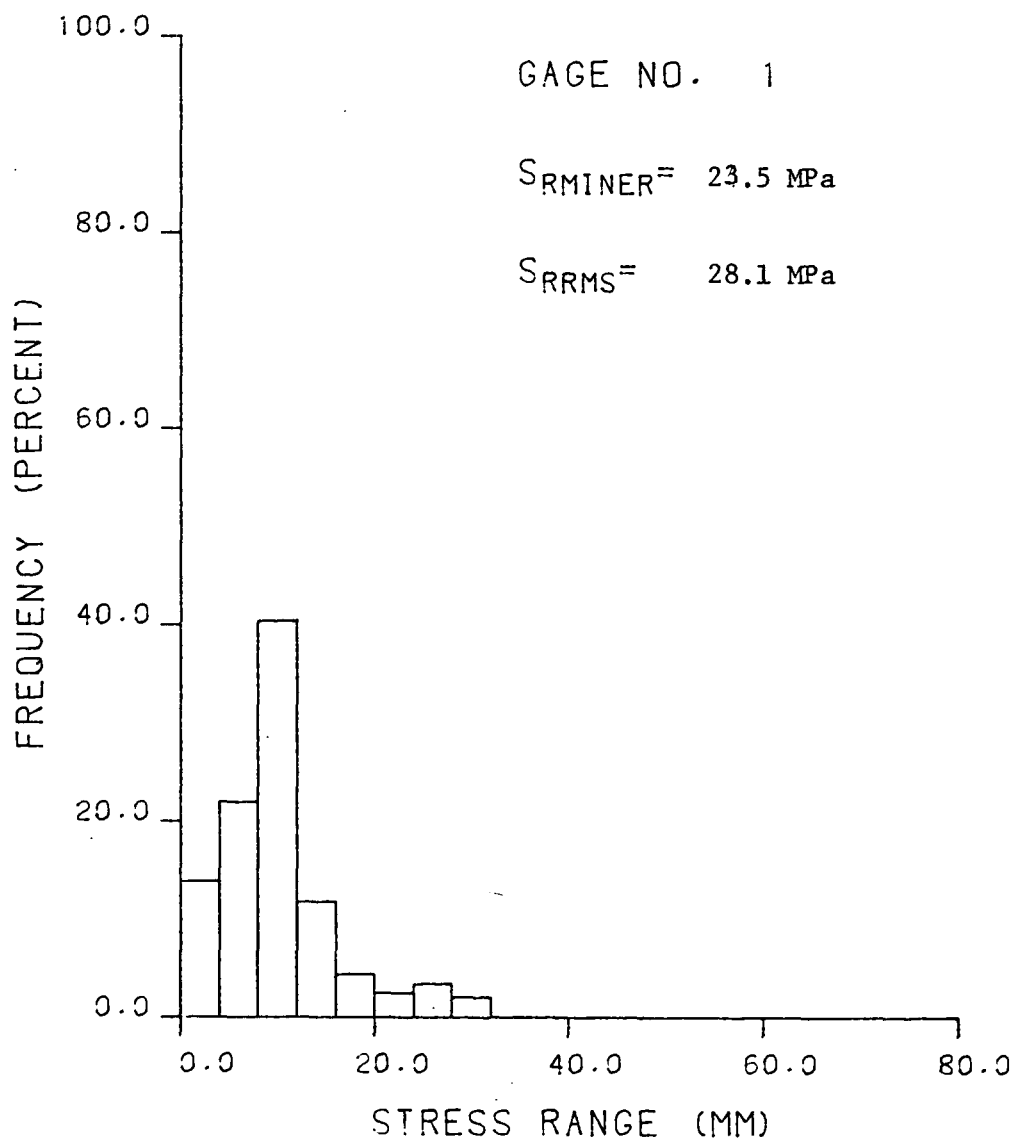
MISC.
TRAINS

GAGE NO. 4

S_{RMINER} = 17.3 MPa

S_{RRMS} = 13.8 MPa

Fig. 5.2 Histogram

Fig. 5.3   S-N Curves

REFERENCES

1. O'Connor, Colin
     DESIGN OF BRIDGE SUPERSTRUCTURES, John Wiley & Sons,
     Inc., New York, New York, 1971.

2. McCormack, Jack C.
     STRUCTURAL STEEL DESIGN, Intext Educational Publishers,
     Scranton, Pennsylvania, 1971.

3. Drew, Freeman, P.
     RECORDED STRESS HISTORIES IN RAILROAD BRIDGES,
     Journal of the Structure Division, Proceedings,
     American Society of Engineers, December 1968.

4. Wirtyachai, A., Chu, K. H. and Garg, V. K.
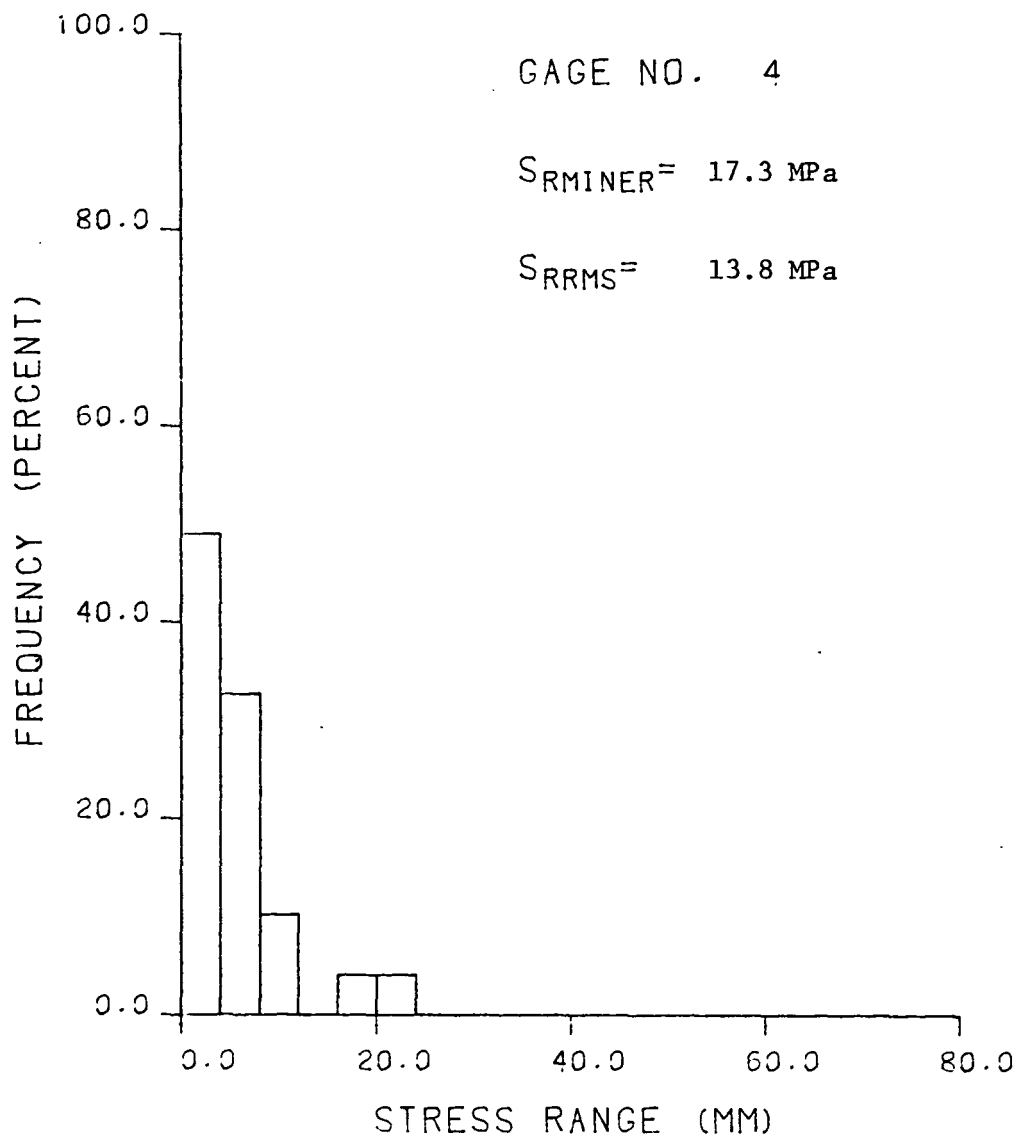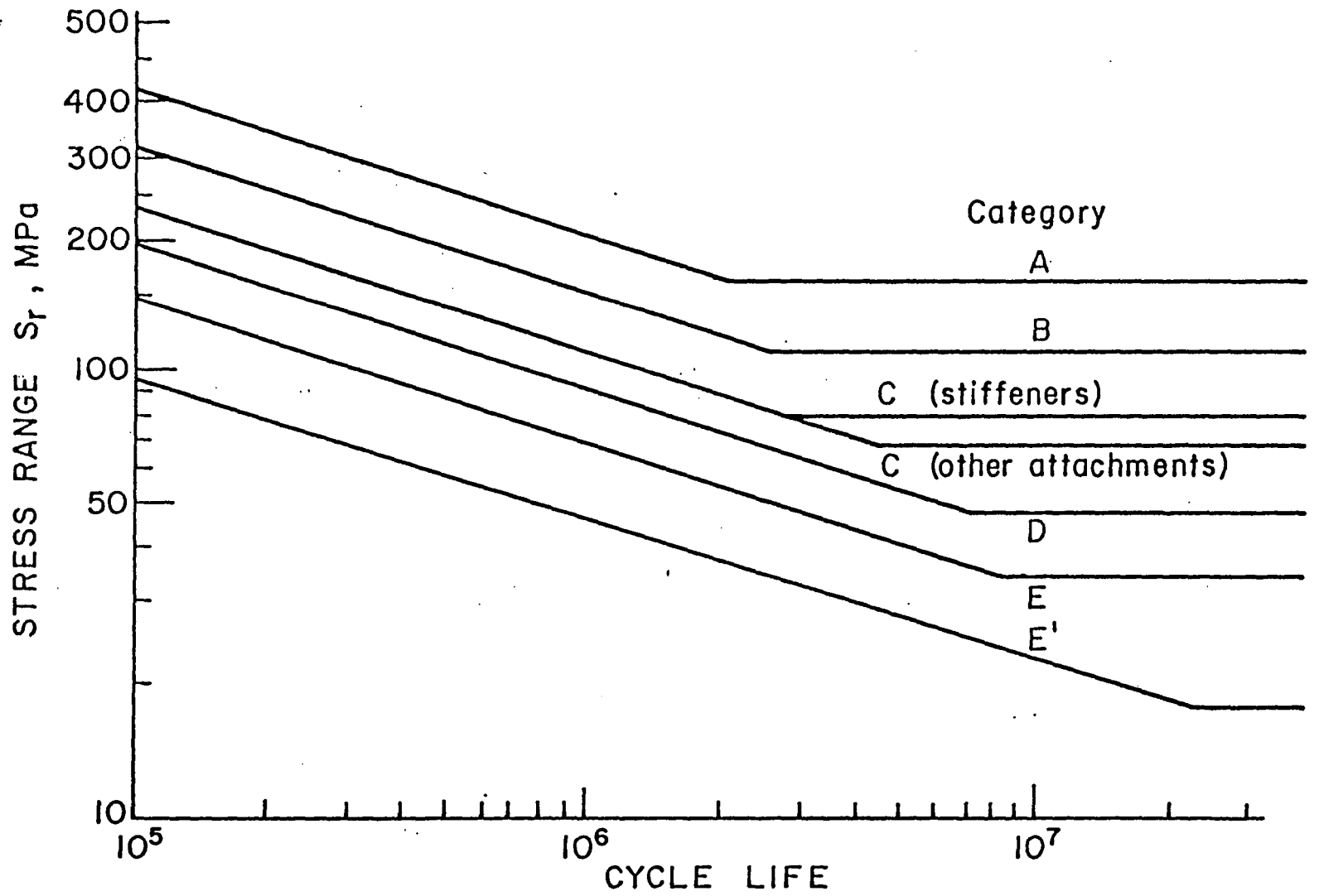   FATIGUE LIFE OF CRITICAL MEMBERS IN A RAILWAY TRUSS
     BRIDGE, Report No. R-472, A & R Technical Center,
     Chicago, Illinois, 1981.

5. Hertzberg, R. W.
     DEFORMATION AND FRACTURE MECHANICS OF ENGINEERING
     MATERIALS, John Wiley & Sons, Inc., New York, New
     York, 1976.

6. Gaylord, Edwin H., Gaylord, Charles N.
     DESIGN OF STEEL STRUCTURES, McGraw Hill Book Company,
     New York, New York, 1972.

7. Fisher, John W., and Struik, John H. A.
     GUIDE TO DESIGN CRITERIA FOR BOLTED AND RIVETED
     JOINTS, John Wiley & Sons, New York, New York, 1974.

8. Fisher, John W.
     BRIDGE FATIGUE GUIDE - DESIGN AND DETAILS, American
     Institute of Steel Construction, Booklet T112-11/77,
     New York, New York, 1977.

9. Sweeney, R. A. P. and Eckholy, I. A. S.
     ESTIMATED FATIGUE DAMAGE IN THE 206'-3" THROUGH TRUSS
     SPAN OF THE OTTAWA RIVER BRIDGE STE. ANNE DEBELLEVUE, P. Q.
     Canadian National Railways, Montreal, Quebec, 1981.

REFERENCES (continued)

10. Eckholy, I. A. S.
    ESTIMATED FATIGUE DAMAGE IN THE 356'-6" THROUGH TRUSS
    SWING SPAN OF THE RAINY RIVER BRIDGE, Rainy River,
    Ontario, Canadian National Railways, Montreal, Quebec,
    1981.

11. Sweeney, R. A. P. and Eckholy, I. A. S.
    ESTIMATED FATIGUE DAMAGE IN THE 116'-10-1/2" THROUGH
    TRUSS SPAN OF THE ASSINBONE RIVER BRIDGE, Nattress,
    Manitoba, Canadian National Railway, Montreal,
    Quebec, 1980.

12. AREA
    MANUAL FOR RAILWAY ENGINEERING, Chicago, Illinois,
    1979.

13. AASHTO
    STANDARD SPECIFICATIONS FOR HIGHWAY BRIDGES,
    Washington, D. C., 1981.

14. Marcotte, D. J.
    FATIGUE OF RIVETED JOINTS, M.S. Thesis, Department
    of Civil Engineering, Lehigh University, Bethlehem,
    Pennsylvania, 1981.

VITA

The author was born in Portland, Maine on January 8, 1953.
He is the first of four offsprings of Mr. and Mrs. Robert R. Ward.

The author received his primary education in the Wantough,
Long Island, New York, Succasanna , New Jersey, Smithtown, Long
Island, New York and Granville, New York school systems. He then
attended Granville Central High School in Granville, New York,
graduating in the spring of 1971. In May of 1975 he received a
Bachelor of Science Degree in Civil Engineering from the College
of Technology, University of Maine in Orono, Maine.

After graduating from college, the author worked for the
consulting engineering firm of E. C. Jordan Company, Inc. of
Portland, Maine from July 1975 through November 1978. His
responsibilities included the design and construction of waste
water treatment systems, highways, and airports. From June of 1977
to September of 1978 he was the project engineer for the design and
reconstruction of the main instrument landing runway at a major
air carrier airport.

In November of 1978, the author began work with the
consulting engineering firm of Hemter Ballew Associates of
Falmouth, Maine. His responsibilities included development of six
airport master plan studies for airports in the New England area, in
conjunction with the Federal Aviation Administration and state
governmental agencies, development and design of waste and storm

water treatment systems for municipal and industrial clients,
transportation studies, and highway reconstruction.

In August of 1980, the author entered Lehigh University.
He has worked as a half-time research assistant on three projects
in the Fatigue and Fracture Division of Fritz Engineering
Laboratory. The projects were out-of-plane displacement induced
fatigue cracking of bridge outrigger brackets, NCHRP Project
12-15(4), Fatigue Behavior of Variably Loaded Bridge Details
Near the Fatigue Limit, and an analysis of the fatigue strength
and ultimate life of five bridges in the Sudan. The exposure to
structural analysis and fatigue has provided the basis for his
thesis work.